Cosmological Implications of Topological Defects

Bryce Cyr

Department of Physics
McGill University
Montreal, Canada

May 2022

A thesis submitted to McGill University in partial fulfillment of the requirements of the degree of Doctor of Philosophy.

Acknowledgements

I would like to thank my supervisor, Robert Brandenberger, for his years of support, guidance, and encouragement. Through my interactions with him, I have learned what it takes to be both a superb researcher, as well as a patient and clear communicator of science. From observing his "always-inquisitive" nature, he has also taught me to treat new ideas with a critical, yet open-minded approach that has proved invaluable many times over. His mentorship has further stoked the flames of my passion for physics, and I am thankful to have had the opportunity to be a part of his research group at McGill.

I would like to next extend my gratitude to the wonderful physicists I have had the opportunity to collaborate with over my time here: Aditya Varna-Iyer, Tim Schaeffer, Rui Shi, and Hao Jiao. I also thank my current collaborators, Gonzalo Alonso-Alvarez, Katelin Schutz, Subodh Patil, and Seva Syvolap, for their patience through this phase of thesis writing. I am grateful to have had officemates who could always offer good conversation, both related and unrelated to cosmology. In particular I would like to acknowledge Elisa G.M. Ferreira, Evan McDonough, Ryo Namba, Ziwei Wang, Guilherme Franzmann, Heliudson Bernardo, and Samuel Laliberte.

I am thankful to the Canada Vanier scholarship, as well as the Natural Sciences and Engineering Research Council of Canada (NSERC) and the McGill Space institute for financial support over these years.

Outside of my immediate research group, I am thankful to have had a fantastic group of friends to help maintain a modicum of mental health during grad school. Pragya Chawla, Shreya Saha, Kale Colville, and Andrea Fodor have all contributed in very unique and specials ways to what was an overall positive journey during our time at McGill.

This experience couldn't have been possible without the continued love and support of my immediate and extended family. My parents, Sherry and Raymond, my brother, Brogan, and our dog, Murphy, have provided the foundation on which I have grown, and they cannot be thanked enough. As well, my friends (with whom I also consider family) Jordan Krasowski and Mar Sanchez-Pulido, I thank you for being a much needed source of love and joy through

some of the most difficult times. I look forward to the next challenges we face together.

Finally, I give my heartfelt thanks to my partner, Andréanne Courtemanche. This journey couldn't have been completed without the unconditional love and support I have received from her, and from our pets (Stella and Rosie), during our time together. Thank you all for providing the perfect home to come back to each night.

Abstract

This thesis investigates the role that topological defects (cosmic strings and textures) can play in producing a variety of cosmological and astrophysical phenomena. The main text is built out of a series of five published works, and one work which was submitted to a preprint archive. Following a general introduction, the thesis is split roughly into three parts. First, the impact of low frequency radiation from cosmic string loops on the global 21-cm signal at cosmic dawn, as well as on the observed distribution of fast radio bursts, is considered. Next, cosmic textures are constrained by considering their energy injection into the cosmic microwave background radiation before recombination. Finally, a mechanism is developed to study the collapse of matter into a black hole in the presence of a cosmic string loop. Black hole formation by cosmic string loops is considered for a range of black hole masses.

Abrégé

Cette thèse étudie le rôle que les défauts topologiques (cosmic strings et cosmic textures) peuvent jouer dans la production d'une variété de phénomènes cosmologiques et astrophysiques. Le texte principal est composé de cinq articles publiés et d'un article soumis en pré-impression à une archive. Le texte qui suit l'introduction générale est divisé en trois parties. La première partie porte sur l'impact du rayonnement à basse fréquence émis par les boucles de cosmic strings sur un signal de global 21-cm pendant le cosmic dawn, de même que sur la distribution de fast radio bursts. La deuxième partie porte sur la contrainte des cosmic textures en considérant leur injection d'énergie dans les radiations du cosmic microwave backgroung avant leur recombination. Dans la troisième partie, un mécanisme pour étudier l'effondrement de la matière en un trou noir en présence de boucles de cosmic strings est développé. La formation de trous noir par les cosmic strings est considérée pour une gamme de masses de trous noirs.

Contents

Preface **1**

I Introduction **4**

1 Introduction to Topological Defects in Cosmology **5**

1.1 Cosmological Phase Transitions 6

1.1.1 Classification of Defects 10

1.1.2 Defects and Cosmological Catastrophes 13

1.2 Cosmic Strings 15

1.2.1 Local $U(1)$ Symmetry Breaking: A Toy Model 16

1.2.2 Superconductivity 19

1.2.3 String Substructure 21

1.2.4 Accretion onto Cosmic String Loops 29

1.2.5 Production of a Loop Network 36

1.2.6 Current Cosmological Constraints 40

1.3 Cosmic Textures 43

Bibliography **46**

II Low Frequency Effects of Cosmic String Loops **53**

2 On the Possible Enhancement of the Global 21-cm Signal at Reionization from the Decay of Cosmic String Cusps **54**

2.1 Introduction 55

2.2 Cusp Emission Mechanism 59

2.3 Global 21-cm Signal at Reionization from Cusp Annihilations 61

2.3.1 Photons Produced Via Bremsstrahlung 61

2.3.2 Photons Produced Via Synchrotron 64
2.4 Comparison with the CMB 66
2.5 Conclusions and Discussion 69

Bibliography **70**

3 Constraints on Superconducting Cosmic Strings from the Global 21-cm Signal before Reionization **78**
3.1 Introduction 79
3.2 Radio Excess and Global 21cm Absorption Signal 82
3.3 Radio Excess from Superconducting Cosmic Strings 84
3.4 Conclusions and Discussion 87

Bibliography **89**

III High Energy Signatures of Cosmic Textures **98**

4 Cosmic Rays and Spectral Distortions from Collapsing Textures **99**
4.1 Introduction 100
4.2 Review of Global Textures and their Scaling Solution 102
4.3 Spectrum of Cosmic Rays Produced by Texture Collapse 105
4.4 Induced Spectral Distortions 109
4.5 Conclusions and Discussion 111

Bibliography **112**

IV Cosmic String Loops and Black Holes **117**

5 Intermediate Mass Black Hole Seeds from Cosmic String Loops **118**
5.1 Introduction 119
5.2 Cosmic String Formation and Evolution 120
5.3 Eddington Accretion and Super-Massive Black Hole Formation 124
5.4 Resulting Distribution of Intermediate Mass Black Holes 125
5.5 Conclusions and Discussion 128

Bibliography **130**

6 Massive black holes at high redshifts from superconducting cosmic strings 138
6.1 Introduction . . . 139
6.2 Cosmic String Overview . . . 140
6.3 Accretion onto Superconducting Cosmic String Loops . . . 143
6.4 Direct Collapse Conditions . . . 145
6.4.1 Sufficient Pristine Mass . . . 146
6.4.2 Atomic Cooling Threshold . . . 149
6.4.3 Lyman-Werner Background . . . 150
6.5 Discussion and Conclusions . . . 154

Bibliography 158

Conclusions 169

List of Figures

1.1 A heuristic illustration of the temperature evolution for different types of symmetry breaking potentials. The transitions occur when $T = T_c$ Left: A second order phase transition with a true vacuum developing at T_c. Once this state is available, the field ϕ readily rolls down from the top of the potential. Right: A first order phase transition, where the true vacua is separated from the false one by a potential barrier. The field must either undergo quantum tunnelling, or experience a significant thermal fluctuation to arrive at the true vacuum. In this scenario, bubble nucleation occurs. 10

1.2 Top: The evolution of the vacuum manifold in a particular class of complex scalar field theories. Finite temperature corrections induce a degeneracy at some critical temperature T_c, giving rise to cosmic strings. Bottom: An illustration of the mapping between physical space (the squares) and field space (the arrows). If we imagine a particular spatial slice to be discretized as shown, the central square is forced to remain in the false vacuum in order to ensure the continuity of ϕ in field space. Many such slices are glued together when extending to a third dimension, with this region of trapped energy (the cosmic string) piercing them, as shown on the right. 12

1.3 A summary of constraints relevant to superconducting cosmic strings, adapted from Miyamoto and Nakayama [32]. Shaded regions are excluded by data. Regions that are inside of a coloured contour but not shaded indicate parameter space that will be excluded by future data. Above the $P_{GW} = P_{EM}$ line, string loops decay primarily into gravitational radiation, whereas below this line, their dominant decay channel is into photons. For details on individual constraints, please see [32] and references therein. 22

1.4 A schematic representation of a cusp annihilation event. The dashed region is the cusp, which will smooth out after annihilation releasing gauge and scalar fields in a tight beam. The arrows represent a particular winding orientation for the string. 25
1.5 Left: An illustration of the scales at play in the Zel'dovich approximation. As an example, we show a mass shell originating outside the loop radius, however, mass shells inside the loop will still be attracted towards the centre, at a slower rate. Right: The evolution of a string-seeded overdensity with redshift. A dark matter halo forms around the loop after matter-radiation equality, followed by baryonic collapse after recombination. The total mass of the overdensity at these redshifts has been roughly estimated in (1.92). . . . 31
1.6 A heuristic picture of loop formation. Left: Loop-loop intersections. Right: Self-intersection of a single loop. Figure adapted from [2] 36
1.7 A recent simulation of a network of cosmic strings in the Nambu-Goto approximation (neglecting the finite width of the strings). One can see a number of long strings running through this Hubble patch, as well as a blue "fog", which indicates an abundance of small loops. Figure adapted from da Cunha et al. [56]. 39
1.8 Left: A simulation of temperature anisotropies on a 20° patch of the sky induced by a network of cosmic strings. The amplitude of the anisotropies is normalized by the string tension, $G\mu/c^2$ (we use $c = 1$ throughout this thesis). Right: The result of applying a spherical gradient to the left image. One experiences a temperature jump (or discontinuity) when traversing a cosmic string (see main text for details), and so strong gradients in the temperature map would be a smoking gun signature of these defects. Figure adapted from [7]. 41

1.9 The gravitational wave spectrum produced by a network of cosmic string loops. The dashed red lines are from the distribution given in (1.100), dashed blue lines from (1.101), and dotted red from (1.102). The solid black line is the total contribution and represents the predicted gravitational wave amplitude per frequency bin. Shaded grey regions represent peak sensitivity frequencies for various GW observatories. Figure adapted and modified from [55] to represent updated upper bounds on $G\mu$ from pulsar timing measurements. It was shown recently that particle emission from cusps introduces a high frequency cutoff to the gravitational wave background, due to the rapid decay of loops with small radii [72]. The exact modification depends on the symmetry breaking scheme, and may have implications for future gravitational wave surveys such as LISA and advanced LIGO. 42

1.10 Possible field configurations in one spatial dimension of a scalar field ϕ winding a vacuum manifold with circular (S^1) topology. Top: A trivial configuration with no texture. Bottom: A texture configuration, with all energy stored in gradients. The field is not trapped to be in its false vacuum at any point. Figure adapted and modified from chapter 3 of [2]. 44

3.1 The shaded regions show the parameter space of superconducting cosmic strings which are ruled out. The light orange region corresponds to constraints from previously considered sources (see [58] and references therein for these constraints), whereas the light blue correspond to regions that are now ruled out by our analysis, assuming the global 21cm absorption signal is not larger than what was reported by the EDGES collaboration. These new regions are bound by the curves along which $\mathcal{R} = 1$ (see the main text for the definition of $\mathcal{R}$). The vertical axis gives the value of $G\mu$, the horizontal axis is the current. The diagonal brown curve corresponds to the critical current as a function of $G\mu$. Above the curve gravitational radiation is the dominate decay mechanism of the loops. Below it, electromagnetic radiation dominates. 90

3.2 The light orange region bounded by the red curve represents the limiting constraints considered by previous works in [58]. The light blue region bounded by the grey curve corresponds to regions of the superconducting string parameter space that constrained via our analysis by requiring $\mathcal{R} \leq 1$. If the signal from strings is less than 10% of what has been reported, the constrained region extends to the orange line (requiring $\mathcal{R} \leq 0.1$). If it is less than 1%, the region extends even further to the purple line ($\mathcal{R} \leq 0.01$). These new constraints all exist in the region where the decay of loops is dominated by their energy loss into EM radiation. Constraints of this analysis from 21cm in the gravitational wave regime are plotted here in magenta, blue, and green, but they do not constrain any regions which haven't been constrained previously. 91

Preface

Preface

This thesis consists of an introduction, followed by five articles. The first four articles were published in peer-reviewed journals, and the fifth article is currently in press and will be published shortly. The introduction (chapter 1) consists of a broad overview of topological defects in cosmology, with an emphasis on cosmic strings. Chapters 2-6 are all original contributions to the field. In high energy physics, authorship on a paper is generally alphabetical. Here I identify my contribution to each of the works.

Author Contributions

Chapter 2: R.H. Brandenberger, B. Cyr, and T. Schaeffer, *On the Possible Enhancement of the Global 21-cm Signal at Reionization from the Decay of Cosmic String Cusps*, JCAP 04 (2019) 020, [arXiv:1810.03219].

I initiated this project after the first observation of the global 21-cm signal from cosmic dawn was reported. Using a new formalism that I had developed after the fast radio burst project, I computed the low frequency spectrum of photons from cosmic strings. T. Schaeffer checked my computations. I wrote the main text of the paper, with helpful suggestions from R. Brandenberger.

Chapter 3: R.H. Brandenberger, B. Cyr, and R. Shi, *Constraints on Superconducting Cosmic Strings from the Global 21-cm Signal before Reionization*, JCAP 09 (2019) 009, [arXiv:1902.08282].

R. Brandenberger and I initiated this project, which was an extension of the previous article to a more complicated class of cosmic strings. R. Shi, R. Brandenberger and myself performed all the computations independently. The writing of the text was shared between myself and R. Brandenberger.

Chapter 4: R.H. Brandenberger, B. Cyr, and H. Jiao, *Cosmic Rays and Spectral Distortions from Collapsing Textures*, JCAP 09 (2020) 035, [arXiv:2005.11099].

This project was conceived as a follow-up to earlier work by R. Brandenberger and H. Jiao. The article is split into two parts, with R. Brandenberger and H. Jiao determining constraints on textures from cosmic ray signatures, while I was in charge of computing the CMB spectral

distortions in the model. I also performed their calculations as a cross-check. I wrote the section on spectral distortions, while R. Brandenberger wrote the rest.

Chapter 5: R.H. Brandenberger, B. Cyr, and H. Jiao, *Intermediate mass black hole seeds from cosmic string loops*, Phys.Rev.D 104 (2021) 12, 123501, [arXiv:2103.14057].

This project was initiated through a joint discussion between the three of us. H. Jiao, R. Brandenberger, and I performed the computations independently, cross-checking at each step. The majority of the text was written by R. Brandenberger.

Chapter 6: B. Cyr, H. Jiao, and R.H. Brandenberger, *Massive black holes at high redshifts from superconducting cosmic strings*, Mon.Not.Roy.Astron.Soc (under review), [arXiv:2202.01799].

Unsatisfied with some assumptions made in the previous paper, I initiated this project as a way to study black hole collapse in an astrophysical environment with a cosmic string loop. I identified the computations that needed to be done, and performed all calculations in tandem with H. Jiao. I wrote the article, with minor suggestions and corrections from R. Brandenberger and H. Jiao.

Part I

Introduction

Chapter 1

Introduction to Topological Defects in Cosmology

Phase transitions are a ubiquitous phenomenon in nature, occurring in environments that are well known to us (for example, a glass of water which freezes), as well as in environments that are less accessible to our everyday senses, such as in low-temperature superconductors, or superfluid systems. From the field theory perspective, a phase transition signifies the emergence of a new, lower energy configuration in the system, known as the *true vacuum*, which is often associated with the breaking of a symmetry in the theory. In some phase transitions, it is possible for regions of space to remain trapped in a *false* vacuum state, for reasons concerning the topology of the true vacuum manifold. Such regions of trapped energy are referred to as topological defects. Phase transitions and topological defect formation are thus intimately related, with the spatial dimensionality of the defect determined by the specific symmetry breaking pattern undergone by the system.

In condensed matter settings, topological defects are not at all uncommon. Superfluid phase transitions, such as in superfluid helium (3HE), are capable of producing one-dimensional (line) defects known as vortex lines [1]. Ferromagnetic materials are also capable of producing defects known as domain walls, two-dimensional surfaces that mark the boundary between different magnetic dipole orientations. In condensed matter physics, the formation of these objects is often bothersome as they can spoil some of the desired properties of a material, and are thus given the negative connotation of being a "defect". In cosmology, however, the formation and evolution of these defects may one day provide us with the key to understanding symmetries present in our universe at the earliest times. Defects are regions of localized energy, and so they may also be referred to as solitons. Thus,

in the cosmological context one may refer to topological defects equally well as topological solitons.

As we shall see, line defects (also known as cosmic strings) are the most viable class of solitons that can obey cosmological constraints. If they exist, cosmic strings will permeate the observable universe, primarily arranging themselves into two different configurations: long straight segments, and loops [2]. These cosmic strings represent regions of trapped energy, and therefore gravitate. Cosmic string loops may act as early non-linearities in the initial matter density field, playing a non-trivial role in cosmic structure formation. In the early 1980's, Zel'dovich [3] and Vilenkin [4] noticed that the observed distribution of galaxies today could potentially be explained by a spectrum of density perturbations sourced by a population of cosmic string loops. This explanation of the initial density fluctuations stood as an alternative to the one proposed by cosmic inflation [5, 6] at the time. However, string-seeded overdensities do not give rise to a series of acoustic peaks in the power spectrum of the cosmic microwave background (see [7] and section 1.2.6 for more details). Therefore, cosmic string loops were relegated to only contributing a subdominant part of the spectrum of density perturbations observed at recombination. Even in this role, however, a rich phenomenology is expected if a distribution of string loops exists in our universe.

In this introduction, we begin with a review of the basic thermal history of our universe. After using this knowledge to motivate the existence of cosmological phase transitions in our universe, we move onto describing the ingredients necessary to produce different types of topological defects. We then show that line defects (cosmic strings) are the most cosmologically well motivated solitons which may exist, and analyse many different aspects of these strings, both microscopically (at the level of fundamental fields) and macroscopically (utilizing an effective action approach). Finally, we conclude with a short discussion on cosmic textures, a class of unstable topological defects. The rest of the thesis is dedicated to studying novel phenomenology arising from these defects. Throughout the introduction and the manuscripts, we use units where $c = k_b = \hbar = 1$.

1.1 Cosmological Phase Transitions

In cosmology, phase transitions often arise due to finite temperature effects, and so we begin with a brief review of the standard thermal history of the universe. The background spacetime is well described by a spatially flat FRLW metric of the form

$$ds^2 = dt^2 - a(t)^2 d\mathbf{x}^2 \tag{1.1}$$

Where t is coordinate time, $a(t)$ is the scale factor which encodes the physical size of the universe at time t, and $\mathbf{x}$ are comoving spatial coordinates. Comoving length scales, by definition, do not evolve in an expanding background, and are related to physical scales by $\mathbf{x}_p = a(t)\mathbf{x}$.

As light propagates on an expanding background, its frequency is modified, $\nu_i = (1+z)\nu_f$ where ν_i is an initial photon frequency, ν_f is its final frequency, and z is the redshift, defined through the scale factor as

$$(1+z) = \frac{a(t_0)}{a(t)}, \tag{1.2}$$

with t_0 being the age of the universe today. Physically, the expansion of space stretches the wavelength of the photon. It is often more convenient to express different times in the thermal history by this redshift factor. The evolution of the scale factor $a(t)$ is determined through Einstein's equations in the presence of an energy momentum tensor, $T_{\mu\nu}$,

$$G_{\mu\nu} = \frac{8\pi}{3M_{pl}^2} T_{\mu\nu}, \tag{1.3}$$

where $G_{\mu\nu}$ is the Einstein tensor, an object consisting of the metric and its derivatives, and $M_{pl} \approx 10^{18}\,\text{GeV}$ is the Planck mass. In order to respect the symmetries of the FRLW metric, the energy momentum tensor takes the form of a perfect fluid

$$T_{\mu\nu} = (\rho + p)u_\mu u_\nu - p g_{\mu\nu}, \tag{1.4}$$

here, ρ and p are the energy density and pressure of the fluid respectively, and u^μ is its four-velocity. Local conservation of this tensor ($D_\mu T^{\mu\nu} = 0$, where D_μ is the covariant derivative, a coordinate-independent generalization of the partial derivative, ∂_μ) allows us to derive a continuity equation for the fluid

$$\dot{\rho} + 3\frac{\dot{a}}{a}(\rho + p) = 0 \tag{1.5}$$

Finally, an equation of state parameter $w = p/\rho$ defines the relationship between the pressure and energy density of the fluid. For (non-relativistic) matter, the pressure is negligible and $w_m = 0$. Radiation is well described by $w_r = 1/3$. With this in hand, it is clear from (1.5) that the energy densities in matter and radiation evolve as $\rho_m \sim a(t)^{-3}$ and $\rho_r \sim a(t)^{-4}$, respectively.

Manipulating the Einstein equations with these ingredients yields the Friedmann equations

$$\left(\frac{\dot{a}}{a}\right)^2 = \frac{8\pi G}{3}\rho_T \tag{1.6}$$

$$\frac{\ddot{a}}{a} = -\frac{4\pi}{3}G(\rho_T + 3p_T) \tag{1.7}$$

Where $\rho_T = \sum \rho_i$ and $p_T = \sum p_i$ are the sums of the individual energy densities and pressures of any fluids present at a given time. Rearranging the first Friedmann equation gives the relationship between physical time t and scale factor when the fluid is dominated by either radiation or matter ($\rho_T \sim \rho_{r/m}$).

$$a(t) \propto \begin{cases} t^{1/2} & \text{(Radiation domination)} \\ t^{2/3} & \text{(Matter domination)} \end{cases} \tag{1.8}$$

After an initial period of inflation (or one of its alternatives [8, 9, 10]), the universe is thought to have entered a phase of radiation domination. During this epoch, a hot, dense plasma of primordial particles permeated the universe. Collisions in this fluid happened sufficiently fast ($\Gamma > H$ where Γ is the rate of interactions, while $H = \dot{a}/a$ describes the expansion rate) that a thermal equilibrium was established. The energy density of this radiation bath is given by

$$\rho_r = \frac{\pi^2}{30}g_*(T)T^4 \tag{1.9}$$

where T is the temperature of the plasma (which redshifts like $T = (1+z)T_0$, where $T_0 \approx 2.3\,\mathrm{K}$ is the temperature of the CMB blackbody today) and $g_*(T)$ is the number of relativistic degrees of freedom at a temperature T. A particle is relativistic when $T \geq m$, and so the value of $g_*(T)$ drops as the temperature is diluted due to expansion and different particle species become nonrelativistic.

After an initial period of radiation domination, the matter content of the universe becomes dominant due to its slower dilution ($\rho_r \sim a(t)^{-4}$ while $\rho_m \sim a(t)^{-3}$). The redshift at which this shift occurs is $z_{eq} \sim 3400$, and it is at this time that the first dark matter structures start to grow. The baryonic content of the standard model doesn't experience this growth initially, as it is remains tightly coupled to a radiation bath of photons which exert considerable pressure forces, resisting gravitational collapse.

As this radiation bath cools further, it is no longer able efficiently ionize newly formed Hydrogen atoms, and the photons start to free-stream. This decoupling of photons and baryons is referred to as *recombination*, and takes place at $z \sim 1100$. After decoupling, these photons are commonly referred to as the cosmic microwave background (CMB). These two epochs will be our primary focus in this thesis.

This thermal history is very well tested in the matter epoch, through a variety of probes such as large scale structure, temperature anisotropies in the CMB, and distortions of the blackbody shape of the the microwave background. When considering beyond the standard model phase transitions, we therefore focus on the radiation epoch, where constraints on such physics are less severe. The presence of a radiation bath induces finite-temperature corrections to the potential energies of coupled fields (for example, $V(\phi) \to V(\phi, T)$ where ϕ is a scalar field). As $V(\phi, T)$ evolves, new, lower energy vacua can develop, and if they do, a phase transition is triggered as ϕ evolves to the true vacuum of the theory. Phase transitions can occur smoothly (in the case of a second order transition), or via bubble nucleation (for first order phase transitions). Fig. 1.1 illustrates the evolution of the potential, $V(\phi, T)$, in these two cases.

Often times, symmetries of the original system are lost after a phase transition. When the true ground state of a theory doesn't exhibit all of the symmetries possessed by the Hamiltonian, the symmetry is said to be spontaneously broken. The spontaneous breaking of local or global symmetries is a necessary (but not sufficient) condition for the formation of topological defects. Symmetry breaking is said to be spontaneous when the ground state of the theory doesn't exhibit all of the symmetries of the original Hamiltonian.

In the current cosmological paradigm, we are confident that at least one example of spontaneous symmetry breaking has taken place. At $T \sim \mathcal{O}(100)\,\mathrm{GeV}$, the evolution of the

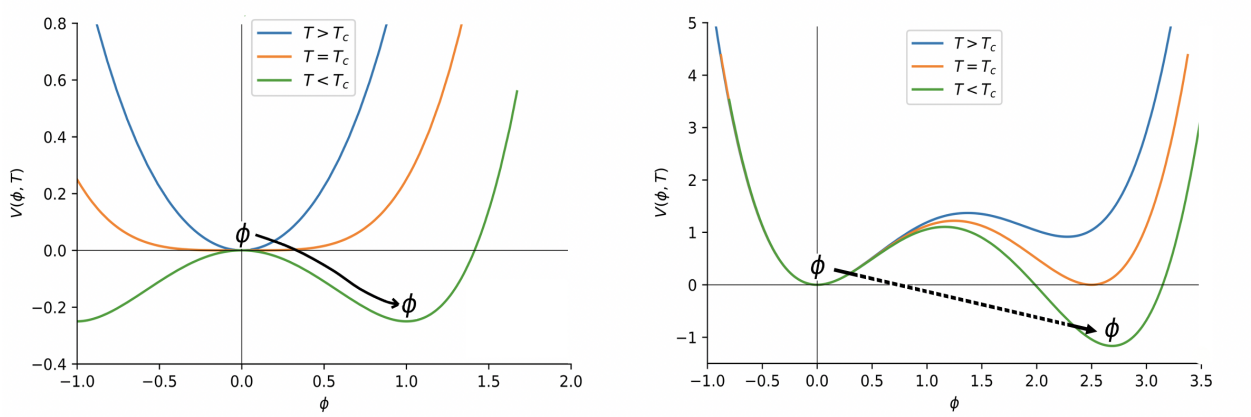

Figure 1.1: A heuristic illustration of the temperature evolution for different types of symmetry breaking potentials. The transitions occur when $T = T_c$ Left: A second order phase transition with a true vacuum developing at T_c. Once this state is available, the field ϕ readily rolls down from the top of the potential. Right: A first order phase transition, where the true vacua is separated from the false one by a potential barrier. The field must either undergo quantum tunnelling, or experience a significant thermal fluctuation to arrive at the true vacuum. In this scenario, bubble nucleation occurs.

Higgs potential triggered a phase transition which reduced the symmetry of the universe from $SU(2) \times U(1) \to U(1)_\gamma$, giving masses to the $W^\pm/Z$ bosons and most of the fermionic content of the standard model. Unfortunately, the topology of the Higgs' vacuum manifold doesn't give rise to stable defect configurations.

Terrestrial particle colliders such as the Large Hadron Collider (LHC) can probe scales up to a center of mass energy of $E_{cm} \sim \mathcal{O}(10^4)\,\text{GeV}$. We know that the effects of quantum gravity become important near the Planck scale ($E_{pl} \sim \mathcal{O}(10^{19})\,\text{GeV}$), and we have reason to expect that a phase transition occurred near the grand unified scale ($E_{GUT} \sim \mathcal{O}(10^{16})\,\text{GeV}$). There are therefore many orders of magnitude in energy which are difficult to probe using conventional methods. However, if topological defects exist in nature, their phenomenological signatures are usually stronger for high scale symmetry breaking. Therefore, topological defects offer a top down approach to probing particle physics, complementary to costly particle collider experiments.

1.1.1 Classification of Defects

In order for defect formation to take place at a phase transition, one requires spontaneous symmetry breaking of global or local symmetries, as well as a certain topological structure of the true vacuum manifold (denoted $\mathcal{M}$). In all instances, the true vacuum of a theory

must be degenerate to produce an ambiguity regarding where the symmetry breaking field (ϕ) will come to rest on scales larger than its correlation length, ξ. In other words, fields separated by $d \geq \xi$ will be completely uncorrelated.

In cosmology this correlation length is typically given by the size of causal horizon during the phase transition, $d_h \sim H(t_{pt})^{-1}$. Since the causal horizon continues increasing with time, regions of the universe with uncorrelated field configurations will be brought into contact and attempt to minimize their energy by smoothly interpolating in field space. The vacuum topology, however, can prevent this smooth interpolation, signalling defect formation. This is often referred to as the Kibble mechanism [11, 12, 13], which states that if the vacuum topology admits defects, they will inevitably form in the cosmological context.

Topological defects represent regions of space where the symmetry breaking (scalar) field is trapped in the false vacuum of a theory due to the conservation of a topological charge. This topological charge is called the winding number, n, as it quantifies the number of complete windings in field space one experiences when traversing a surface defect (domain wall), circling a line defect (cosmic string), or surrounding a point defect (monopole), in configuration space. If a phase transition takes place at an energy scale η, the interior of the defect is a region of trapped energy with that characteristic value. The following subsection describes some of the catastrophic gravitational effects of this trapped energy.

In three spatial dimensions, there are three types of (stable) defect configurations:

- **Domain Walls:** A vacuum manifold with degenerate, disconnected minima (such as a double well potential) will admit domain wall solutions. Domain wails are two dimensional regions of trapped energy that border parts of space where the scalar field has fallen into opposing vacua. Smooth interpolation in field space requires the scalar field to be raised in its potential to the false vacuum in the centre of the wall. Domain walls have no ends, they (generally) stretch through the Hubble patch at any given time. This can lead to them contributing heavily to the total energy density of the universe if they form.

- **Cosmic Strings:** These objects form when the vacuum manifold is degenerate, and not simply connected, such as in the case of a circle, S^1 (see figure 1.2). In this case, a one dimensional line defect is produced with the scalar field winding the vacuum manifold as one circles around the string in configuration space. Although extended mostly in one direction, cosmic strings possess a finite width associated with the Compton wavelength of the scalar field, $w \sim m_\phi$. Cosmic strings exist as both *long* strings, which run through the whole Hubble patch, and smaller string *loops*, which we discuss

in detail in section (1.2).

- **Monopoles:** The formation of point-like defects known as monopoles is precipitated by a phase transition whose vacuum structure is that of a sphere (S^2). In practice, any grand unified theory (GUT) that eventually leaves $U(1)_\gamma$ as a symmetry will produce monopoles [14]. Monopole solutions have radial magnetic field configurations (hence their name), where the type of magnetic field is determined via the precise symmetry breaking pattern. For the pattern $SO(3) \to U(1)_\gamma$ (as considered by 't Hooft [15] and Polyakov [16, 17]), these would be magnetic monopoles of standard electromagnetism.

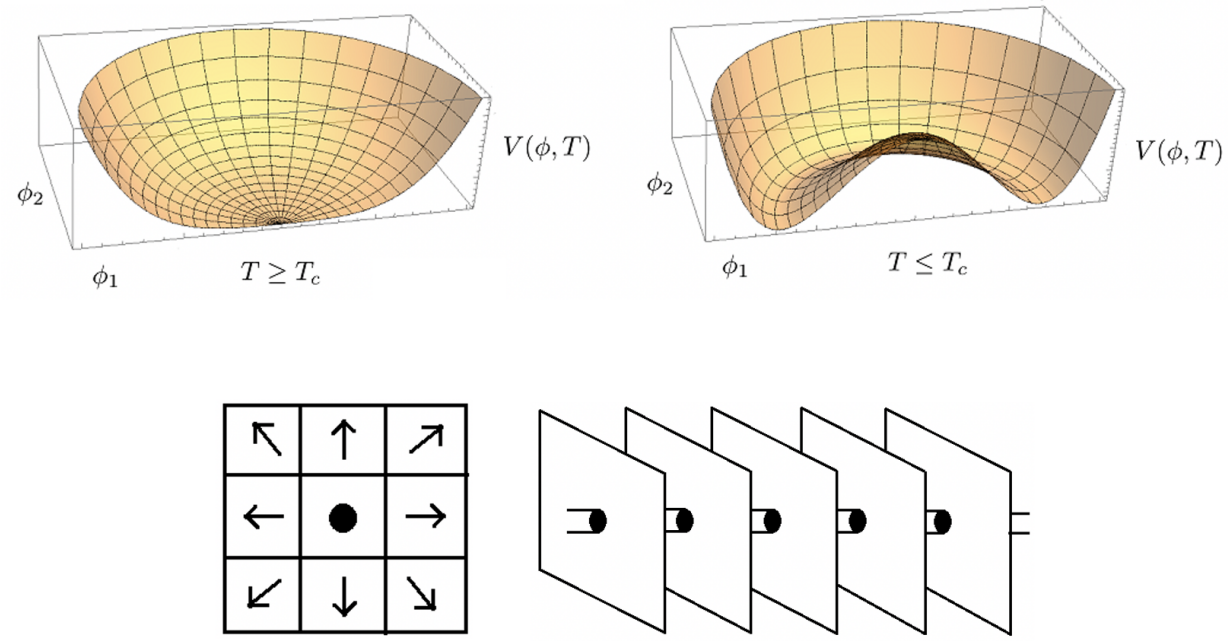

Figure 1.2: Top: The evolution of the vacuum manifold in a particular class of complex scalar field theories. Finite temperature corrections induce a degeneracy at some critical temperature T_c, giving rise to cosmic strings. Bottom: An illustration of the mapping between physical space (the squares) and field space (the arrows). If we imagine a particular spatial slice to be discretized as shown, the central square is forced to remain in the false vacuum in order to ensure the continuity of ϕ in field space. Many such slices are glued together when extending to a third dimension, with this region of trapped energy (the cosmic string) piercing them, as shown on the right.

A fourth type of defect known as a cosmic texture is also possible, although it does not possess a topologically conserved quantity and thus is unstable to collapse. Cosmic textures are discussed in more detail in section (1.3).

The breaking of a local symmetry produces a qualitatively different defect than the breaking of a global one, due to the presence of gauge fields. As we show later, the gradient energy of a local defect is screened by the presence of these gauge fields, yielding a well-defined core region. Global defects, on the other hand, have their energy density more smeared out. This can lead to divergences in their total energy which need to be regulated by physical considerations. As no gauge screening occurs for global defects, they are also capable of imparting long-range non-gravitational forces on each other, while local defects can not.

1.1.2 Defects and Cosmological Catastrophes

Our previous discussion indicates that there are three different classes of stable defects, each of which can be local (gauge) or global, that may be present in our universe. Half of these options however, are strictly constrained by cosmological considerations. While cosmic strings are relatively well behaved in the energy scaling of their network, local/global domain walls, and local monopoles can be disastrous. Here we closely follow the arguments made by Vilenkin and Shellard [2].

The domain wall problem

Domain walls, if they exist, would quickly overclose the universe [18]. Perhaps the simplest example to consider is that of a real scalar field ϕ subject to a double well potential:

$$\mathcal{L} = \frac{1}{2}(\partial_\mu \phi)^2 - \frac{\lambda}{4}(\phi^2 - \eta^2)^2 \tag{1.10}$$

The Euler-Lagrange equations yield

$$\partial_\mu \partial^\mu \phi + \lambda \phi(\phi^2 - \eta^2) = 0, \tag{1.11}$$

and by requiring the solution to be solitonic (time-independent), one finds the ϕ^4-kink solution

$$\phi(x) = \eta \tanh\left[\eta \left(\frac{\lambda}{2}\right)^{1/2} x\right], \tag{1.12}$$

which describes the evolution of ϕ across a domain wall lying at $x = 0$ in the $y - z$ plane. The width of the domain wall can be read off from the extent of the tanh function, $w \sim (\sqrt{\lambda}\eta)^{-1} \sim m_\phi^{-1}$. Kibble's mechanism implies that at least one domain wall is present in any Hubble volume at any time. The energy density inside the domain wall is $\rho_{dw} = \lambda\eta^4/4$ (given when $\phi = 0$ is in the false vacuum), and so its contributions to the energy budget of the universe is

$$\rho_{dw} = \frac{E_{dw}}{V_H} \tag{1.13}$$

$$= \sqrt{\lambda}\eta^3 t^{-1} \tag{1.14}$$

where $E_{dw} = \rho_{dw}\, w\, d_H^2$ is the total energy of the domain wall, $V_H = d_H^3$ is the volume of a Hubble patch, and $d_H = H^{-1}$ ($\sim t$ during matter or radiation domination) is the Hubble length. Comparing this with the critical density required to maintain spatial flatness, $\rho_c = 3H^2/8\pi G$ yields the troubling result

$$\frac{\rho_{dw}}{\rho_c} \approx \sqrt{\lambda}\eta \left(\frac{\eta}{M_{pl}}\right)^2 t \tag{1.15}$$

with $M_{pl} \approx 10^{18}\,\mathrm{GeV}$. This result grows with time. Inserting GUT scale parameters for the phase transition, $\eta = 10^{16}\,\mathrm{GeV}$, $\lambda \sim \mathcal{O}(1)$, and evaluating the contribution of this domain wall today $t = t_0$ shows that $\rho_{dw}/\rho_c \approx 10^{52}$, severely overclosing the universe.

It should be noted that local domain walls fare no better, as this effect is due to the trapped energy density in the defect, and not any gradient energies that could be compensated by gauge fields. Therefore, both local and global (stable) domain walls are ruled out by the data. However, metastable domain walls such as those appearing in axion theories are still allowed, provided they are short lived [19, 20].

The (local) monopole problem

If monopoles form at some time t_i the Kibble mechanism predicts an initial number density of at least

$$n_m(t_i) \geq p t_i^{-3} \qquad\qquad p \approx 0.1, \tag{1.16}$$

where p depends on the shape of the vacuum topology and we have quoted the result for $\mathcal{M} \sim S^2$ [11, 12, 13]. Local monopoles experience no long range interactions (thanks to the shielding presence of gauge fields) making it difficult for them to annihilate with each other. As a result, their comoving number density doesn't decrease by any appreciable amount [21]. Their contribution to the energy density of the universe therefore scales as

$$\rho_m = m n_m(t) \sim a(t)^{-3} \tag{1.17}$$

The critical energy density during radiation domination scales as $a(t)^{-4}$, and so if monopoles are produced at early enough times (high enough temperature scales), they can quickly come to dominate the universe.

As mentioned before, GUT scale theories which leave $U(1)_\gamma$ intact at low energies generically produce monopoles. For typical GUT scale energies ($T_{GUT} \sim 10^{16}\,\text{GeV}$), this type of monopole overproduction is in major conflict with observations and is often referred to as the *monopole problem* [22]. A popular way to get around this problem is by invoking cosmic inflation after GUT scale symmetry breaking, effectively inflating these monopoles outside of our observable universe before they can cause any harm.

Global monopoles don't possess such a problem. The mass of a monopole in typical symmetry breaking examples (such as $SO(3) \to SO(2)$) is given by

$$m \approx 4\pi\eta^2 \ell \tag{1.18}$$

where η is the scale of the phase transition and ℓ is the average separation of monopoles. Monopoles and antimonopoles therefore possess an attractive force, $F \approx 4\pi\eta^2$ that is independent of distance, in contrast to the local monopole. This allows them to find each other and annihilate rather efficiently, diluting their contribution to the energy density of the universe before it becomes relevant.

1.2 Cosmic Strings

Cosmic strings are nearly one-dimensional line defects which form when the vacuum manifold of a theory is degenerate and not simply connected (such as the circle, S^1). In this case, the scalar field ϕ winds nontrivially around excited string configurations, ensuring stability

through a conserved quantity known as the winding number. Strings that form through the breaking of a gauge symmetry are known as local, and possess a well-defined core region, outside of which their gradient energies are screened by compensating gauge fields. Global strings don't have such gauge fields present, and so their core region is less well-defined, leading to diveregences in their energies that have to be regulated by physical considerations.

If a network of strings form, they reach what is known as a *scaling solution*, in which the relative energy density ($\Omega_{cs} = \rho_{cs}/\rho_c$) in the network is roughly constant over all time. They are usually parametrized by one free parameter, μ, the mass per unit length of the string, related to the symmetry breaking scale η through $\mu \sim \eta^2$. This parameter is usually introduced in dimensionless form as $G\mu$, also known as the string tension, where G is Newton's gravitational constant. Superconducting cosmic strings can possess electromagnetic currents ($\mathcal{I}$), and are usually parametrized by both $G\mu$ and $\mathcal{I}$ when applying phenomenological constraints.

The network of strings consists of long strings (strings with curvature radius greater than the Hubble horizon), and of smaller, sub-Hubble loops which form mainly by the intersections and self-intersections of the long strings. Both types of objects source interesting phenomenology, however this thesis will focus exclusively on different effects of the cosmic string loops, which we now describe.

1.2.1 Local $U(1)$ Symmetry Breaking: A Toy Model

It is prudent to start a discussion on cosmic strings by considering one of the simplest cases: the Abelian-Higgs model. We roughly follow the discussions of [2]. The action for this model is given by a complex scalar field ϕ and a gauge field A_μ

$$\mathcal{S} = \int d^4x\sqrt{-g}\left[(\bar{D}_\mu\bar{\phi})(D^\mu\phi) - \frac{1}{4}F_{\mu\nu}F^{\mu\nu} - \frac{1}{4}\lambda(|\phi|^2 - \eta^2)^2\right], \tag{1.19}$$

where overbars represent complex conjugates, $F_{\mu\nu} = \partial_\mu A_\nu - \partial_\nu A_\mu$ is the gauge invariant field strength tensor, $D_\mu = \partial_\mu + ieA_\mu$ is the covariant derivative, e is the gauge coupling strength, and η is the symmetry breaking scale. This action is invariant under the local $U(1)$ gauge transformations, $\phi(x) \to \phi(x)e^{i\alpha(x)}$ and $A_\mu \to A_\mu + e^{-1}\partial_\mu\alpha(x)$ where $\alpha(x)$ is the local generator of the symmetry.

Spontaneous symmetry breaking gives a mass to both ϕ and A_μ. To illustrate this, we can briefly choose a gauge where ϕ is real, representing it in its vacuum state as

$$\phi = \eta + \frac{1}{\sqrt{2}}\phi_1 \tag{1.20}$$

Expanding the action around this point we find

$$\mathcal{S} = \int d^4x\sqrt{-g}\left[\frac{1}{2}(\partial_\mu\phi_1)^2 - \frac{1}{4}F_{\mu\nu}F^{\mu\nu} - \frac{1}{2}\lambda\eta^2\phi_1^2 + e^2\eta^2 A_\mu A^\mu\right] + \mathcal{S}_{int} \tag{1.21}$$

where $\mathcal{S}_{int}$ contains cubic and higher order terms in the expansion. One can identify the mass terms by inspection of the quadratic (non-derivative) part of the action. This yields a mass for the scalar field of $m_\phi = \sqrt{\lambda}\eta$ and for the gauge field $m_A = \sqrt{2}e\eta$. The typical thickness of a cosmic string is given by the Compton wavelength of the scalar field, so $w \sim \eta^{-1}$.

Computing now the Euler-Lagrange equations for the initial action (1.19) we find

$$(\partial_\mu - ieA_\mu)(\partial^\mu - ieA^\mu)\phi + \frac{\lambda}{2}\phi(|\phi|^2 - \eta^2) = 0 \tag{1.22}$$

$$\partial_\mu F^{\mu\nu} - 2ie(\bar{\phi}(\partial^\nu - ieA^\nu)\phi) = 0 \tag{1.23}$$

Solving this expression is, in general, a complicated task. To search for the existence of cosmic strings, we first envision a straight string lying on the z axis and take an ansatz for the fields which exhibits cylindrical symmetry. One such ansatz is given by Nielson and Oleson [23].

$$\phi_{NO}(\mathbf{r}) = \eta e^{in\tilde{\theta}}\, f(r), \qquad A_{NO,\theta}(\mathbf{r}) = -\eta\frac{n}{er}\alpha(r), \tag{1.24}$$

where r, θ are the cylindrical coordinates, $\tilde{\theta}$ is the phase of the scalar field in the vacuum state, and n is the winding number. We must solve the equations of motion for $f(r)$ and $\alpha(r)$ to construct our solution. We also make use of Lorentz gauge, $\partial_\mu A^\mu = 0$. Plugging this ansatz back into the equations of motion gives us a coupled second order differential equation. In the large r limit, we require that $\phi \to \eta$ and a finite energy configuration, yielding the asymptotic forms $\alpha(r \to \infty) = f(r \to \infty) = 1$. Inside the core the symmetry is restored and $\alpha(0) = f(0) = 0$. Solving the differential equations in these asymptotic limits gives (See [24] and [2] for more numerical results).

$$f(r) \sim \begin{cases} (m_A\, r)^n & r \to 0 \\ 1 & r \to \infty \end{cases} \qquad \alpha(r) \sim \begin{cases} (m_A\, r)^2 & r \to 0 \\ 1 & r \to \infty \end{cases} \tag{1.25}$$

Numerical results for $f(r)$ and $\alpha(r)$ show the existence of static, cylindrically symmetric solutions to the equations of motion which are interpreted to be cosmic strings. The energy per unit length of this configuration is given by the Hamiltonian of the system,

$$\mu = \int r dr d\theta \left[|(\nabla - ie\mathbf{A})\phi|^2 + \frac{1}{2}(\mathbf{E}^2 + \mathbf{B}^2) + V(|\phi|) \right] \tag{1.26}$$

At large r (far from the string core), the $\mathbf{E}$ and $\mathbf{B}$ fields approach 0, and $V(|\phi|) \to 0$ as $\phi \to \eta$. We can see that the gauge fields effectively screen the gradient energy of ϕ, and by employing numerical techniques, the string tension is found to be [2]

$$\mu_{local} \approx 2\pi n^2 \eta^2 g(\lambda/2e^2) \sim \eta^2 \tag{1.27}$$

where $g(\lambda/2e^2)$ is a slowly varying function of the model parameters, and is equal to 1 when $\lambda = 2e^2$. For a crude analytic approximation of this computation, one can refer to section 4.1 of [2], or the original reference [25].

Without the presence of a gauge field, one can see that the string tension will be divergent. Consider integrating this energy density from the edge of the core (a distance w from the centre) to a distance L away

$$\mu_{global} \approx 2\pi \int_w^L dr\, r \left[\frac{1}{r} \frac{\partial \phi}{\partial \theta} \right]^2 \tag{1.28}$$

$$\approx 2\pi n^2 \eta^2 \left[\frac{\partial \tilde{\theta}}{\partial \theta} \right]^2 \ln\left(\frac{L}{w} \right) \tag{1.29}$$

While this result may formally look divergent as L becomes large, in practice for a network of strings, L is usually cut off by the typical string separation distance, $L = d_{sep}$. Finally, the winding number of the string can be computed by tracing the evolution of the phase of ϕ as one traverses a physical loop around the string

$$n = \frac{1}{2\pi}\int_0^{2\pi} \frac{d\tilde{\theta}}{d\theta} d\theta \tag{1.30}$$

We now move to a slightly more complex example where cosmic strings can exhibit superconductivity.

1.2.2 Superconductivity

Cosmic strings offer a wide array of observational signatures simply due to their gravitational influences. It is also possible, however, for an electromagnetic current to run along the length of a cosmic string in certain symmetry breaking schemes. When electromagnetism ($U(1)_\gamma$) is spontaneously broken in an object, it is said to be superconducting. An object that is superconducting suppresses magnetic fields in its interior by screening it with a current that runs along its boundary. This is known as the Meissner effect.

We outline now the simplest case of cosmic string superconductivity as proposed by Witten [26] and retold by [2] who we follow here. Beginning with an action comprised of two complex scalar fields, ϕ and χ, and two gauge fields A_μ and B_μ we have

$$\mathcal{S} = \int d^4x \sqrt{g}\left[|D_\mu \chi|^2 + |D^B_\mu \phi|^2 - \frac{1}{4}F_{\mu\nu}F^{\mu\nu} - \frac{1}{4}F^B_{\mu\nu}F^{\mu\nu,B} - V(\chi,\phi)\right] \tag{1.31}$$

$$V(\chi,\phi) = \frac{1}{4}\lambda_\phi(|\phi|^2 - \eta_\phi^2)^2 + \frac{1}{4}\lambda_\chi(|\chi|^2 - \eta_\chi^2)^2 + \alpha|\phi|^2|\chi|^2 \tag{1.32}$$

where superscript B pertains to the covariant derivative (with gauge coupling g) and field strength tensor of the B_μ field. We identify the A_μ in this setup as the standard model photon with gauge coupling e. The above action enjoys both a $U(1)_\gamma$ and a $U(1)_B$ gauge invariance. The heuristic picture is as follows

- At low energies, we want the $U(1)_B$ to be broken, giving rise to cosmic strings, while the $U(1)_\gamma$ remains unbroken. We can realize this if $\lambda_\phi\eta_\phi^4 > \lambda_\chi\eta_\chi^4$. This ensures that the photon doesn't acquire a mass which would put it in severe violation of data. The vacuum is then characterized by $|\chi| = 0$ and $|\phi| = \eta_\phi$.
- Outside of the string core, the χ field has a mass term of

$$m_\chi^2 = \alpha\eta_\phi^2 - \frac{1}{2}\lambda_\chi\eta_\chi^2 \tag{1.33}$$

which must remain positive to maintain stability of the vacuum of the system. This gives another condition on the model parameters

$$\frac{2\alpha}{\lambda_\chi} \geq \left(\frac{\eta_\chi}{\eta_\phi}\right)^2 \tag{1.34}$$

- Inside the string core, however, $|\phi| \to 0$ as it creeps back up to its false vacuum. In this region, it is possible for the χ vacuum to become unstable, causing $U(1)_\gamma$ to break in the centre of the string and signifying the onset of superconductivity. For this particular model, parameters that satisfy [27, 28]

$$\frac{\alpha}{\lambda_\chi} \leq \frac{1}{4}\left(\frac{\lambda_\chi}{\lambda_\phi}\right)\left(\frac{\eta_\chi}{\eta_\phi}\right)^4 \tag{1.35}$$

  will give rise to superconductivity on the string.

In this case, cosmic strings act analogously to thin, superconducting wires, and their microstructure can give rise to strong electromagnetic signals, as we will see shortly.

While the above picture provides a proof-of-concept that cosmic strings can carry electromagnetic currents, it is by no means the only example. Since this original paper by Witten, many models have been presented using both Bose and Fermi charge carriers in Abelian and non-Abelian symmetry breaking patterns (see [29] for an early review).

With this plethora of models, it is often times inefficient to look at the fundamental equations of motion when considering the current generation on a string. As a result, approaches have been developed based on an effective action to describe the motion of charge carrier on the string [26, 30, 31]. A derivation of the effective action is beyond the scope of this thesis, and so we quote the results for the current generated on a closed string loop in an external electric field, E_0, which is of most relevance to this thesis

$$\frac{d\mathcal{I}}{dt} = \kappa e^2\left(E_0 - L\frac{d\mathcal{I}}{dt}\right) \tag{1.36}$$

$$= \kappa e^2 E_0\left(1 + 2\kappa e^2 \ln\left(\frac{R_c}{w}\right)\right)^{-1} \tag{1.37}$$

where κ is a model dependent coefficient and is typically $\mathcal{O}(1)$. The presence of an external electric field continuously builds up current on the loop, while the presence of this current induces a counteracting electric field proportional to the inductance of the string, given by

$L = 2\ln(R_c/w)$. The cutoff radius R_c is given by the minimum of either the diameter of the string loop, or the coherence length of the electric field. String loops oscillate under their own tension, and so the presence of a primordial magnetic field will look like an electric field in the rest frame of the loop.

Unfortunately, it is exceedingly difficult to track both a distribution of superconducting string loops, as well as the coherence lengths and amplitudes of magnetic and electric fields over cosmic time. Indeed, if strings form at a high symmetry breaking scale, the universe exists as a tightly coupled plasma and the evolution of current on just one string loop becomes impossible to follow. As a result, when considering phenomenological effects one makes the following simplifying assumptions:

- The string current $\mathcal{I}$ on a loop is constant over the lifetime of the loop. In this view, the loop is effectively formed with its initial current, which does not get enhanced or dissipated by interactions with subsequent electromagnetic fields.
- A string loop network has a large distribution of radii, and all loops possess the same current $\mathcal{I}$. In other words, the static current on the loops are radius independent.

The advantage of taking these assumptions is that the parameter space of superconducting string models can be neatly displayed as a function of only the string tension ($G\mu$) and the (static) current present on all loops ($\mathcal{I}$). Though these assumptions are perhaps a bit restrictive, they are standard in works computing phenomenological signals from superconducting cosmic strings. A relatively recent review of constraints in this parameter space are shown in figure 1.3, modified from a paper by Miyamoto and Nakayama [32].

1.2.3 String Substructure

The field theory example presented in section (1.2.1) provides a good introduction to the core structure of a cosmic string. However, to study the dynamics and evolution of the entire string in such a formalism is cumbersome. In the case of local symmetry breaking, the bulk properties of cosmic strings away from their core regions are largely similar between different models as gauge fields screen any long range interactions. With this in mind, we introduce the Nambu-Goto action[1]

$$\mathcal{S} = -\mu \int d^2\zeta \sqrt{-\gamma}, \tag{1.38}$$

[1]In this section of the string review we follow arguments presented in chapter 6 of [2]

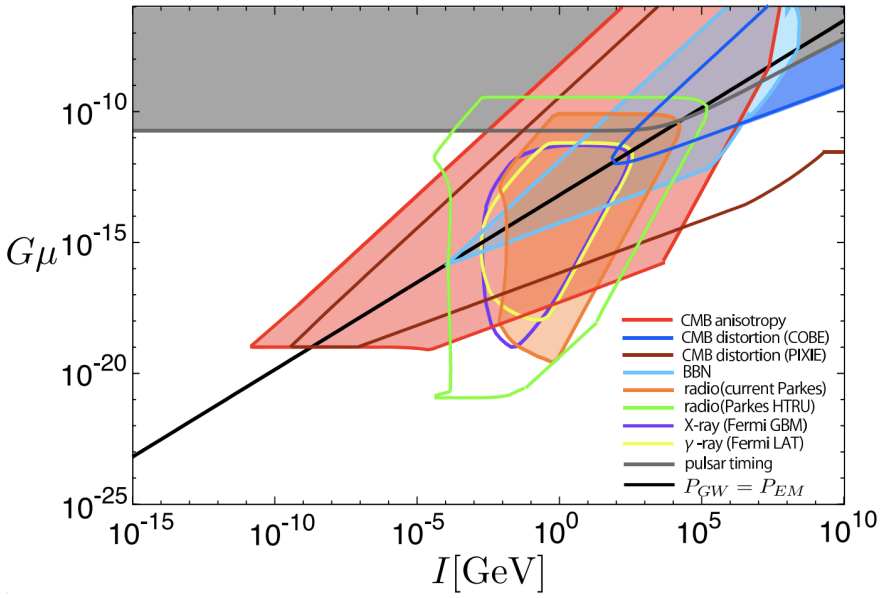

Figure 1.3: A summary of constraints relevant to superconducting cosmic strings, adapted from Miyamoto and Nakayama [32]. Shaded regions are excluded by data. Regions that are inside of a coloured contour but not shaded indicate parameter space that will be excluded by future data. Above the $P_{GW} = P_{EM}$ line, string loops decay primarily into gravitational radiation, whereas below this line, their dominant decay channel is into photons. For details on individual constraints, please see [32] and references therein.

an effective description for the qualitative features of a string, valid when the radius of curvature of the string is much larger than the width ($R \gg w$). Here, μ is the mass per unit length (string tension), ζ^0 and ζ^1 are timelike and spacelike parametrizations of the worldsheet swept out by the string. In other words, a point on the string can be labelled by the "point" ζ^1 at a given "time" ζ^0. Finally, γ is the determinant of the induced metric on the worldsheet, related to the four dimensional metric $g_{\mu\nu}$ through

$$\gamma_{ab} = g_{\mu\nu} \frac{\partial x^\mu}{\partial \zeta^a} \frac{\partial x^\nu}{\partial \zeta^b} \tag{1.39}$$

As with any action, one can vary it with respect to the metric $g_{\mu\nu}$ to determine the energy momentum tensor $T_{\mu\nu}$, and with respect to the coordinates $x^\mu(\zeta^a)$, determining the equations of motion for the string which encode its dynamical evolution. By considering the flat space limit ($g_{\mu\nu} \to \eta_{\mu\nu}$) the equations of motion for the string are

$$\frac{\partial}{\partial\zeta^a}\left(\sqrt{-\gamma}\gamma^{ab}\frac{\partial x^\mu}{\partial\zeta^b}\right)=0 \tag{1.40}$$

We have the liberty to choose any parametrizations for ζ^0 and ζ^1 as we like, and so we choose to work in *conformal* gauge by fixing two components of the metric as follows

$$\gamma_{01}=0 \qquad \longrightarrow \qquad \dot{x}_\mu x^{\mu\,\prime}=0 \tag{1.41}$$

$$\gamma_{00}+\gamma_{11}=0 \qquad \longrightarrow \qquad \dot{x}_\mu\dot{x}^\mu+x'_\mu x^{\mu\,\prime}=0 \tag{1.42}$$

where primes and dots represent derivatives with respect to ζ^1, ζ^0 respectively. There still remains a residual gauge freedom which is fixed when we identify $\zeta^0=t$, the physical time coordinate. In conformal gauge the induced metric simplifies $\gamma^{ab}=(-\gamma)^{-1/2}\eta^{ab}$ and so (1.40) becomes a wave equation:

$$\ddot{x}^\mu-x^{\mu\,\prime\prime}=0 \tag{1.43}$$

By splitting x_μ into three vector notation ($x_\mu x^\mu=x_0x^0+x_ix^i$) where $x^0=t$ our gauge conditions and string equations of motion take on suggestive forms

- The first gauge condition becomes

$$\dot{x}_\mu x^{\mu\,\prime}=0 \qquad \longrightarrow \qquad \dot{\mathbf{x}}\cdot\mathbf{x}'=0 \tag{1.44}$$

  from which we infer that $\dot{\mathbf{x}}$ is the transverse velocity of the string, since it is perpendicular to a derivative along its length. Longitudinal boosts of a string are unobservable, so $\dot{\mathbf{x}}$ represents the observable velocity of a segment of string.

- The other gauge condition yields

$$\dot{x}_\mu\dot{x}^\mu+x'_\mu x^{\mu\,\prime}=0 \qquad \longrightarrow \qquad \dot{\mathbf{x}}^2+\mathbf{x}^{2\,\prime}=1 \tag{1.45}$$

  which is a statement regarding the invariant energy of the string. Intuitively, the total energy of a string is given by $E=\mu\int d\zeta^1$. Rearranging this condition to solve for $d\zeta^1$

we can see that

$$E = \mu \int (1 - \dot{\mathbf{x}}^2)^{-1/2} d|\mathbf{x}| \tag{1.46}$$

Where $(1 - \dot{\mathbf{x}}^2)^{-1/2}$ is the relativistic gamma factor for the loop.

- The wave equation keeps a similar form

$$\ddot{x}^\mu - x^{\mu\,\prime\prime} = 0 \qquad \longrightarrow \qquad \ddot{\mathbf{x}} - \mathbf{x}'' = 0 \tag{1.47}$$

The local curvature radius of a string is given by $R = |d^2x/(d\zeta^1)^2|^{-1}$ (in the rest frame of the string, $\dot{\mathbf{x}} = 0$). Therefore, the wave equation looks like

$$\ddot{\mathbf{x}} = R^{-1} \tag{1.48}$$

This implies that if a part of a string is curved, it will attempt to straighten.

We now focus specifically on the case of cosmic string loops, closed objects with total energy $E = \beta\mu R$, where R is the radius of the loop, and β is a parameter that sets the circularity of the loop (with a perfectly circular loop having $\beta = 2\pi$). When long (Hubble length) strings intersect and self-intersect, it is often energetically favourable for a loop to detach and undergo an independent evolution. The formation of a network of such loops will be discussed in section (1.2.5).

String loop oscillations

Once a loop is formed, it will begin to oscillate under its own tension. If we assume perfectly circular loops, the period can be inferred by examining the invariant energy of a loop of radius $R(t)$

$$E(R) = E_0 = \beta\mu R(t)\gamma(R(t)) \tag{1.49}$$

where $\gamma(R(t)) = (1-\dot{R})^{-1/2}$ is the relativistic gamma factor. Solving the resulting differential equation gives the evolution of the loop radius

$$R(t) = R_0 \cos(t/R_0) \tag{1.50}$$

Where $R_0 = E_0/\beta\mu$, is the radius of the loop at its maximal extent. The period of a loop oscillation is thus $T = R_0$.

The full wave equation (1.47) can be solved in terms of objects known as left-movers and right-movers, excitations that travel along the string in opposite directions. It was shown early on [33] that once per oscillation time, points on the string can reach the speed of light, $\dot{\mathbf{x}}(t, \zeta^1) = 1$. The interpretation of these objects is that they are regions of the string that have a cusp-like structure, with the string effectively doubling back on itself. This structure can liberate energy from the string loop, allowing it to slowly decay as it oscillates.

Interconnections of strings can also give rise to substructure on a loop known as a *kink*, where the left and write movers have discontinuous derivatives, and the string possess a sharp edge. Kinks and kink-kink collisions may also cause the string to lose energy, however, they are typically a subdominant decay channel when compared with cusps. As a result, we focus solely on cosmic string cusp decays.

Gravitational waves from cosmic string cusps

The liberation of energy from a cosmic string cusp is relatively straightforward to understand heuristically. Consider a cosmic string loop with a particular winding orientation (either clockwise or anticlockwise around the string core). In the region where a cusp forms, the string has essentially doubled back on itself, creating an overlap region as illustrated in figure 1.4. The only difference between a cosmic string, and a cosmic antistring, is the direction of this winding orientation. By tracing this winding up to the overlap region, we see that the cusp itself locally looks like a string-antistring configuration, and will thus annihilate.

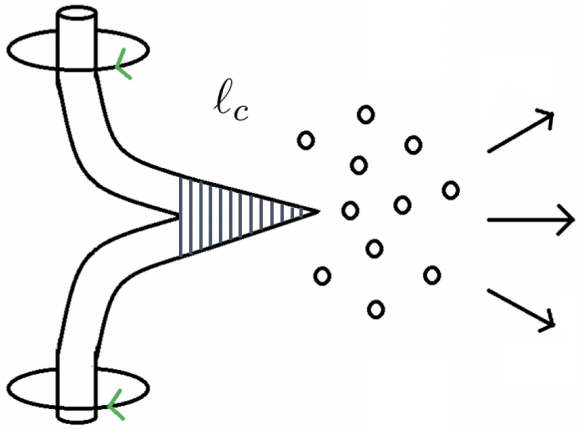

Figure 1.4: A schematic representation of a cusp annihilation event. The dashed region is the cusp, which will smooth out after annihilation releasing gauge and scalar fields in a tight beam. The arrows represent a particular winding orientation for the string.

This annihilation produces a small number of gauge and scalar fields that were present in the previously unbroken state of the universe, whose lifetimes are very short for high scale symmetry breaking, $\tau \sim m^{-1} \sim \eta^{-1}$. After the annihilation, the cusp is smoothed. In contrast to this direct particle creation, the ultrarelativistic motion of substructure on a loop (the cusp itself) is responsible for sourcing powerful bursts of gravitational waves, whose magnitude we estimate now.

One can get the proper parametric dependence on the energy loss to gravitational waves by the usual quadrupole formula[2], which for an oscillating loop yields

$$P_{GW} \sim -G \left\langle \frac{d^3 J_{ij}}{dt^3} \frac{d^3 J^{ij}}{dt^3} \right\rangle \tag{1.51}$$

$$\sim -G M_{loop}^2 R^4 \frac{1}{T^6} \tag{1.52}$$

$$\sim -G\mu^2 \tag{1.53}$$

where J_{ij} is the reduced quadrupole moment of the system, $M_{loop} = \beta\mu R$ is the total mass of the loop, R is the radius, and $T \sim R$ is the frequency of oscillation. A more precise calculation taking into account the formation of cusps in the presence of precise loop trajectories was given in [35] and [36], where the power radiated by a single string loop in gravitational waves was determined to be

$$P_{GW} = \Gamma_{GW} G\mu^2, \tag{1.54}$$

with $\Gamma_{GW} \sim \mathcal{O}(100)$ being a dimensionless constant determined by numerics. A distribution of string loops, therefore, is capable of producing a stochastic background of gravitational waves. Indeed, constraints from pulsar timing arrays provide some of the most stringent bounds on $G\mu$. We discuss this further in section (1.2.5).

Particle production from cosmic string cusps

If cosmic strings are formed through a symmetry breaking pattern that eventually descends to our symmetry group through a pattern such as

[2] A nice derivation of this can be found in Carroll [34]

$$G \to H \to \cdots \to SU_C(3) \times SU_L(2) \times U(1)_h \to SU_C(3) \times U(1)_\gamma, \tag{1.55}$$

the scalar and gauge bosons will naturally decay into some combination of their standard model counterparts. Unlike gravitational waves, standard model gauge boson production comes from the direct decay of higher energy particles and is thus proportional to the (invariant) size of the cusp region on a loop. Taking the proper Lorentz contractions into account, Blanco-Pillado and Olum [37] found that this cusp length is given by

$$\ell_c = w^{1/2} R^{1/2}. \tag{1.56}$$

with $w \sim \eta^{-1/2}$ being the width of the string. In addition, the authors also considered the number of particles produced during a cusp annihilation. As mentioned above, the typical mass of a scalar field inside the string is $m_\phi \sim \eta \sim \mu^{1/2}$, and so by taking into account the boost factor of the produced particles ($\gamma_\phi \sim \sqrt{R/w}$) they find

$$N_\phi \sim \frac{E_c}{\gamma_\phi m_\phi} \tag{1.57}$$

$$\sim \frac{\mu \ell_c}{\mu^{1/2}\sqrt{R/w}} \tag{1.58}$$

$$\sim 1 \tag{1.59}$$

One usually assumes that symmetry breaking happens in such a way that these ϕ fields decay equally into photons, $W^\pm/Z$, and gluons (at low energies). For the $U(1)_\gamma$ and $SU(2)$ gauge bosons, only a small number of particles are produced which makes their detection prospects slim. However, the production of gluons will lead to hadronic showers which may be observable through the decay of neutral and charged pions. The QCD multiplicity function provides an empirical description of the spectrum of particles present in a hadronic shower. The number of photons per unit energy produced by the decays of neutral pions at a cosmic string cusp is given by [38]

$$\frac{dN_\gamma}{dE} = \frac{15}{16}\frac{\mu\ell_c}{Q_f^2}\left[\frac{16}{3} - 2\left(\frac{E}{Q_f}\right)^{1/2} - 4\left(\frac{E}{Q_f}\right)^{-1/2} + \frac{2}{3}\left(\frac{E}{Q_f}\right)^{-3/2}\right] \tag{1.60}$$

where Q_f is the initial energy of the QCD jet. Since this spectrum is sourced via decaying pions, it is only valid for $m_{\pi^0} \leq E \leq Q_f$. While this makes it useful for computing gamma ray (and with slight modifications, neutrino) fluxes [39], it cannot be used to make radio photon predictions (which have $E_\gamma \ll E_{\pi^0}$). In astrophysical environments, however, methods developed in [40] allow for the computation of a low energy spectrum sourced by the Bremsstrahlung and synchrotron emission of charged pions in an ionized environment.

Photons from (superconducting) cosmic string cusps

Strings which are superconducting, on the other hand, are capable of sourcing a strong burst of photons over a wide range of frequencies (including radio frequencies) near their cusps. A charged loop which undergoes oscillations will emit dipole radiation, though the fact that the oscillations are relativistic throw into question the validity of such a simple assumption.

The first detailed computation was performed by Vilenkin and Vachaspati [41] who used a saddle point method to determine the electromagnetic radiation emitted near a cusp region on a cosmic string. The result of their calculation was that in the vicinity of a cusp, photons are emitted with a spectrum given by

$$\frac{dP_{em}}{d\omega} = \beta^{1/3}\mathcal{I}^2 R^{1/3}\omega^{-2/3} \tag{1.61}$$

Where $\beta \approx \mathcal{O}(10)$ encodes the shape factor of the loop, $\mathcal{I}$ is the (constant) current on the loop, R is the radius of the loop, and ω the frequency of emitted radiation. They also found that the emitted radiation is tightly beamed, being emitted in a solid angle of order $\Omega \sim (\beta\omega R)^{-2/3}$.

Interestingly, the total power emitted by a cusp is dominated by the highest frequencies of photons emitted, $P_{em} \sim \omega_{max}^{1/3}$. To estimate the total power in a cusp event, one therefore needs to determine a maximum cutoff frequency. A natural way to determine this is to integrate (1.61) over frequencies and average over a loop oscillation to determine the mean energy released per period T

$$\langle E_{em} \rangle_T = \beta^{4/3} \mathcal{I}^2 R^{4/3} \omega_{max}^{1/3}. \tag{1.62}$$

This energy should be compared with the total energy available in the cusp region. The size of the cusp is modified in the case of superconducting strings, $\ell_c^{SC} \sim \beta^{2/3} R^{2/3} \omega_{max}^{1/3}$ and so the requirement that $\langle E_{em} \rangle_T \leq \mu \ell_c^{SC}$ yields

$$\omega_{max} = \beta^{-1} \mathcal{I}^{-3} \mu^{3/2} R^{-1}. \tag{1.63}$$

Therefore the total power radiated in photons from a superconducting cosmic string cusp is

$$P_{em} = \Gamma_{em} \mathcal{I} \sqrt{\mu}, \tag{1.64}$$

where $\Gamma_{em} \approx \mathcal{O}(10)$ is determined by a full numerical solution. In some regions of parameter space for superconducting strings, this energy loss mechanism will be dominant over gravitational wave production, leading to different phenomenology. Summarizing, superconducting string loops can source a powerful burst of beamed radiation, with spectral shape given by (1.61), valid for any frequencies satisfying $\omega \leq \omega_{max}$. The photon production from kinks and kink-kink collisions was considered in [42], and found to be subdominant to that of cusps.

1.2.4 Accretion onto Cosmic String Loops

Cosmic string loops are localized regions of trapped energy density, allowing them to gravitate and accrete matter, acting as early seeds of structure formation. In the days before detailed observations of the CMB power spectrum, a distribution of these string loop seeds were considered a viable alternative to seeds sourced by quantum fluctuations of the inflaton. However, it is now known that the role of string loops on structure formation must be subdominant to a stronger, gaussian component.

Even though the large scale structure of the universe cannot be described solely by cosmic strings, their existence in the universe after matter radiation equality will lead to early non-linearities in the density field, and could precipitate the formation of objects such as ultracompact minihalos (UCMHs) [43] or even black holes [44, 45, 46]. Roughly speaking, a pocket of the universe is said to be non-linear when it is no longer well described by linear

perturbation theory. This happens when the density contrast, $\delta(\mathbf{x}) = \delta\rho(\mathbf{x})/\rho_c$ exceeds 1, where $\delta\rho$ is the energy density at a localized point $\mathbf{x}$, and ρ_c is the critical energy density, given by the first Friedmann equation as

$$\rho_c(z) = \frac{3H^2(z)}{8\pi G}. \tag{1.65}$$

In physical coordinates, a spherical shell of matter surrounding an overdensity (for example, around a string loop) has its dynamics determined by two competing effects. The gravitational force of the overdensity will act inwards on the shell, causing it to fall towards the centre. This is counteracted by the expansion of the universe, which resists the gravitational collapse. We now study the collapse of spherical shells of matter around a cosmic string loop in a formalism known as the Zel'dovich approximation [47].

For simplicity we consider only gravitational interactions, and denote the physical distance of a spherical shell of matter from the centre of the overdensity as

$$h(q,t) = a(t)(q - \psi(q,t)) \tag{1.66}$$

where q is the initial comoving distance of the shell, and $\psi(q,t)$ denotes a correction to the trajectory of the shell in the presence of a string loop. Initially, shells are expanding outwards with the Hubble flow. A shell is said to have "turned around" when $\dot{h}(q,t) = 0$, indicating that it is no longer receding due to expansion, and will now fall into the overdensity. See figure 1.5 for a heuristic picture of this procedure.

Importantly, for a given loop radius R_0 the physical distance, h of the matter shell can either be inside ($h < R_0$) or outside ($h > R_0$) the loop. Mass shells with $h > R_0$ see the loop as a point particle, with all of its mass concentrated at the origin, whereas shells that are inside the radius see only a fraction of the total loop mass. We describe both cases noting that the computation for $h < R_0$ is original work.

The mass shell evolves according to the Newtonian potential as

$$\ddot{h} = -\frac{\partial\Phi}{\partial h} \tag{1.67}$$

$$\nabla_h^2\Phi = 4\pi G(\rho_{bg} + \rho_{loop}) \tag{1.68}$$

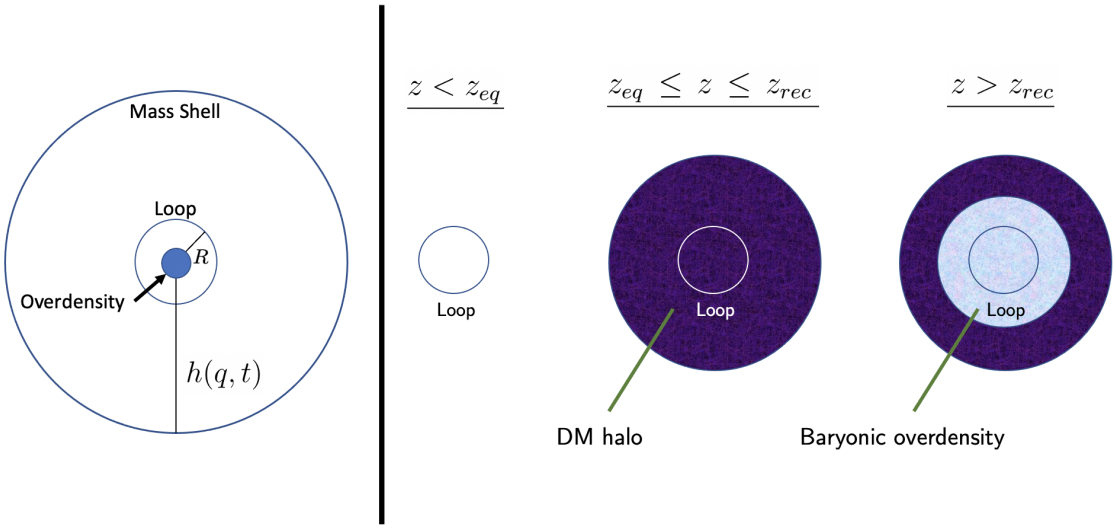

Figure 1.5: Left: An illustration of the scales at play in the Zel'dovich approximation. As an example, we show a mass shell originating outside the loop radius, however, mass shells inside the loop will still be attracted towards the centre, at a slower rate. Right: The evolution of a string-seeded overdensity with redshift. A dark matter halo forms around the loop after matter-radiation equality, followed by baryonic collapse after recombination. The total mass of the overdensity at these redshifts has been roughly estimated in (1.92).

where in the second line we note that the potential is determined through the Poisson equation in the presence of background energy density and the loop itself. The mass element dM inside a physical volume dh^3 should be conserved in comoving coordinates, giving the useful relation

$$\rho_{bg}(h,t)dh^3 = a^3(t)\rho_c(t)dq^3 \tag{1.69}$$

which implies

$$\rho_{bg}(h,t) = a^3(t)\rho_c(t)\frac{q^2}{h^2}\frac{\partial q}{\partial h} \tag{1.70}$$

$$\approx \rho_c(t)\left(1 + 2\frac{\psi}{q} + \frac{\partial\psi}{\partial q}\right) \tag{1.71}$$

at linear order in the perturbation, ψ. The Newtonian potential consists of two terms (Φ_{bg} and Φ_{loop}) which can be determined by different methods. The determination of the background component is relatively straightforward. Noting spherical symmetry, one needs

to solve

$$\frac{1}{h^2}\frac{\partial}{\partial h}\left(h^2\frac{\partial \Phi_{bg}}{\partial h}\right) = 4\pi G\rho_c(t)\left(1+2\frac{\psi}{q}+\frac{\partial\psi}{\partial q}\right) \tag{1.72}$$

for the derivative, $\partial\Phi_{bg}/\partial h$ in order to determine the background dynamics of the shell. At linear order, the computation proceeds as

$$\frac{\partial \Phi_{bg}}{\partial h} = \frac{1}{h^2}\int dh\, 4\pi G\rho_c(t)h^2\left(1+2\frac{\psi}{q}+\frac{\partial\psi}{\partial q}\right) \tag{1.73}$$

$$\approx \frac{4\pi aG\rho_c(t)}{(q-\psi)^2}\int dq\, q^2 \tag{1.74}$$

$$\approx \frac{4\pi aG\rho_c(t)}{3}(q+2\psi). \tag{1.75}$$

The potential from the string loop is slightly more complicated. Mass shells with $h > R_0$ (where R_0 is the radius of a string loop) will feel the full potential of the loop, and we can model the loop energy density as a delta function source located at the origin, $h = 0$. However, for $h < R_0$, the mass distribution of the loop is smeared out, due to its rapid oscillations. Therefore, shells inthis regime effectively see only a fraction of the total loop mass. To model this effect, consider the time averaged energy density of a loop oscillating with period T,

$$\langle\rho(r)\rangle_T = \frac{2}{\pi R_0}\int_0^{\pi R_0/2} dt\,\rho(r,t), \tag{1.76}$$

where $\langle\rho(r)\rangle_T$ is the average energy density at some $r < R_0$. The full energy density of an oscillating loop can be written as

$$\rho(r,t) = \frac{\beta\mu R_0}{4\pi r^2}\delta(r-R(t)) \tag{1.77}$$

$$R(t) = R_0\cos\left(\frac{t}{R_0}\right) \tag{1.78}$$

where $R(t)$ was derived earlier in equation (1.50) by considering the invariant energy of a loop. The time average is over a quarter period as this is the amount of time it takes a

loop to contract to a point (in a further quarter period, the loop expands back to R_0 in an inverted configuration). Solving this yields

$$\langle \rho(r) \rangle_T = \frac{\beta\mu}{2\pi^2 r^2} \left[1 - \left(\frac{r}{R_0} \right)^2 \right]^{-1/2} \tag{1.79}$$

The average energy (or equivalently, the effective mass) of the string loop inside a radius $h < R_0$ is then

$$E(h \leq R_0) = \int_0^R dr\, 4\pi r^2 \langle \rho(r) \rangle_T \tag{1.80}$$

$$= \frac{2}{\pi} \beta\mu R_0 \arcsin\left(\frac{h}{R_0} \right) \tag{1.81}$$

The total mass of the loop is simply $M_{loop} = \beta\mu R_0$ and so we see the effect of these oscillations is to introduce an arcsin modulation. The derivative of the potential of the loop can be written as a piecewise function, noting that $\Phi_{loop}(h) = -GM_{loop}^{eff}/h$, which gives

$$\frac{\partial \Phi_{loop}}{\partial h} = \begin{cases} \beta G\mu \frac{R_0}{h^2} & (h \geq R_0) \\ \beta G\mu \frac{R_0}{h^2} \left[\frac{2}{\pi} \arcsin\left(\frac{h}{R_0} \right) \right] & (h < R_0) \end{cases} \tag{1.82}$$

Finally, we are ready to determine the trajectory of a mass shell. Expanding (1.67) with (1.75) and (1.82) yields the equation of motion for ψ,

$$\ddot{\psi} + \frac{4}{3t}\dot{\psi} - \frac{2}{3t^2}\psi = \frac{\partial \Phi_{loop}}{\partial h} \tag{1.83}$$

where we restrict ourselves to the matter dominated epoch and normalize $a(t_0) = 1$ so that $a(t) = (t/t_0)^{2/3}$. The effects of ρ_{bg} are included on the left hand side of this expression. The homogeneous part of this differential equation has a familiar solution in this epoch

$$\psi_h = A \left(\frac{t}{t_i} \right)^{2/3} + B \left(\frac{t}{t_i} \right)^{-1}. \tag{1.84}$$

Here, A and B are constants to be solved for after determining a particular solution ψ_p and applying initial conditions, and t_i is the initial collapse time. In the case of no string loop, overdensities grow as $t^{2/3}$, a well known result.

There are three distinct phases to the evolution of a particular mass shell. First, the shell is expanding with the Hubble flow. At some turnaround time, t_{ta}, the mass shell decouples from the Hubble flow, and begins falling inwards towards the overdensity. This turnaround time is computed by finding when $\dot{h} = 0$. Once a shell has turned around, it virializes in what is known as a "free-fall" time, where $t_{ff} \sim H^{-1}$.

We are most interested in knowing the turnaround time, t_{ta} of a particular mass shell. This leaves us with three distinct regimes in which to solve the differential equation: shells which originate and turn around inside the loop ($h < R_0$), shells which originate and turn around outside the loop ($h > R_0$), and shells which originate inside ($h < R_0$) but turn around outside the loop ($h > R_0$).

- **Shells originating and turning around inside the loop**: In this instance, we solve (1.83) with the initial conditions $\psi(t_i) = \dot{\psi}(t_i) = 0$. The particular solution (in all instances) is readily found by method of variation of parameters, after we employ the approximation arcsin(x) $\approx x$. This approximation is good for shells close to the centre of the string loop, but becomes gradually worse as $h \approx R_0$. However, even at $h = R_0$ the error is small, roughly $\pi/2$. Therefore, this approximation will not significantly disturb an order of magnitude estimate such as this. The full solution ($\psi = \psi_h + \psi_p$) is then

$$\psi(t) \approx \frac{6}{5\pi}\frac{\beta G\mu t_i^2}{q}\left(\frac{t_0}{t_i}\right)^{4/3}\left[\frac{3}{5}\left(\frac{t}{t_i}\right)^{-1} - \frac{3}{5}\left(\frac{t}{t_i}\right)^{2/3} + \left(\frac{t}{t_i}\right)^{2/3}\ln\left(\frac{t}{t_i}\right)\right] \tag{1.85}$$

  For a given comoving scale q, one can define a time t_q from the requirement that $h < R_0$ for which this solution is valid. We find the regime of validity to be $t < t_q = t_0\left(\frac{R_0}{q}\right)^{3/2}$.

- **Shells originating and turning around outside the loop**: Here, the string loop always looks like a point mass. This solution is a standard result, also computed in [2, 48]. It is

$$\psi(t) = \frac{3}{2}\frac{\beta G\mu R_0 t_i^2}{q^2}\left(\frac{t_0}{t_i}\right)^2\left[\frac{3}{5}\left(\frac{t}{t_i}\right)^{2/3} + \frac{2}{5}\left(\frac{t}{t_i}\right)^{-1} - 1\right] \tag{1.86}$$

In contrast to the previous case, this is valid for $t > t_q = t_0\left(\frac{R_0}{q}\right)^{3/2}$.

- **Originating inside, but turning around outside the loop**: For this case, we start with the solution (1.85) and evolve it forward until t_q, the time at which the shell is at R_0. We then solve the differential equation (1.83) again using new initial conditions from this first stage of evolution. These initial conditions are

$$\psi(t_q) = \frac{6}{5\pi}\frac{\beta G\mu t_0^2 R_0}{q^2} \qquad \dot{\psi}(t_q) = \frac{2}{3}\frac{6}{5\pi}\frac{\beta G\mu t_0}{q^{1/2}R_0^{1/2}} \tag{1.87}$$

The perturbation in this regime looks like

$$\psi(t) \approx \frac{\beta G\mu t_0^2}{q}\left[\left(\frac{6}{5\pi} + \frac{9}{10}\right)\left(\frac{t}{t_0}\right)^{2/3} + \frac{3}{5}\left(\frac{R_0}{q}\right)^{7/2}\left(\frac{t}{t_0}\right)^{-1} - \frac{3}{2}\left(\frac{R_0}{q}\right)\right] \tag{1.88}$$

As an example, lets consider the growth of a dark matter halo when we are exclusively in the second regime. Here, one can find the comoving non-linear radius through

$$\dot{h} = 0 \qquad \longrightarrow \qquad q_{nl} = 2\psi(t_{ta}) \tag{1.89}$$

Once we have this, we can relate it (at zeroth order) to a physical radius $h_{nl} = a(t)q_{nl}$. Once more making use of a perfectly spherical collapse, one can compute the total mass that has gone non-linear at some time t through

$$M_{nl} \approx \frac{4}{3}\pi h_{nl}^3\rho_c \tag{1.90}$$

$$\approx \frac{2}{5}\beta\mu R_0\left(\frac{t}{t_i}\right)^{2/3} \tag{1.91}$$

When we consider the dominant piece of (1.86) at late tims. All mass shells with $h < h_{nl}$ will have already gone non-linear at time t_{nl} and so are bound to a halo which forms around the string loop. If we set the initial collapse time to $t_i = t_{eq}$ which will be the case for dark matter particles, we can see how the mass grows with redshift

$$M_{nl} \approx \beta \mu R_0 \left(\frac{1 + z_{eq}}{1 + z} \right) \tag{1.92}$$

It is of course possible in principle to compute M_{nl} for the other regimes, but (1.92) is a good approximation for the late time growth of a halo of matter around a string loop.

1.2.5 Production of a Loop Network

In this section, we expand on our previously alluded to claim that a distribution of small, sub-Hubble loops can be produced by a long string network. As the long strings evolve, they will undergo intersections with other long strings, as well they can experience self-intersections. In doing so, it is energetically favourable to "chop-off" segments of the long strings into smaller, sub-Hubble loops (see figure 1.6 below, as well as chapter 4 of [2]).

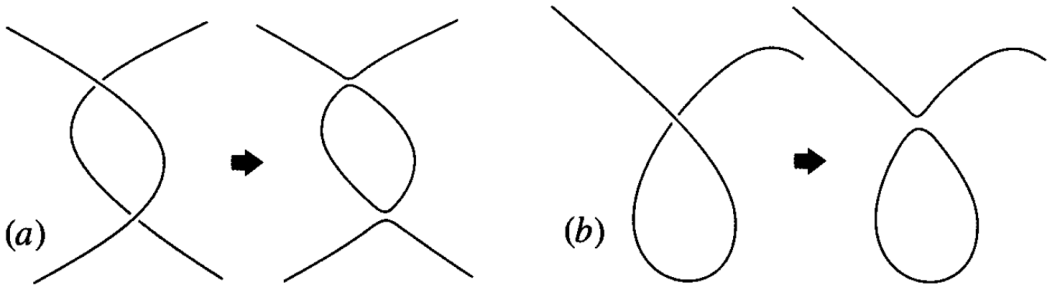

Figure 1.6: A heuristic picture of loop formation. Left: Loop-loop intersections. Right: Self-intersection of a single loop. Figure adapted from [2]

The typical size of a loop at its formation is given by a fraction of the Hubble radius, $d_H \sim t$

$$R_f \approx \alpha t_f \tag{1.93}$$

where α is the known as the "chopping" coefficient ($\alpha \sim \mathcal{O}(10^{-1})$). Over time, this chopping procedure seeds a distribution of cosmic string loops which evolve independently of the long

strings, and may source a wide variety of astrophysical and cosmological phenomena.

By the Kibble mechanism, there exists a few long strings per Hubble volume. The energy density in these strings at any time is roughly $\rho_\infty \sim \mu/d_H^2$. As the universe expands, $\rho_\infty \sim a^{-2}$, while the energy density in matter or radiation redshifts like a^{-3} and a^{-4} respectively. In order to not overclose the universe, long strings require an additional way to lose energy, which they thankfully possess through their fragmentation into loops. We now discuss how energy leaves the network through the decay of string loops.

Energy dissipation in loops

Once produced, a loop will oscillate and lose its energy to gravitational radiation, or in the case of high current superconducting strings, through photon emission. This causes the loops to shrink and subsequently decay away, liberating energy that was originally trapped in the cosmic string network. The gravitational power radiated by a loop was given in (1.51), but we restate it here for completeness

$$P_{GW} = \Gamma_{GW} G\mu^2, \qquad \Gamma_{GW} \sim \mathcal{O}(100) \tag{1.94}$$

Most of the power is produced near the cusp regions. By recalling that $E = \beta\mu R_0$ for a loop of radius R_0, one can track the evolution of the maximal radius of a loop over time due to this energy release (using $R_0(t_f) = R_f$ as the initial condition)

$$R_0(t) = R_f - \gamma_{GW} G\mu(t - t_f), \qquad \gamma_{GW} = \Gamma_{GW}/\beta \sim \mathcal{O}(10) \tag{1.95}$$

The gravitational radiation starts to affect the loop size only at times when $t \sim (\alpha/\gamma_{GW} G\mu)t_f$. For typical values of the parameters, $\alpha \sim 0.1$, $\gamma_{GW} \sim 10$, $G\mu \sim 10^{-10}$, this occurs only at late times when $t \gg t_f$. As a result, one often defines a gravitational cutoff radius,

$$R_c^{GW} = \gamma_{GW} G\mu t, \tag{1.96}$$

where loops with $R < R_c^{GW}$ decay within one Hubble time and disappear from the network. Similarly, one can look at the rate of energy loss from photon production on superconducting strings. For $P_{EM} = \Gamma_{EM}\mathcal{I}\sqrt{\mu}$, we can find an electromagnetic cutoff radius of

$$R_c^{EM} = \kappa_{EM} \mathcal{I} \mu^{-1/2} t, \qquad \kappa_{EM} = \Gamma_{EM}/\beta \sim \mathcal{O}(1) \tag{1.97}$$

In the above we make the simplifying assumption that all loops possess the same steady state current $\mathcal{I}$ as is typical in the literature. To determine whether a current carrying loop decays primarily through photon emission or gravitational waves, we can equate the two cutoff radii to determine a critical current,

$$\mathcal{I}_c = \frac{\gamma_{GW}}{\kappa_{EM}} M_{pl} \left(G\mu\right)^{3/2} \tag{1.98}$$

For a given string tension $G\mu$, loops with $\mathcal{I} > \mathcal{I}_c$ will decay primarily into photons with a cutoff radius set by R_c^{EM}, while if $\mathcal{I} < \mathcal{I}_c$, the energy is produced mainly in gravitational waves and the loop distribution will obey a lower cutoff given by R_c^{GW}.

We should also mention that particle production from cusp decay will also induce energy losses in a string loop. However, energy loss from this mechanism is highly subdominant for $G\mu \geq 10^{-18}$ [49]. Most string phenomenology scales with the string tension, and so string loops with a value of $G\mu$ this low do not generally source interesting signals, and so we neglect this effect in what follows.

Loop distribution functions

At any given time, t, a loop distribution is populated by long string intersections and self-intersections. This distribution has well defined maximum and minimum radii,

$$R_c^{GW/EM}(t) \leq R \leq R_f(t) \tag{1.99}$$

It has been shown using both analytic arguments [4, 50] and numerical simulations [51, 52, 53, 54, 55] that the string network achieves a "scaling" solution, in which the comoving energy density in the strings is constant over all time. In such a "one-scale" model, the properties of the network are determined solely by the horizon size. In other words, the number of loops in some comoving fraction of a horizon volume will be constant over time.

The precise distribution of cosmic string loops has been calculated by utilising simulations [53, 54] to infer the loop production rate. The results of this semi-analytic work are [55]

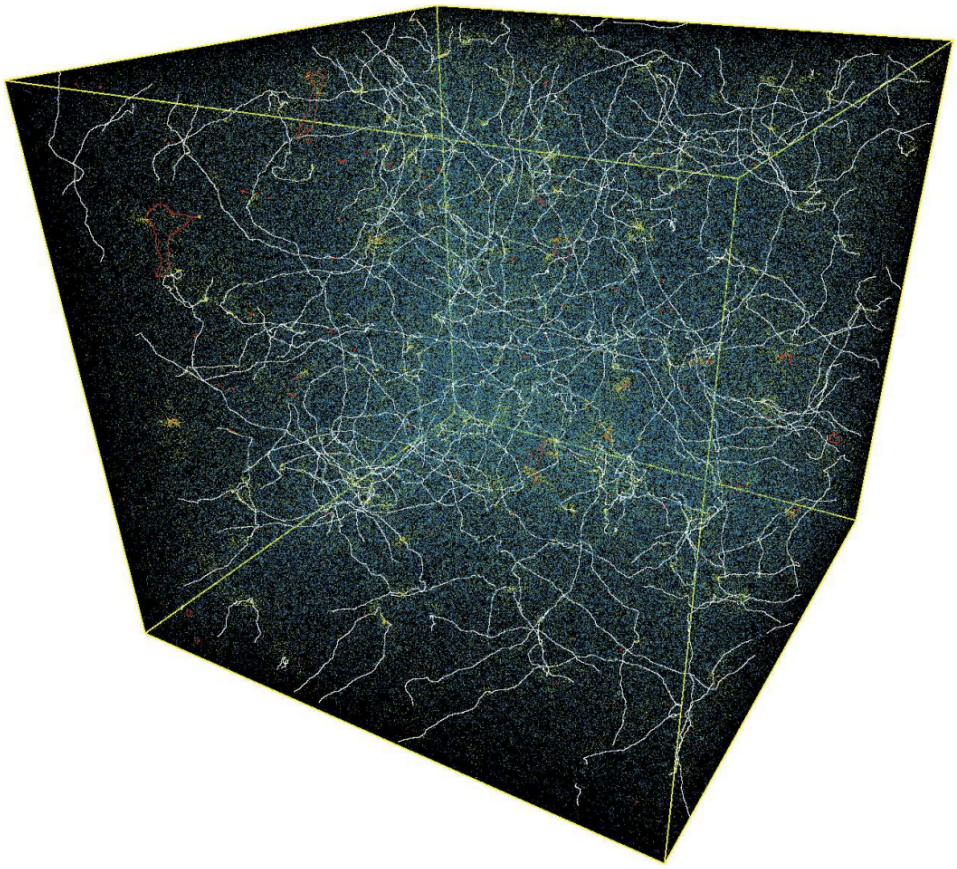

Figure 1.7: A recent simulation of a network of cosmic strings in the Nambu-Goto approximation (neglecting the finite width of the strings). One can see a number of long strings running through this Hubble patch, as well as a blue "fog", which indicates an abundance of small loops. Figure adapted from da Cunha et al. [56].

$$n_r(t,R) \approx \frac{0.18}{t^{3/2}(\beta R + \Gamma_{GW} G\mu t)^{5/2}} \qquad (t_f < t_{eq} \text{ and } t < t_{eq}) \tag{1.100}$$

$$n_m(t,R) \approx \frac{0.27 - 0.45(\beta R/t)^{0.31}}{t^2(\beta R + \Gamma_{GW} G\mu t)^2} \qquad (t_f > t_{eq} \text{ and } t > t_{eq}) \tag{1.101}$$

$$n_r(t > t_{eq},R) \approx \frac{0.18 t_{eq}^{1/2}}{t^2(\beta R + \Gamma_{GW} G\mu t)^{5/2}} \qquad (t_f < t_{eq} \text{ and } t > t_{eq}) \tag{1.102}$$

Here, $n(t,R)$ represents the number density of loops (in physical coordinates), per unit radius. The last expression represents loops which were formed in the radiation era, but persist into the matter domination epoch.

For the work presented in this thesis, we make consistent use of the "sudden decay"

approximation. That is, we neglect the slow shrinking of a loop due to the emission of gravitational (or electromagnetic) radiation over its lifetime. In other words, a loop is formed with radius $R_f(t_f)$ at some time t_f, and maintains this radius until $R_c^{GW/EM}(t) = R_f(t_f)$, at which point it decays away within a Hubble time. Doing this allows a slight simplification to the distribution for sufficiently small ($\beta R \ll t$) loops

$$n(t,R) \approx \begin{cases} 0.18\beta^{-5/2}t^{-3/2}R^{-5/2} & (t_f < t_{eq} \text{ and } t < t_{eq}) \\ 0.27\beta^{-2}t^{-2}R^{-2} & (t_f > t_{eq} \text{ and } t > t_{eq}) \\ 0.18\beta^{-5/2}t_{eq}^{1/2}t^{-2}R^{-5/2} & (t_f < t_{eq} \text{ and } t > t_{eq}) \end{cases} \tag{1.103}$$

which we utilize in many parts of this thesis.

1.2.6 Current Cosmological Constraints

Both ordinary and superconducting cosmic strings exhibit gravitational effects due to their string tension, and so $G\mu$ is the primary parameter of interest in any model. The most robust constraints on $G\mu$ come from the predicted effect of long strings on the CMB temperature anisotropies. The spacetime around a cosmic string is conical, with a deficit angle given by $\Delta = 8\pi G\mu$. Therefore, CMB photons that pass near a string on their way to us will experience a Doppler shift [57, 58] as they traverse this conical geometry. The result is that one should observe line discontinuities (temperature jumps) in CMB temperature anisotropy maps with an amplitude of $\delta T/T \approx 10G\mu$, as shown in figure 1.8.

On top of these temperature discontinuities, one can also simulate and construct the power spectrum expected from a scaling distribution of cosmic strings (see figure 3 of [7] for an example). In contrast to the observed power spectrum of the CMB which features a series of acoustic peaks, a defect-dominated power spectrum contains only one broad peak. Unsuccessful searches for these features in CMB datasets therefore provide a robust uppeer bound on the string tension, set by the Planck collaboration to be [7],

$$(G\mu)_{CMB}^{NG} \leq 1.3 \times 10^{-7} \tag{1.104}$$

The above constraint is from Nambu-Goto simulations of the cosmic string network, in which the width of the strings are neglected and they are evolved using the Nambu-Goto

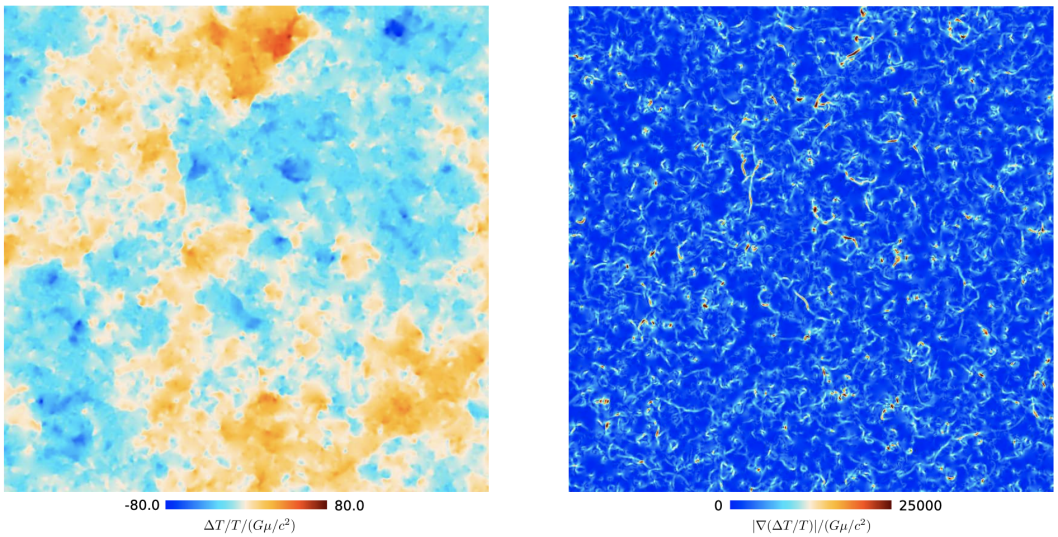

Figure 1.8: Left: A simulation of temperature anisotropies on a 20° patch of the sky induced by a network of cosmic strings. The amplitude of the anisotropies is normalized by the string tension, $G\mu/c^2$ (we use $c = 1$ throughout this thesis). Right: The result of applying a spherical gradient to the left image. One experiences a temperature jump (or discontinuity) when traversing a cosmic string (see main text for details), and so strong gradients in the temperature map would be a smoking gun signature of these defects. Figure adapted from [7].

effective action, discussed earlier. For field theory simulations, in which the microphysics are specified (usually given by the Abelian-Higgs model, with action (1.19)), the bound is similar, $(G\mu)^{AH}_{CMB} \leq 3.2 \times 10^{-7}$. However, we should note that Nambu-Goto simulations [59, 60, 61, 62, 63, 64, 65, 66] do not agree with field theory simulations [67, 68, 69] when establishing the existence of a loop distribution. Indeed, our discussion in the previous subsection assumes Nambu-Goto strings, whereas Abelian-Higgs simulations predict no long-lived population of loops. This subject has been under debate in the literature for a considerable amount of time, with no resolution as of yet.

The strongest bounds on the string tension (for regular and low-current superconducting strings) currently come from pulsar timing arrays [70, 71]. Pulsars are rapidly rotating neutron stars which emit bursts of electromagnetic radiation from their poles during each oscillation. As the periods of these neutron stars are often highly stable, they represent some of the most reliable clocks in nature. Pulsar timing is a technique in which the most stable pulsars are measured repeatedly over decades. Accurate timing data from a web of these pulsars can then be analyzed. Correlated irregularities in pulse arrival times across these pulsars could therefore indicate the passage of a gravitational wave, or a stochastic

background of gravitational waves.

A network of cosmic string loops following a scaling distribution, such as the one presented in equation (1.103) are capable of sourcing such a stochastic gravitational wave background. As each loop oscillates it sources gravitational waves with characteristic wavelengths related to the loop radius, R_0. Blanco-Pillado, Olum, and Shlaer have computed the expected power in gravitational waves for a variety of string tensions, and we reproduce their figure below.

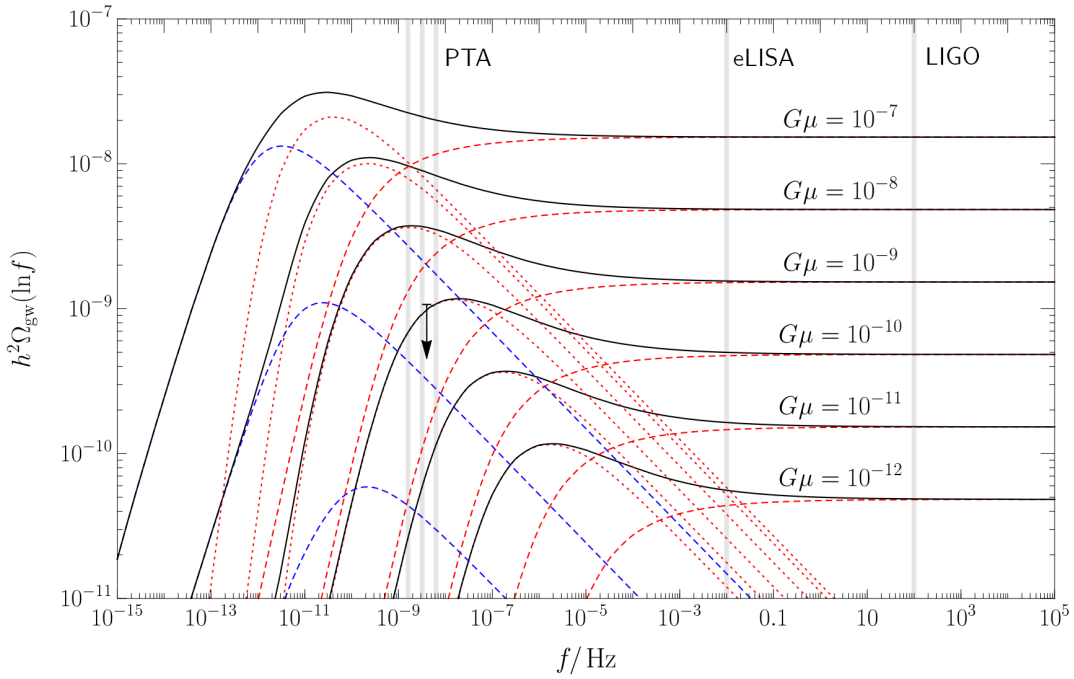

Figure 1.9: The gravitational wave spectrum produced by a network of cosmic string loops. The dashed red lines are from the distribution given in (1.100), dashed blue lines from (1.101), and dotted red from (1.102). The solid black line is the total contribution and represents the predicted gravitational wave amplitude per frequency bin. Shaded grey regions represent peak sensitivity frequencies for various GW observatories. Figure adapted and modified from [55] to represent updated upper bounds on $G\mu$ from pulsar timing measurements. It was shown recently that particle emission from cusps introduces a high frequency cutoff to the gravitational wave background, due to the rapid decay of loops with small radii [72]. The exact modification depends on the symmetry breaking scheme, and may have implications for future gravitational wave surveys such as LISA and advanced LIGO.

In the nearly ten years since this figure was produced, pulsar timing data has improved substantially, and the constraint on $G\mu$ from gravitational wave emission stands at roughly

$$(G\mu)_{PT} \leq 10^{-10} \tag{1.105}$$

One should note that this constraint is not necessarily robust, as it applies only when a substantial loop distribution is present, such as in the case of Nambu-Goto simulations. If the true nature of cosmic strings match instead with field theory simulations, this bound does not apply.
It should also be mentioned that recently, the NANOGrav [73], PPTA [74], and EPTA [75] pulsar timing array collaborations have reported on the detection of a common spectrum process that may have a gravitational wave interpretation. If confirmed, it is possible that the signal could be due to a loop distribution of cosmic strings with $G\mu \sim 10^{-10}$ [76].

Finally, for superconducting cosmic strings, the allowed parameter space is enlarged to include the current, $\mathcal{I}$. Instead of enumerating the wide variety of phenomena that these strings can source, we instead refer back to figure 1.3, where the parameter space of these models was displayed. Additional details can be found in [32].

1.3 Cosmic Textures

To close out our review on topological defects that are relevant for this thesis, we very briefly discuss cosmic textures. Textures are formed when the vacuum manifold ($\mathcal{M}$) of a theory is given by a three sphere, S^3. In three spatial dimensions, it is possible to wind this manifold non-trivially, yielding a defect. However, unlike other defects we have mentioned, the scalar fields which initiate the phase transition are not necessarily lifted off of $\mathcal{M}$, they may always remain in the vacuum state. A symmetry breaking potential of the form

$$V(\phi) = \frac{\lambda}{4}\sum_{i=1}^{d+1}(\phi_i^2 - \eta^2)^2 \tag{1.106}$$

will always give rise to texture configurations (where d is the number of spatial dimensions).

Perhaps the simplest way to visualize a texture is to consider a 1+1 dimensional universe, which undergoes a phase transition with a symmetry braking potential of thee form of (1.106). In one spatial dimension the vacuum manifold will be the circle, S^1. In this case, the difference between a trivial mapping of the scalar field to the vacuum manifold and a nontrivial are presented in figure 1.10.

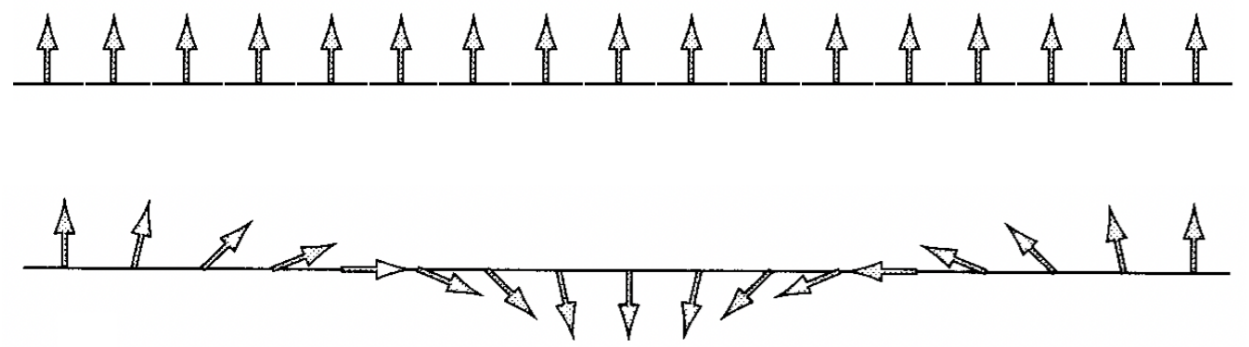

Figure 1.10: Possible field configurations in one spatial dimension of a scalar field ϕ winding a vacuum manifold with circular (S^1) topology. Top: A trivial configuration with no texture. Bottom: A texture configuration, with all energy stored in gradients. The field is not trapped to be in its false vacuum at any point. Figure adapted and modified from chapter 3 of [2].

This twisted configuration is sometimes referred to as a topological "knot". The energy in a texture configurations resides solely in its gradients, as the field is in no place trapped at the top of its potential.

Previous discussion on the qualitative differences between global and local defects still hold. Therefore, no well-localized texture configurations exist from the breaking of gauge (local) symmetries. The reason for this being that gauge fields act to locally screen gradient energies of a defect, and so local textures are essentially unobservable. Only textures formed from the breaking of a global symmetry may induce interesting phenomenology.

Global textures are unstable to collapse, as can be seen from the scaling of their total energy

$$E = \frac{1}{2}\int d^3x\,(\nabla\phi_i)^2 \tag{1.107}$$

where a sum over i is implicit. If we perform a radial rescaling of the coordinates[3], $\mathbf{x} \to \alpha\mathbf{x}$, ($\alpha > 1$ implies a collapsing texture, while $\alpha < 1$ an expanding one) we can see that

$$E_\alpha = \frac{1}{2}\alpha^{-1}\int d^3x\,(\nabla\phi_i)^2. \tag{1.108}$$

[3]This scaling argument was originally introduced by Derrick in [77] and applies not just to textures, but all defects. The introduction of gauge fields avoids this instability for local strings. Global strings are technically non-local, as they have no well defined core radius, and thus these arguments do not apply.

It is clear that the energy is minimized as α is increased. From this we infer that once a texture is formed, it will collapse relativistically. As the texture collapses, the energy in field gradients continues to increase until $(\nabla\phi_i)^2 \approx V(0) \sim \eta^4$, at which time the field has enough energy to jump over the potential barrier and "unwind" its topological knot. In doing so, it radiates ϕ_i fields which are then free to decay, potentially into standard model fields.

The Kibble mechanism once again assures us that on scales larger than the correlation length of the field ($\xi \leq d_H$), texture configurations will appear with initial size $r \sim d_H$. These collapse relativistically in one Hubble time ($t_H \sim H^{-1}$) leading to a burst of particles. As the field always remains uncorrelated outside the horizon, textures will continuously enter the horizon and subsequently collapse. Turok [78] has estimated the number of texture collapses per horizon volume per Hubble time

$$\frac{dn_{tex}}{dt} \approx \kappa d_H^{-4} \tag{1.109}$$

where $\kappa \approx 0.04$ from simulations [79]. Collapsing textures also produce gravitational fields, and collapses taking place near recombination can introduce so called "cold-spots" in CMB temperature maps [80]. They also introduce fluctuations in the power spectrum which have been constrained by Planck [7] to yield the constraint

$$G\eta^2 \leq 1.1 \times 10^{-6} \tag{1.110}$$

where η is the symmetry breaking scale at which the first textures were formed. Thanks to their gravitational interactions, textures may also aid in structure formation (see chapter 15 of [2] and references therein). In this thesis, we consider the constraining power of present and future generation CMB spectral distortion instruments on the texture energy scale, $G\eta^2$.

Bibliography

[1] A. P. Finne, V. B. Eltsov, R. Hanninen, N. B. Kopnin, J. Kopu, M. Krusius, M. Tsubota, and G. E. Volovik, "Dynamics of vortices and interfaces in superfluid 3He," *Rept. Prog. Phys.* **69** (2006) 3157–3230, arXiv:cond-mat/0606619.

[2] A. Vilenkin and E. P. S. Shellard, *Cosmic Strings and Other Topological Defects*. Cambridge University Press, 7, 2000.

[3] Y. B. Zeldovich, "Cosmological fluctuations produced near a singularity," *Mon. Not. Roy. Astron. Soc.* **192** (1980) 663–667.

[4] A. Vilenkin, "Cosmological Density Fluctuations Produced by Vacuum Strings," *Phys. Rev. Lett.* **46** (1981) 1169–1172. [Erratum: Phys.Rev.Lett. 46, 1496 (1981)].

[5] A. H. Guth, "The Inflationary Universe: A Possible Solution to the Horizon and Flatness Problems," *Phys. Rev. D* **23** (1981) 347–356.

[6] A. D. Linde, "A New Inflationary Universe Scenario: A Possible Solution of the Horizon, Flatness, Homogeneity, Isotropy and Primordial Monopole Problems," *Phys. Lett. B* **108** (1982) 389–393.

[7] **Planck** Collaboration, P. A. R. Ade *et al.*, "Planck 2013 results. XXV. Searches for cosmic strings and other topological defects," *Astron. Astrophys.* **571** (2014) A25, arXiv:1303.5085 [astro-ph.CO].

[8] J. Khoury, B. A. Ovrut, P. J. Steinhardt, and N. Turok, "The Ekpyrotic universe: Colliding branes and the origin of the hot big bang," *Phys. Rev. D* **64** (2001) 123522, arXiv:hep-th/0103239.

[9] R. H. Brandenberger and C. Vafa, "Superstrings in the Early Universe," *Nucl. Phys. B* **316** (1989) 391–410.

[10] M. Novello and S. E. P. Bergliaffa, "Bouncing Cosmologies," *Phys. Rept.* **463** (2008) 127–213, arXiv:0802.1634 [astro-ph].

[11] T. W. B. Kibble, "Topology of Cosmic Domains and Strings," *J. Phys. A* **9** (1976) 1387–1398.

[12] T. W. B. Kibble, "Phase Transitions in the Early Universe," *Acta Phys. Polon. B* **13** (1982) 723.

[13] T. W. B. Kibble, "Some Implications of a Cosmological Phase Transition," *Phys. Rept.* **67** (1980) 183.

[14] J. Preskill, "Cosmological Production of Superheavy Magnetic Monopoles," *Phys. Rev. Lett.* **43** (1979) 1365.

[15] G. 't Hooft, "Magnetic Monopoles in Unified Gauge Theories," *Nucl. Phys. B* **79** (1974) 276–284.

[16] A. M. Polyakov, "Particle Spectrum in Quantum Field Theory," *JETP Lett.* **20** (1974) 194–195.

[17] A. M. Polyakov, "Isomeric States of Quantum Fields," *Zh. Eksp. Teor. Fiz.* **68** (1975) 1975.

[18] Y. B. Zeldovich, I. Y. Kobzarev, and L. B. Okun, "Cosmological Consequences of the Spontaneous Breakdown of Discrete Symmetry," *Zh. Eksp. Teor. Fiz.* **67** (1974) 3–11.

[19] P. Sikivie, "Of Axions, Domain Walls and the Early Universe," *Phys. Rev. Lett.* **48** (1982) 1156–1159.

[20] M. Dine and W. Fischler, "The Not So Harmless Axion," *Phys. Lett. B* **120** (1983) 137–141.

[21] J. Magueijo and R. H. Brandenberger, "Cosmic defects and cosmology," in *IPM School on Cosmology 1999: Large Scale Structure Formation*. 1, 2000. arXiv:astro-ph/0002030.

[22] Y. B. Zeldovich and M. Y. Khlopov, "On the Concentration of Relic Magnetic Monopoles in the Universe," *Phys. Lett. B* **79** (1978) 239–241.

[23] H. B. Nielsen and P. Olesen, "Vortex Line Models for Dual Strings," *Nucl. Phys. B* **61** (1973) 45–61.

[24] M. B. Hindmarsh and T. W. B. Kibble, "Cosmic strings," *Rept. Prog. Phys.* **58** (1995) 477–562, arXiv:hep-ph/9411342.

[25] J. Preskill, "VORTICES AND MONOPOLES," in *Les Houches School of Theoretical Physics: Architecture of Fundamental Interactions at Short Distances*, pp. 235–338. 1987.

[26] E. Witten, "Superconducting Strings," *Nucl. Phys. B* **249** (1985) 557–592.

[27] D. Haws, M. Hindmarsh, and N. Turok, "SUPERCONDUCTING STRINGS OR SPRINGS?," *Phys. Lett. B* **209** (1988) 255–261.

[28] A. C. Thompson, "Dynamics of Cosmic String," *Phys. Rev. D* **37** (1988) 283–297.

[29] E. J. Copeland, "Cosmic Strings and Superconducting Cosmic Strings," in *International School of Particle Astrophysics, 2nd Course: Dark Matter in the Universe*. 8, 1988.

[30] E. M. Chudnovsky, G. B. Field, D. N. Spergel, and A. Vilenkin, "SUPERCONDUCTING COSMIC STRINGS," *Phys. Rev. D* **34** (1986) 944–950.

[31] M. Aryal, A. Vilenkin, and T. Vachaspati, "NOTES ON SUPERCONDUCTING COSMIC STRINGS," *Phys. Lett. B* **194** (1987) 25–29.

[32] K. Miyamoto and K. Nakayama, "Cosmological and astrophysical constraints on superconducting cosmic strings," *JCAP* **07** (2013) 012, arXiv:1212.6687 [astro-ph.CO].

[33] N. Turok, "Grand Unified Strings and Galaxy Formation," *Nucl. Phys. B* **242** (1984) 520–541.

[34] S. M. Carroll, *Spacetime and Geometry*. Cambridge University Press, 7, 2019.

[35] T. Vachaspati and A. Vilenkin, "Gravitational Radiation from Cosmic Strings," *Phys. Rev. D* **31** (1985) 3052.

[36] T. Damour and A. Vilenkin, "Gravitational wave bursts from cosmic strings," *Phys. Rev. Lett.* **85** (2000) 3761–3764, arXiv:gr-qc/0004075.

[37] J. J. Blanco-Pillado and K. D. Olum, "Form of cosmic string cusps," *Phys. Rev. D* **59** (1999) 063508, arXiv:gr-qc/9810005. [Erratum: Phys.Rev.D 103, 029902 (2021)].

[38] J. H. MacGibbon and R. H. Brandenberger, "Gamma-ray signatures from ordinary cosmic strings," *Phys. Rev. D* **47** (1993) 2283–2296, arXiv:astro-ph/9206003.

[39] J. H. MacGibbon and R. H. Brandenberger, "High-energy neutrino flux from ordinary cosmic strings," *Nucl. Phys. B* **331** (1990) 153–172.

[40] R. Brandenberger, B. Cyr, and T. Schaeffer, "On the Possible Enhancement of the Global 21-cm Signal at Reionization from the Decay of Cosmic String Cusps," *JCAP* **04** (2019) 020, arXiv:1810.03219 [astro-ph.CO].

[41] A. Vilenkin and T. Vachaspati, "Electromagnetic Radiation from Superconducting Cosmic Strings," *Phys. Rev. Lett.* **58** (1987) 1041–1044.

[42] Y.-F. Cai, E. Sabancilar, D. A. Steer, and T. Vachaspati, "Radio Broadcasts from Superconducting Strings," *Phys. Rev. D* **86** (2012) 043521, arXiv:1205.3170 [astro-ph.CO].

[43] M. Anthonisen, R. Brandenberger, and P. Scott, "Constraints on cosmic strings from ultracompact minihalos," *Phys. Rev. D* **92** no. 2, (2015) 023521, arXiv:1504.01410 [astro-ph.CO].

[44] S. F. Bramberger, R. H. Brandenberger, P. Jreidini, and J. Quintin, "Cosmic String Loops as the Seeds of Super-Massive Black Holes," *JCAP* **06** (2015) 007, arXiv:1503.02317 [astro-ph.CO].

[45] R. Brandenberger, B. Cyr, and H. Jiao, "Intermediate mass black hole seeds from cosmic string loops," *Phys. Rev. D* **104** no. 12, (2021) 123501, arXiv:2103.14057 [astro-ph.CO].

[46] B. Cyr, H. Jiao, and R. Brandenberger, "Massive black holes at high redshifts from superconducting cosmic strings," arXiv:2202.01799 [astro-ph.CO].

[47] Y. B. Zeldovich, "Gravitational instability: An Approximate theory for large density perturbations," *Astron. Astrophys.* **5** (1970) 84–89.

[48] M. Pagano and R. Brandenberger, "The 21cm Signature of a Cosmic String Loop," *JCAP* **05** (2012) 014, arXiv:1201.5695 [astro-ph.CO].

[49] R. Brandenberger, B. Cyr, and R. Shi, "Constraints on Superconducting Cosmic Strings from the Global 21-cm Signal before Reionization," *JCAP* **09** (2019) 009, arXiv:1902.08282 [astro-ph.CO].

[50] T. W. B. Kibble, "Evolution of a system of cosmic strings," *Nucl. Phys. B* **252** (1985) 227. [Erratum: Nucl.Phys.B 261, 750 (1985)].

[51] B. Allen and E. P. S. Shellard, "Cosmic string evolution: a numerical simulation," *Phys. Rev. Lett.* **64** (1990) 119–122.

[52] C. Ringeval, M. Sakellariadou, and F. Bouchet, "Cosmological evolution of cosmic string loops," *JCAP* **02** (2007) 023, arXiv:astro-ph/0511646.

[53] J. J. Blanco-Pillado, K. D. Olum, and B. Shlaer, "Large parallel cosmic string simulations: New results on loop production," *Phys. Rev. D* **83** (2011) 083514, arXiv:1101.5173 [astro-ph.CO].

[54] J. J. Blanco-Pillado, K. D. Olum, and B. Shlaer, "A new parallel simulation technique," *J. Comput. Phys.* **231** (2012) 98–108, arXiv:1011.4046 [physics.comp-ph].

[55] J. J. Blanco-Pillado, K. D. Olum, and B. Shlaer, "The number of cosmic string loops," *Phys. Rev. D* **89** no. 2, (2014) 023512, arXiv:1309.6637 [astro-ph.CO].

[56] D. C. N. da Cunha, C. Ringeval, and F. R. Bouchet, "Stochastic gravitational waves from long cosmic strings," arXiv:2205.04349 [astro-ph.CO].

[57] N. Kaiser and A. Stebbins, "Microwave Anisotropy Due to Cosmic Strings," *Nature* **310** (1984) 391–393.

[58] J. R. Gott, III, "Gravitational lensing effects of vacuum strings: Exact solutions," *Astrophys. J.* **288** (1985) 422–427.

[59] A. Albrecht and N. Turok, "Evolution of Cosmic Strings," *Phys. Rev. Lett.* **54** (1985) 1868–1871.

[60] D. P. Bennett and F. R. Bouchet, "Evidence for a Scaling Solution in Cosmic String Evolution," *Phys. Rev. Lett.* **60** (1988) 257.

[61] B. Allen and E. P. S. Shellard, "Cosmic string evolution: a numerical simulation," *Phys. Rev. Lett.* **64** (1990) 119–122.

[62] C. Ringeval, M. Sakellariadou, and F. Bouchet, "Cosmological evolution of cosmic string loops," *JCAP* **02** (2007) 023, arXiv:astro-ph/0511646.

[63] V. Vanchurin, K. D. Olum, and A. Vilenkin, "Scaling of cosmic string loops," *Phys. Rev. D* **74** (2006) 063527, arXiv:gr-qc/0511159.

[64] L. Lorenz, C. Ringeval, and M. Sakellariadou, "Cosmic string loop distribution on all length scales and at any redshift," *JCAP* **10** (2010) 003, arXiv:1006.0931 [astro-ph.CO].

[65] J. J. Blanco-Pillado, K. D. Olum, and B. Shlaer, "Large parallel cosmic string simulations: New results on loop production," *Phys. Rev. D* **83** (2011) 083514, arXiv:1101.5173 [astro-ph.CO].

[66] J. J. Blanco-Pillado, K. D. Olum, and B. Shlaer, "The number of cosmic string loops," *Phys. Rev. D* **89** no. 2, (2014) 023512, arXiv:1309.6637 [astro-ph.CO].

[67] N. Bevis, M. Hindmarsh, M. Kunz, and J. Urrestilla, "CMB power spectrum contribution from cosmic strings using field-evolution simulations of the Abelian Higgs model," *Phys. Rev. D* **75** (2007) 065015, arXiv:astro-ph/0605018.

[68] M. Hindmarsh, J. Lizarraga, J. Urrestilla, D. Daverio, and M. Kunz, "Scaling from gauge and scalar radiation in Abelian Higgs string networks," *Phys. Rev. D* **96** no. 2, (2017) 023525, arXiv:1703.06696 [astro-ph.CO].

[69] M. Hindmarsh, J. Lizarraga, J. Urrestilla, D. Daverio, and M. Kunz, "Type I Abelian Higgs strings: evolution and Cosmic Microwave Background constraints," *Phys. Rev. D* **99** no. 8, (2019) 083522, arXiv:1812.08649 [astro-ph.CO].

[70] **NANOGrav** Collaboration, P. Demorest, J. Lazio, and A. Lommen, "Gravitational Wave Astronomy Using Pulsars: Massive Black Hole Mergers & the Early Universe," arXiv:0902.2968 [astro-ph.CO].

[71] G. Hobbs *et al.*, "The international pulsar timing array project: using pulsars as a gravitational wave detector," *Class. Quant. Grav.* **27** (2010) 084013, arXiv:0911.5206 [astro-ph.SR].

[72] P. Auclair, D. A. Steer, and T. Vachaspati, "Particle emission and gravitational radiation from cosmic strings: observational constraints," *Phys. Rev. D* **101** no. 8, (2020) 083511, arXiv:1911.12066 [hep-ph].

[73] **NANOGrav** Collaboration, Z. Arzoumanian *et al.*, "The NANOGrav 12.5 yr Data Set: Search for an Isotropic Stochastic Gravitational-wave Background," *Astrophys. J. Lett.* **905** no. 2, (2020) L34, arXiv:2009.04496 [astro-ph.HE].

[74] B. Goncharov *et al.*, "On the Evidence for a Common-spectrum Process in the Search for the Nanohertz Gravitational-wave Background with the Parkes Pulsar Timing Array," *Astrophys. J. Lett.* **917** no. 2, (2021) L19, arXiv:2107.12112 [astro-ph.HE].

[75] S. Chen *et al.*, "Common-red-signal analysis with 24-yr high-precision timing of the European Pulsar Timing Array: inferences in the stochastic gravitational-wave background search," *Mon. Not. Roy. Astron. Soc.* **508** no. 4, (2021) 4970–4993, arXiv:2110.13184 [astro-ph.HE].

[76] J. J. Blanco-Pillado, K. D. Olum, and J. M. Wachter, "Comparison of cosmic string and superstring models to NANOGrav 12.5-year results," *Phys. Rev. D* **103** no. 10, (2021) 103512, arXiv:2102.08194 [astro-ph.CO].

[77] G. H. Derrick, "Comments on nonlinear wave equations as models for elementary particles," *J. Math. Phys.* **5** (1964) 1252–1254.

[78] N. Turok, "Global Texture as the Origin of Cosmic Structure," *Phys. Rev. Lett.* **63** (1989) 2625.

[79] D. N. Spergel, N. Turok, W. H. Press, and B. S. Ryden, "Global texture as the origin of large scale structure: numerical simulations of evolution," *Phys. Rev. D* **43** (1991) 1038–1046.

[80] M. Cruz, E. Martinez-Gonzalez, P. Vielva, J. M. Diego, M. Hobson, and N. Turok, "The CMB cold spot: texture, cluster or void?," *Mon. Not. Roy. Astron. Soc.* **390** (2008) 913, arXiv:0804.2904 [astro-ph].

Part II

Low Frequency Effects of Cosmic String Loops

Chapter 2

On the Possible Enhancement of the Global 21-cm Signal at Reionization from the Decay of Cosmic String Cusps

R.H. Brandenberger, B. Cyr, and T. Schaeffer, *On the Possible Enhancement of the Global 21-cm Signal at Reionization from the Decay of Cosmic String Cusps*, JCAP 04 (2019) 020, [arXiv:1810.03219].

Addendum for thesis

In 2018, the Experiment to Detect the Global EoR (epoch of reionization) Signature (EDGES) released a surprising result to the astronomy community. They claimed to have detected the global (sky-averaged) 21-cm signal at cosmic dawn. Specifically, this signal measures the absorption of 21-cm wavelength photons by neutral hydrogen atoms at the time of formation of the first stars. The amplitude of the signal is characterized by a brightness temperature δT_b (among other things), and the EDGES collaboration reported that they had seen an amplitude twice that of the δT_b expected from our standard cosmological model.

R. Brandenberger and I, together with an undergraduate student from Paris that I was mentoring, T. Schaeffer, set out to determine the effect of a distribution of cosmic string loops on this global 21-cm signal. As in the previous chapter, we studied cusp annihilations, this time taking into account the proper parametrization of the cusp size.

As well, we utilized a formalism I had developed after the last project, in order to determine the low energy photon spectrum from a cusp decay. This formalism took as input the spectrum of charged pions coming from QCD jets after a cusp decay, and computed the Bremsstrahlung and synchrotron emission produced by their interactions with the charged medium present in a galaxy.

The effect of cosmic string cusp annihilations on this brightness temperature δT_b is miniscule, proving this to be more of an academic exercise as no stringent constraints were derived. It should also be noted that in the recent months, results from another experiment (SARAS-2) have cast doubt on the validity of the EDGES detection. Likely, the signal seen by EDGES is an unchecked systematic, and not of physical origin.

Abstract

We consider cosmic string cusp annihilations as a possible source of enhancement to the global background radiation temperature in 21-cm photons at reionization. A soft photon spectrum is induced via the Bremsstrahlung and Synchrotron emission of electrons borne out of QCD jets formed off the cusp. The maximal energy density background comes from synchrotron induced photons with a string tension of $G\mu \sim 10^{-18}$. In this instance, the radiation background at reionization is heated up by $5 \cdot 10^{-3}\ K$. We find that the depth of the absorption trough (δT_b) in 21-cm at reionization is altered by one part in 10^4 from the strings, requiring high precision measurements to be detectable. This mechanism cannot explain the δT_b observed by the EDGES experiment.

2.1 Introduction

Cosmic strings are one dimensional topological defects that can form in the early universe. They form if the universe undergoes a phase transition in which the true vacuum state is degenerate, and not simply connected. If they form, the string region has a small (but non-zero) and is made up of scalar and gauge particles related to the previously unbroken symmetry group (see e.g. [1, 2, 3] for some reviews). Detection of these strings would provide invaluable insights into the mathematical structure of matter in the very early universe, and could be an alternative to expensive particle physics experiments when studying physics at these very high energies (see e.g. [4]). The theory of cosmic strings is an elegant one to work with, particularly because they possess only one free parameter, the string tension

μ. This parameter is often expressed in a dimensionless way as $G\mu$, where G is Newton's gravitational constant.

The strings themselves have been proposed as candidates for many unsolved mysteries in astrophysics and cosmology. Historically they were first thought of as a competition with inflation for providing the seeds of the large scale structure, though this required a string tension of $G\mu \sim 10^{-6}$ [5, 6, 7, 8]. In contrast to inflation, a cosmological model in which the fluctuations are due to strings exclusively does not give rise to acoustic oscillations in the angular power spectrum of the cosmic microwave background (CMB) [9, 10, 11]. Detailed studies of the acoustic peak structure of the angular power spectrum of the CMB now limits the string tension to values $G\mu < 10^{-7}$ [12, 13, 14]. Since strings predict [15, 16] lines in the sky across which the temperature of the CMB jumps, searches for these non-Gaussian features in the CMB has the potential of reducing this upper bound by a couple of orders of magnitude [17, 18, 19, 20, 21, 22, 23]. Even if strings are only a subdominant mechanism for structure formation, they leave behind distinctive non-Gaussian localized signals in the distribution of structure in the universe. Long string segments produce wakes [24, 25, 26, 27, 28, 29], planar overdensities, while string loops seed compact clumps which correspond to nonlinear density fluctuations at early times. These nonlinear seed fluctuations could yield an explanation for the origin of globular clusters [30, 31], fast radio bursts [32, 33, 34, 35, 36, 37, 38, 39], and they could seed supermassive black holes [40]. Provided that the distribution of strings includes a scaling distribution of string loops (which is indicated by certain numerical studies [41, 42, 43, 44, 45, 46, 47, 48]), pulsar timing arrays could provide a stronger constraint, $G\mu < 10^{-11}$ coming from the observational upper bound on the amplitude of the stochastic gravitational wave background [49].

The energy scale η of particle physics models which yields cosmic strings could, however, be many orders of magnitude lower than that which yields a value of $G\mu$ corresponding to the upper bounds mentioned above. The non-observation of new physics beyond the particle physics Standard Model at the Large Hadron Collider sets a lower bound on $G\mu$ of the order of 10^{-30} (making use of the relation $\mu \simeq \eta^2$). As we will review below, the number of cosmic string loops at any given time increases as $G\mu$ decreases. Hence, it is possible that searching for effects of cosmic strings in the sky might lead to a lower bound on the cosmic string tension. In this work we will consider possible constraints on the cosmic string tension arising from an observational upper bound on the excess photon radiation at redshifted 21cm wavelenghts. We find that the strongest signal arises from very low string tensions of $G\mu \sim 10^{-18}$, but that the predicted signal lies below the current observational bounds.

Recently there has been some excitement regarding an anomalous radio background detected by the ARCADE-2 experiment [50]. This experiment detected a new radiation field that dominates over the CMB at low energies ($\nu < 1\ GHz$). The effective frequency dependent temperature of the background radiation was fitted to a power law [51]

$$T(\nu) \,=\, T_{CMB} + \xi T_R \left(\frac{\nu}{\nu_0}\right)^{\beta} , \tag{2.1}$$

with $T_R = 1.19\ K$, $\nu_0 = 1\ GHz$, and a spectral index of $\beta = -2.62$ [1]. Since the detected signal hasn't been fully disentangled from the background, the parameter ξ sets the fraction of the excess radiation that was present at early times. This signal is not currently explained by radio point sources, galactic emission, or CMB spectral distortions.

The inclusion of a new radiation field present at early times can have a substantial effect on the 21-cm signal predicted at reionization. When neutral hydrogen undergoes the "forbidden" hyperfine transition between its triplet and singlet state, it emits a 21-cm photon. Conversely, CMB photons can be absorbed by cold clouds of neutral hydrogen by exciting hydrogen molecules to their excited state (see e.g. [52] for a review). Thus, detection of these photons provides an accurate way to probe the distribution of neutral hydrogen in the universe. Recently, the first detection of a global (i.e. averaged over the sky) 21-cm signal from the epoch of reionization was reported by the EDGES experiment [53, 54]. The global signal detected was larger than what was expected according to the standard cosmological paradigm. While met with some scepticism about its validity [55], we are entering a time when this signal will likely be probed by other collaborations. What is certain is that the global 21cm signal is not larger than the reported value from the EDGES collaboration.

In this work we will compute the contribution of cosmic string loops to the global 21cm signal [2], and we investigate whether, using the value reported by the EDGES collaboration as an upper bound for a possible signal, constraints on the cosmic string tension can be derived.

The observable measured for such a signal is the so-called differential brightness temperature,

$$\delta T_b(\nu) \,=\, T_b(\nu) - T_{CMB}\,, \tag{2.2}$$

[1] T_{CMB} is the temperature of the CMB.

[2] See [56] for recent work computing the contribution of cosmic string wakes to this signal.

where the brightness temperature at the frequency ν is

$$T_b(\nu) \approx I_\nu c^2/2k_B\nu^2\,, \tag{2.3}$$

where I_ν is the radiation intensity at frequency ν, c is the speed of light and k_B is Boltzmann's constant [3]. The differential brightness temperature is

$$\delta T_b \propto 1 - \frac{T_\gamma}{T_{spin}}\,, \tag{2.4}$$

where T_γ is the temperature of the photon radiation, and T_{spin} is the spin temperature of the hydrogen, a weighted average of the CMB temperature, kinetic temperature from collisions with other particles, and scattering by Lyman α photons. Interestingly, the EDGES collaboration detected a value of δT_b in absorption that was roughly twice what was predicted by the standard cosmological paradigm.

To explain this result, a flurry of papers were written to either lower the spin temperature (for example, by coupling to milli-charged dark matter as a way to sap energy from the hydrogen gas [57, 58, 59]), or increase the background radiation temperature. Feng and Holder showed that if $\mathcal{O}(1\%)$ of the radio background detected by ARCADE-2 was present at reionization, the detected brightness temperature could be achieved [51].

If a distribution of cosmic string loops form, they will naturally persist throughout most of our cosmic history. These loops possess mechanisms that allow them to source electromagnetic radiation. We compute the induced background of 21-cm photons present at reionization by this mechanism, in an attempt to source any part of this anomalous radio background.

In the following section, we review the *cusp annihilation* mechanism by which non-superconducting strings yield bursts of particles including photons. In Section III we compute the flux of radio frequency photons produced by the distribution of cosmic string loops present between the time t_{rec} of recombination and the time of reionization (the time relevant for the global 21cm signal). In Section IV we then infer the contribution which cosmic string loops make to the global 21cm signal.

[3] In the following we shall use natural units in which c, k_B and Planck's constant are set to one.

2.2 Cusp Emission Mechanism

If a phase transition in the very early universe permits the production of cosmic strings, a network of strings will inevitably form [60, 61]. The network of strings consists of both long strings (strings with curvature radius which is comparable or larger than the Hubble radius t) and loops. Due to their relativistic motion, the long string network coarsens with time by splitting off string loops. By causality [60, 61], the string network has to persist until the current time. As can be shown using analytical arguments [1, 2, 3], the long string network approaches a *scaling solution* for which the curvature radius of the strings tracks the Hubble radius t at all times. There are good reasons to believe that the distribution of string loops will also approach a scaling solution [62, 63, 64] according to which the statistical properties of the loop distribution are independent of time is all lengths are scaled to t. Numerical simulations [41, 42, 43, 44, 45, 46, 47, 48] of the evolution of cosmic string networks using the Nambu-Goto action (i.e. neglecting the finite width of the strings) confirm that such a scaling solution is achieved, although field theory simulations [65] still yield a different result (in these simulations it is the classical scalar and gauge field equations which are evolved). In this work, we will assume a scaling distribution of string loops.

By considering the Nambu-Goto action for a string, one can derive its equations of motion. From these equations of motion, it follows [66] that for each string loop with radius R, there will be at least one cusp per loop oscillation time R^{-1}. A cusp is a point on the string where the string velocity reaches the speed of light, and the string doubles back on itself. Since the string has a finite width, at each cusp point there will be an interval of length l_c on the string where the two string segments (the parts of the string on either side of the cusp point) overlap. This region is called the cusp. Whereas a long straight string is protected against decaying by topology, the cusp region looks like a string and an anti-string (strings with opposite winding numbers). It is not protected against decay, and so this overlapping region self-annihilates (in analogy to particle - antiparticle annihilation), producing a jet of gauge and scalar particles that make up the string [67]. Previous work has been done on high energy gamma ray and neutrino signals from these annihilations [68] [69, 70], but these used an incorrect parametrization of the cusp length. We should note that it is possible to construct loop configurations with no cusps, but most generic models exhibit this feature [71].

By considering special relativistic effects, one can show that the proper parametrization

for the cusp yields the following form [72] for the cusp length

$$l_c \sim R^{1/2} w^{1/2} \tag{2.5}$$

where $w \sim \mu^{-1/2}$ is the microscopic width of the string [73], and μ is the mass per unit length of the string. A consequence of this parametrization discussed in [72] is that we get $\mathcal{O}(1)$ particles produced per cusp annihilation. Particles produced at the cusp are thought to decay to superheavy fermions with mass Q_f, before transferring their energy into a jet of standard model particles. The jets thus formed are similar to those produced at the LHC, containing pions, photons, etc. Previous works have considered this idea [68], and by using the Pion multiplicity function, it is possible to show that the low energy ($E_\pi << Q_f$) spectrum of neutral and charged pions emanating from a cusp is

$$\frac{dN}{dE} = \frac{15}{24} \frac{\mu l_c}{Q_f^2} \left(\frac{Q_f}{E} \right)^{3/2} \tag{2.6}$$

The dominant pion decay channels are

$$\begin{aligned} \pi^0 &\to 2\gamma \\ \pi^+ &\to \mu^+ + \nu_\mu \\ \pi^- &\to \mu^- + \bar{\nu}_\mu \end{aligned}$$

And so photons with energies $E_\gamma > m_\pi$ will be sourced by neutral pion decay and follow the above spectrum, scaling with $E^{-3/2}$. However, we are interested in radio photons which are *soft* in comparison to the pion mass. For these photons we cannot apply the above scaling of the photon flux as a function of energy. Whereas there will be primordial soft photons from jets, their spectrum is not known (at least to us). Hence, we will consider more robust production mechanisms for these soft photons.

We consider the decays of the charged pions into muons (and quickly thereafter, electrons). Assuming no further interactions of the electrons after production, they traverse the universe from the time of their production until today. As they travel, they interact with electric and magnetic fields, which source the production of photons through Bremsstrahlung and Synchrotron emission. The pion-produced electrons will once again follow the same spectrum above for $E_e > m_\pi$. From this distribution, we closely follow [74] for computing the Bremsstrahlung and Synchrotron photon spectra, which can safely be extrapolated down to 21-cm energies.

Finally, we note that the emission of low frequency photons from the cusp can transfer a significant amount of energy to the surrounding plasma. When this happens, the particles in the plasma are accelerated to very high energies and can create a hydrodynamic flow in the immediate vicinity of the cusp. This flow ceases with a shockwave, which can be a source of gamma ray photons. This idea has been studied by Berezinsky et al. [71] in the context of gamma ray bursts from superconducting cosmic strings. This effect is difficult to study analytically, and we neglect it in the computations below.

2.3 Global 21-cm Signal at Reionization from Cusp Annihilations

2.3.1 Photons Produced Via Bremsstrahlung

First, let us compute the soft photon spectrum at reionization produced by electrons via the Bremsstrahlung process. The distribution of electrons produced by cusp annihilations at any one point in time is given by integrating (2.6) over all of the loops present. Loops form at a time t with a characteristic radius $R = \alpha t$, and an analysis of the decay of these loops by gravitational radiation [75] gives a cutoff radius $R_c = \gamma G\mu t$, below which loops live less than one Hubble expansion time and for which the energy density is negligible. Here, $\alpha \sim 1$, $\gamma \sim 10$ are dimensionless numerical constants fit by simulation [41, 42, 43, 44, 45, 46, 47, 48]. For electrons emitted off of cusps at a time t'', their energy distribution is given by

$$\frac{dn_e(t'')}{dE(t'')dt''} = \int_{\gamma G\mu t''}^{\alpha t''} n_{R,loops}(t'')\frac{dN}{dE}\frac{1}{R}dR\,, \tag{2.7}$$

where the factor of $1/R$ comes from the fact that cusp annihilations occur on average once every oscillation time, $1/R$, and $n_{R,loops}$ is the number density of loops.

The loop distribution follows a scaling solution which for $R > \gamma G\mu t$ is given by [1, 2, 3]

$$n_{R,loops}(t) = \begin{cases} \nu R^{-5/2}t^{-3/2} & t < t_{eq} \\ \nu R^{-5/2}t_{eq}^{1/2}t^{-2} & t > t_{eq} \quad t_f < t_{eq} \\ \nu R^{-2}t^{-2} & t > t_{eq} \quad t_f > t_{eq} \end{cases} \tag{2.8}$$

where ν is a coefficient of the order one [4] which is determined from numerical simulations

[4] This constant has nothing to do with the frequency ν used earlier in the text.

[41, 42, 43, 44, 45, 46, 47, 48], and t_{eq} is the time of equal matter and radiation. We take $Q_f \sim \eta$, the symmetry breaking scale at which the strings formed (note also that $\eta \simeq \mu^{1/2}$). The integral over R is dominated by the lower cutoff radius $\gamma G\mu t$. For values of $G\mu$ smaller than the current upper bound, loops of such radii are produced in the radiation phase. On the other hand, we only consider the contribution of electrons after the time of recombination to the global 21cm signal. Hence, when evaluating the integral (2.7), we must use the expression for the loop distribution given in the second line of the above equation. Hence, the dominant piece of this integral yields

$$\frac{dn_e(t'')}{dE(t'')dt''} \sim \nu\gamma^{-2}(G\mu)^{-3/2}t_{eq}^{1/2}t''^{-4} \cdot E(t'')^{-3/2}G^{-1/2}\,. \tag{2.9}$$

This expression gives us the energy spectrum of electrons emitted from cusps at time t''.

The next step is to determine the spectrum of electrons present at time t' coming from electrons emitted from cusps at earlier times t''. To obtain this, we integrate over time from recombination to some $t' > t_{rec}$ to determine the electron distribution from all cusp annihilations over that timeframe. We have to take into account both the redshifting of the electron number density and the Jacobian of the energy ratio. By noting that the Jacobian transformation between energies at different times is

$$E^{3/2}(t'')\frac{dn_e(t'')}{dE(t'')} = E^{3/2}(t')\frac{dn_e(t')}{dE(t')}\left(\frac{t'}{t''}\right)^{1/3}\left(\frac{t'}{t''}\right)^{2} \tag{2.10}$$

and including the redshifting of the number density of the electrons, we find

$$\begin{aligned}\frac{dn_e(t')}{dE(t')} &= \nu\gamma^{-2}(G\mu)^{-3/2}t_{eq}^{1/2}E(t')^{-3/2}G^{-1/2} \\ &\quad \times \int_{t_{rec}}^{t'} dt''\left(\frac{t''}{t'}\right)^{1/3}\left(\frac{t''}{t'}\right)^{2}t''^{-4} \\ &\sim \nu\gamma^{-2}(G\mu)^{-3/2}G^{-1/2}E(t')^{-3/2}t_{eq}^{1/2}t'^{-7/3}t_{rec}^{-2/3}\end{aligned} \tag{2.11}$$

Now that we have a time dependent expression for the electron distribution, we can compute the induced soft photon spectrum. Following [74], in the weak shielding limit the induced photon distribution per unit time is

$$\frac{dn_\gamma(t')}{dE(t')dt'} \approx \left(\frac{8}{3}m_\pi^{-1/2}\right)\alpha_{em}r_0^2K_e(t')E(t')^{-1}\sum_s n_s(t')\tilde{\phi}_w\,, \tag{2.12}$$

where α_{em} is the EM fine structure constant, r_0 is the reduced Compton wavelength of the electrons, $r_0 = m_e^{-1}$, n_s is the number density of a species of charged particles that our induced electrons interact with (we include a summation over different types of scatterers), and $\tilde{\phi}_w \sim 300$ is a dimensionless weak shielding coefficient (its value is taken from that of neutral hydrogen). This expression is for a power law of electrons going as $E^{-3/2}$, and K_e is set by the expression $dn_e(t')/dE(t') = K_e(t')E(t')^{-3/2}$ [5].

To obtain the photon spectrum at the time t when the global 21cm signal is computed, we must integrate the above result (3.17) in time over all times when photons can travel without scattering, i.e. from t_{rec} to time t. In computing this integral, we must take into account the Jacobian arising from converting $E(t')$ to $E(t)$ which is

$$E(t')\frac{dn_\gamma(t')}{dE(t')} \;=\; E(t)\frac{dn_\gamma(t)}{dE(t)}\left(\frac{t}{t'}\right)^2 \tag{2.13}$$

as well as the redshifting of the number density of photons. Integrating over time and including the abovementioned effects, the spectrum of soft photons by Bremsstrahlung emission is

$$\begin{aligned}\frac{dn_\gamma(t)}{dE(t)} &\approx \nu\gamma^{-2}(G\mu)^{-3/2}G^{-1/2}(\Lambda\tilde{\phi}_w)E(t)^{-1}t_{eq}^{1/2}t_{rec}^{-2/3} \\ &\quad\times\int_{t_{rec}}^{t}\left(n_s(t)\left(\frac{t}{t'}\right)^2\right)\left(\frac{t'}{t}\right)^2 t'^{-7/3}dt' \\ &\sim \nu\gamma^{-2}(G\mu)^{-3/2}G^{-1/2}(\Lambda\tilde{\phi}_w n_s(t))E(t)^{-1}t_{eq}^{1/2}t_{rec}^{-2}\,,\end{aligned} \tag{2.14}$$

where

$$\Lambda \;=\; \frac{8}{3}\alpha_{em}r_0^2 m_\pi^{-1/2}\,. \tag{2.15}$$

Note that the integral is dominated by the earliest times, i.e. t_{rec}. Note that the amplitude of the spectrum increases as $G\mu$ decreases, the reason being that the increase in the number of loops as $G\mu$ decreases is a more important factor than the decrease in the cusp energy of an individual loop [6].

At first glance it appears that as the value of the string tension decreases one would get a large and observable signal. However, as was shown in [76], there is a crossover value of $G\mu$ below which gravitational radiation is not the dominant decay mechanism, and

[5] To obtain this expression, we consider the spectrum of photons produced by a single high energy electron, and then integrate over the distribution of electrons computed above.

[6] This phenomenon was already seen in the computations of the high energy gamma and neutrino fluxes from string loops.

cusp annihilation becomes the more efficient method to lose energy. Assuming that cusp radiation dominates over gravitational radiation, one obtains an effective cutoff radius in the loop distribution which at time t is

$$R_c^{cusp} = \left(\frac{3}{2}\mu^{-1/4}\beta^{-1}t\right)^{2/3}, \tag{2.16}$$

with $\beta \sim 10$ being a parameter that measures how circular the loops are on average (perfectly circular loops have $\beta = 2\pi$). If R_c^{cusp} is larger than the gravitational radiation cutoff radius $\gamma G\mu t$ the cusp annihilation is the dominant decay process.

For values of $G\mu$ below the value where the gravitational cutoff radius equals R_c^{cusp} at the time of recombination (the time which dominates in the integrals we perform), the computation of the soft photon distribution has to be redone, replacing the gravitational cutoff radius by R_c^{cusp}.This yields a soft photon spectrum of

$$\begin{aligned}\frac{dn_\gamma^{cusp}(t)}{dE} &\approx \nu\beta^{4/3}(G\mu)^{5/6}G^{-5/6}E(t)^{-1}(\Lambda\tilde{\phi}_w n_s(t)) \\ &\quad \times t_{eq}^{1/2}\int_{t_{rec}}^{t} dt' t'^{-7/3}\ln\left(\frac{t'}{t_{rec}}\right).\end{aligned} \tag{2.17}$$

In this region of values of $G\mu$, the signal decreases as μ decreases. Hence, we see that the largest soft photon signal is produced by values of $G\mu$ where the gravitational radiation cutoff equals R_c^{cusp} at t_{rec}.

By equating the cutoff radii in the two regimes, the crossover value of the string tension can be derived. This value depends on time t_c and is

$$G\mu = \left(\left(\frac{2}{3}\right)^{2/3}\gamma\beta^{2/3}G^{-1/6}t_c^{1/3}\right)^{-6/7}. \tag{2.18}$$

Equivalently, we can fix $G\mu$, and in this case for times before t_c cusp annihilation is the dominant decay mechanism, and for times after, gravitational radiation takes over. Taking our crossover time to be recombination, we find that $\frac{dn_\gamma(t)}{dE}$ is the proper expression for $G\mu > 10^{-18}$, and for smaller values of the tension we must use $\frac{dn_\gamma^{cusp}(t)}{dE}$.

2.3.2 Photons Produced Via Synchrotron

Next, we consider the soft photon produced by Synchrotron emission over the same time-frame. The computation of $dn_e(t')/dE(t')$ proceeds in the same way as for the Bremsstrahlung

computation. From [74], the induced Synchrotron spectrum from a power law distribution of electrons, from recombination to reionization, is

$$\begin{aligned}\frac{dn_\gamma(t')}{dE(t')dt'} &= \frac{2D_e(t')e^3}{m_e}B(t')^{(p+1)/2}\left(\frac{3e}{4\pi m_e}\right)^{(p-1)/2} \\ &\quad \times a(p)E(t')^{-(p+1)/2}(2\pi)^{(p-1)/2}\,, \end{aligned} \tag{2.19}$$

where $B(t')$ is the magnetic field at time t', $a(p)$ is a dimensionless constant of order 10^{-1}, and $D_e(t')$ is defined by the equation

$$\frac{dn_e(t')}{d\Gamma'} = \frac{D_e(t')}{4\pi}\Gamma'^{-p}\,, \tag{2.20}$$

where $\Gamma' = E(t')/m_e$. For our case, $D_e(t')$ is

$$D_e(t') = 4\pi\gamma^{-2}(G\mu)^{-3/2}G^{-1/2}m_e^{-1/2}t_{eq}^{1/2}t_{rec}^{-2/3}t'^{-7/3}\,. \tag{2.21}$$

As well, the power law is unchanged for the electrons so $p = 3/2$. In deriving this expression, it was assumed that the cusp was an isotropic emitter of electrons. If a more detailed analysis is required, one must take into account the fact that the QCD jets coming off the cusp are beamed into a solid angle related to the strong coupling constant [68].

To obtain the photon spectrum at some late time t, we must integrate over the rate of production at earlier times t', taking into accouint the redshifting of the number density, and of the Jacobian transformation of the energies, which for this power law integral is

$$E^{5/4}(t')\frac{dn_\gamma(t')}{dE'} = E^{5/4}(t)\frac{dn_\gamma(t)}{dE(t)}\left(\frac{t}{t'}\right)^{1/6}\left(\frac{t}{t'}\right)^2\,. \tag{2.22}$$

The computation yields a photon spectrum of

$$\begin{aligned}\frac{dn_\gamma(t)}{dE(t)} &= \Omega E^{-5/4}(t)(G\mu)^{-3/2}t_{eq}^{1/2}t_{rec}^{-2/3} \\ &\quad \times\int_{t_{rec}}^{t}dt'\left(B(t_{rec})\left(\frac{t_{rec}}{t'}\right)^{4/3}\right)^{5/4} \\ &\quad \times\left(\frac{t'}{t}\right)^{1/6}\left(\frac{t'}{t}\right)^2 t'^{-7/3} \\ &= \Omega(G\mu)^{-3/2}E^{-5/4}(t)B^{5/4}(t_{rec})t_{eq}^{1/2}t_{rec}^{1/6}t^{-13/6}\,, \end{aligned} \tag{2.23}$$

with

$$\Omega \;=\; 4\pi \frac{2e^3}{m_e^{3/2}} \left(\frac{3e}{2m_e}\right)^{1/4} a\left(\frac{3}{2}\right) \gamma^{-2} G^{-1/2}\,. \tag{2.24}$$

Since we intend to use the upper bound on the magnitude of the B field from CMB observations, we have replaced $B(t')$ by $B(t_{rec})$, taking into account the appropriate redshift factor. Similarly to the Bremsstrahlung analysis, this spectrum is only valid for $10^{-18} < G\mu$ when gravitational radiation is the dominant decay mechanism. For smaller values of $G\mu$, we again use the cutoff radius for cusp decay, and find

$$\begin{aligned}
\frac{dn_\gamma^{cusp}(t)}{dE} &= \Omega' E(t)^{-5/4} B^{5/4}(t_{rec}) (G\mu)^{5/6} t_{eq}^{1/2} \\
&\quad \times \int_{t_{rec}}^{t} dt' \left(\frac{t_{rec}}{t'}\right)^{5/3} \left(\frac{t'}{t}\right)^{13/6} t'^{-7/3} \ln\left(\frac{t'}{t_{rec}}\right) \\
&= \Omega' (G\mu)^{5/6} E^{-5/4}(t) B^{5/4}(t_{rec}) t_{eq}^{1/2} t_{rec}^{5/3} t^{-13/6} \\
&\quad \times \int_{t_{rec}}^{t} dt' t'^{-11/6} \ln\left(\frac{t'}{t_{rec}}\right)\,,
\end{aligned} \tag{2.25}$$

with

$$\Omega' \;=\; 4\pi \frac{2e^3}{m_e^{3/2}} \left(\frac{3e}{2m_e}\right)^{1/4} a\left(\frac{3}{2}\right) \beta^{4/3} G^{-5/6} \tag{2.26}$$

The above expressions must be evaluated and compared to the energy density in the CMB at 21-cm wavelengths to infer any possible effects.

2.4 Comparison with the CMB

The first measurements of the global 21-cm signal at reionization have started to come back [53, 54], and they seem to be in tension with current theory computations. In addition, the ARCADE-2 experiment has detected an anomalous radio background that may have some cosmological origin [50]. The global 21-cm signal is characterized by an absorption depth (δT), and a shape. The signal reported by the EDGES experiment indicates that this depth may be twice as deep as was expected. The depth goes as $\delta T \propto T_r/T_{spin}$, where T_r is the background radiation temperature at that time. Hence, a larger depth of the signal could be explained either by decreasing the spin temperature or by increasing the photon temperature. Usually, the radiation temperature T_r is taken to be $T_r = T_{CMB}$. However, if there is extra production of soft photons then T_r can be boosted. As we have seen, cosmic string cusp annihilation leads to a flux of soft photons and hence increases the effective

radiation temperature at 21cm frequencies. In this section we will compute the magnitude of the resulting absorption feature.

The energy density at 21-cm in the CMB at reionization is given in natural units by

$$\begin{aligned} \frac{d\rho_{CMB}}{dE} &= \frac{8\pi h}{c^3}\frac{E^3}{e^{hE/kT}-1} \\ &\approx E^2 T \\ &\approx 10^{-40}\ GeV^3 \end{aligned} \tag{2.27}$$

when computed at a temperature of $T_{reion} = 50\ K$. We wish to compute the ratio of the energy density from our string induced soft photon spectra, to that in the CMB. We define this ratio as

$$\mathcal{F} = \frac{d\rho_{21-cm}/dE}{d\rho_{CMB}/dE} \tag{2.28}$$

where the energy density in 21-cm at reionization can be evaluated by computing $E_{21}\frac{dn_\gamma(t_{reion})}{dE}$ with $E_{21} \sim 10^{-15}\ GeV$.

In the Bremsstrahlung analysis, the scatterers which contribute are the ionized particles which are present after recombination. The ionization fraction f drops from $f = 1$ close to recombination to $f \sim 10^{-4}$ at later times (but before reionization) [77]. We hence use

$$n_s(t) = f\rho_B(t)m_B^{-1}\,, \tag{2.29}$$

where ρ_B is the baryon density and m_B is the baryon (hydrogen) mass. The ratio $\mathcal{F}$ then becomes

$$\begin{aligned} \mathcal{F} \sim\ & \nu\gamma^{-2}(G\mu)^{-3/2} f\frac{m_{pl}}{m_B}\left(\frac{m_{pl}}{m_\pi}\right)^{1/2}\left(\frac{T_{rec}}{E}\right)^2\left(\frac{r_0}{t_0}\right)^2 \\ & \times\frac{t^{2/3}t_{eq}^{1/3}}{t_{rec}}\left(\frac{t_0}{t}\right)^2\,, \end{aligned} \tag{2.30}$$

where t_0 is the present time.

With this, the ratio in energy densities in 21-cm at reionization (for interesting values of $G\mu$) is

$$\begin{aligned} \mathcal{F}_{Brem} &\sim 10^{-26} \qquad \text{For } G\mu = 10^{-7} \\ \mathcal{F}_{Brem} &\sim 10^{-10} \qquad \text{For } G\mu = 10^{-18}\,. \end{aligned} \tag{2.31}$$

The ratio peaks at $G\mu \sim 10^{-18}$ when the crossover occurs, and drops off as $(G\mu)^{5/6}$ for smaller values.

In the case of Synchrotron radiation, we give an upper bound on the possible effect by using the upper bound on the primordial magnetic field obtained by the analysis of the CMB. The bound is [78]

$$B(t_{rec}) \; < \; 10^{-9}\text{Gauss}\,, \tag{2.32}$$

with appropriate redshifting to later times. Using this input, we find that the resulting upper bounds on the fraction $\mathcal{F}$ for these same values of $G\mu$ are

$$\begin{aligned} \mathcal{F}_{Sync} &\sim 10^{-23} \qquad \text{For } G\mu = 10^{-7} \\ \mathcal{F}_{Sync} &\sim 10^{-6} \qquad \text{For } G\mu = 10^{-18}\,. \end{aligned} \tag{2.33}$$

Once again, the maximal energy density in 21-cm radiation peaks at the crossover value of $G\mu$ when evaluated at the time t_{rec}.

The total energy density will be a superposition of the photons produced by Bremsstrahlung and by Synchrotron emission. Though Synchrotron seems to win by about $3-4$ orders of magnitude, we urge the reader to be cautious since we have used an upper bound on the primordial magnetic field and, in addition, a more detailed Synchrotron analysis (taking into account the beaming angle of the cusp emission, for example), may change the Synchrotron prediction considerably.

In the Rayleigh-Jeans limit, we find that the maximum induced temperature coming from a background of synchrotron photons sourced by cusp annihilations is

$$T_{sync}^{strings} \; \sim \; 5 \cdot 10^{-3} \text{ K}\,. \tag{2.34}$$

We can compute the differential brightness temperature at reionization from the expression

$$\delta T_b = 27 x_{HI} \left(1 - \frac{T_r}{T_s}\right) \sqrt{\frac{1+z}{10}\frac{0.15}{\Omega_m h^2}} \left(\frac{\Omega_b h^2}{0.023}\right) \text{ mK} \tag{2.35}$$

Where x_{HI} is the fraction of neutral hydrogen, and T_s is the spin temperature of the hydrogen gas. We also define

$$T_r = T_{CMB} + T_{sync}^{strings} + T_{Brem}^{strings} \tag{2.36}$$

As our new background temperature. We parametrize our enhancement over the standard

CMB signal as

$$\frac{\delta T_b}{\delta T_b^{CMB}} = 1 + \frac{T_{sync}^{strings} + T_{Brem}^{strings}}{T_{CMB} - T_s} \tag{2.37}$$

Where δT_b^{CMB} is the differential brightness temperature in the case where the whole background is sourced by the CMB only. At reionization the spin and background temperatures can be calculated using the 21cmFAST code [51] with $T_{CMB} \sim \mathcal{O}(10)$ K and $T_s \sim \mathcal{O}(1)$ K. This implies our maximum departure from standard CMB predictions is

$$\frac{\delta T_b}{\delta T_b^{CMB}} \sim 1 + \mathcal{O}(10^{-4}) \tag{2.38}$$

Thus, a precision of one part in 10^4 is required by future experiments to constrain even the strongest of our signals. Currently, the only global measurement of this signal is from the EDGES collaboration, who are reporting a signal twice as strong as expected from CMB considerations alone ($\delta T_b^{EDGES}/\delta T_b^{CMB} \sim 2$). Our mechanism cannot explain this EDGES signal, though it could still have a small effect on the depth of the absorption trough that could be constrained if precision measurements of this global 21-cm signal are achieved.

2.5 Conclusions and Discussion

In this work, we have considered the effects of cusp annihilations of cosmic strings on the radio frequency radiation background present at reionization. We have utilized the fact that QCD jets emanating from cusp annihilations will produce a cascade of neutral and charged pions, which will quickly decay into electrons. These electrons interact with the dilute gas of hydrogen that exists between recombination and reionization, inducing a soft photon spectrum via Bremsstrahlung and Synchrotron radiation.

We have computed number density and energy density distributions for both of these processes. These computations are valid for any $E_\gamma < m_\pi$ and any time between recombination and reionization. For our purposes, we computed the additional contribution to the background radiation temperature in 21-cm at reionization, in the hopes of using the upper bound on the global 21cm absorption signal at times of reionization to constrain the cosmic string tension. We found that the induced effect of cosmic strings increases as the string tension decreases, hence opening the possibility that a lower bound on the string tension could be established. However, since for low string tensions cusp annihilation becomes the

dominant string decay mechanism and changes the string loop distribution, we found that the soft photon spectrum from strings peaks at a valuie of $G\mu \sim 10^{-18}$, and that even for that value of $G\mu$, the soft photons from cusp annihilation do not have a sufficient impact on the radiation temperature to yield an effect on the global 21cm signal which exceeds the upper bound set by the EDGES experiment (recall that we are using the value reported in [53, 54] as an upper bound on the possible effect).

Concerning the Bremsstrahlung effect, we have not taken into account electrons produced from cosmic string cusp annihilations before the time of recombination. Taking these into account could potentially increase the cosmic string signal.

Concerning the effect due to Synchrotron radiation, we should note that the computation of the emission spectrum uses a simplifying assumption that the cusp emission is isotropic, which is not the case. A more detailed analysis taking the beaming effect into account might change the amplitude of $d\rho/dE$.

As well, backreaction on the cusp may also reduce any observational signal. Gravitational backreaction is capable of reducing the cusp region, yielding a decrease in the emitted energy off of a cusp [79].

Finally, we have neglected the effects of gamma ray fireballs that may be produced by the injection of low energy photons into the plasma surrounding a cusp [71]. Since the universe is quite neutral during the epoch between recombination and reionization, however, there may not be many of these fireballs produced. The production of any of these fireballs could cause patches of the Universe to reionize too early, and so future work should consider their effects.

As a conclusion, we find that cosmic string cusp annihilation provides too weak of a soft photon flux to lead to constraints on the parameter space of the theory. We have, however, neglected soft photons produced directly from the jets. At the current time we do not know how to predict the magnitude of this effect.

Acknowledgements

The research at McGill is supported in part by funds from NSERC and from the Canada Research Chair program. BC is supported in part by an MSI fellowship. We are grateful to Oscar Hernandez for stimulating discussions.

Bibliography

[1] A. Vilenkin and E. P. S. Shellard, *Cosmic Strings and Other Topological Defects*. Cambridge University Press, 7, 2000.

[2] M. B. Hindmarsh and T. W. B. Kibble, "Cosmic strings," *Rept. Prog. Phys.* **58** (1995) 477–562, arXiv:hep-ph/9411342.

[3] R. H. Brandenberger, "Topological defects and structure formation," *Int. J. Mod. Phys. A* **9** (1994) 2117–2190, arXiv:astro-ph/9310041.

[4] R. H. Brandenberger, "Probing Particle Physics from Top Down with Cosmic Strings," *The Universe* **1** no. 4, (2013) 6–23, arXiv:1401.4619 [astro-ph.CO].

[5] A. Vilenkin, "Cosmological Density Fluctuations Produced by Vacuum Strings," *Phys. Rev. Lett.* **46** (1981) 1169–1172. [Erratum: Phys.Rev.Lett. 46, 1496 (1981)].

[6] N. Turok and R. H. Brandenberger, "Cosmic Strings and the Formation of Galaxies and Clusters of Galaxies," *Phys. Rev. D* **33** (1986) 2175.

[7] H. Sato, "Galaxy Formation by Cosmic Strings," *Prog. Theor. Phys.* **75** (1986) 1342.

[8] A. Stebbins, "Cosmic Strings and Cold Matter," *apjl* **303** (1986) L21.

[9] J. Magueijo, A. Albrecht, D. Coulson, and P. Ferreira, "Doppler peaks from active perturbations," *Phys. Rev. Lett.* **76** (1996) 2617–2620, arXiv:astro-ph/9511042.

[10] U.-L. Pen, U. Seljak, and N. Turok, "Power spectra in global defect theories of cosmic structure formation," *Phys. Rev. Lett.* **79** (1997) 1611–1614, arXiv:astro-ph/9704165.

[11] L. Perivolaropoulos, "Spectral analysis of microwave background perturbations induced by cosmic strings," *Astrophys. J.* **451** (1995) 429–435, arXiv:astro-ph/9402024.

[12] T. Charnock, A. Avgoustidis, E. J. Copeland, and A. Moss, "CMB constraints on cosmic strings and superstrings," *Phys. Rev. D* **93** no. 12, (2016) 123503, arXiv:1603.01275 [astro-ph.CO].

[13] C. Dvorkin, M. Wyman, and W. Hu, "Cosmic String constraints from WMAP and the South Pole Telescope," *Phys. Rev. D* **84** (2011) 123519, arXiv:1109.4947 [astro-ph.CO].

[14] **Planck** Collaboration, P. A. R. Ade *et al.*, "Planck 2013 results. XXV. Searches for cosmic strings and other topological defects," *Astron. Astrophys.* **571** (2014) A25, arXiv:1303.5085 [astro-ph.CO].

[15] N. Kaiser and A. Stebbins, "Microwave Anisotropy Due to Cosmic Strings," *Nature* **310** (1984) 391–393.

[16] R. Moessner, L. Perivolaropoulos, and R. H. Brandenberger, "A Cosmic string specific signature on the cosmic microwave background," *Astrophys. J.* **425** (1994) 365–371, arXiv:astro-ph/9310001.

[17] R. J. Danos and R. H. Brandenberger, "Canny Algorithm, Cosmic Strings and the Cosmic Microwave Background," *Int. J. Mod. Phys. D* **19** (2010) 183–217, arXiv:0811.2004 [astro-ph].

[18] S. Amsel, J. Berger, and R. H. Brandenberger, "Detecting Cosmic Strings in the CMB with the Canny Algorithm," *JCAP* **04** (2008) 015, arXiv:0709.0982 [astro-ph].

[19] A. Stewart and R. Brandenberger, "Edge Detection, Cosmic Strings and the South Pole Telescope," *JCAP* **02** (2009) 009, arXiv:0809.0865 [astro-ph].

[20] L. Hergt, A. Amara, R. Brandenberger, T. Kacprzak, and A. Refregier, "Searching for Cosmic Strings in CMB Anisotropy Maps using Wavelets and Curvelets," *JCAP* **06** (2017) 004, arXiv:1608.00004 [astro-ph.CO].

[21] J. D. McEwen, S. M. Feeney, H. V. Peiris, Y. Wiaux, C. Ringeval, and F. R. Bouchet, "Wavelet-Bayesian inference of cosmic strings embedded in the cosmic microwave background," *Mon. Not. Roy. Astron. Soc.* **472** no. 4, (2017) 4081–4098, arXiv:1611.10347 [astro-ph.IM].

[22] R. Ciuca and O. F. Hernández, "A Bayesian Framework for Cosmic String Searches in CMB Maps," *JCAP* **08** (2017) 028, arXiv:1706.04131 [astro-ph.CO].

[23] R. Ciuca, O. F. Hernández, and M. Wolman, "A Convolutional Neural Network For Cosmic String Detection in CMB Temperature Maps," *Mon. Not. Roy. Astron. Soc.* **485** (2019) 1377, arXiv:1708.08878 [astro-ph.CO].

[24] J. Silk and A. Vilenkin, "COSMIC STRINGS AND GALAXY FORMATION," *Phys. Rev. Lett.* **53** (1984) 1700–1703.

[25] M. Rees, "Baryon concentrations in string wakes at $z \sim 200$: implications for galaxy formation and large-scale structure," *Mon. Not. Roy. Astron. Soc.* **222** (1986) 27.

[26] T. Vachaspati, "Cosmic Strings and the Large-Scale Structure of the Universe," *Phys. Rev. Lett.* **57** (1986) 1655–1657.

[27] A. Stebbins, S. Veeraraghavan, R. H. Brandenberger, J. Silk, and N. Turok, "Cosmic String Wakes," *Astrophys. J.* **322** (1987) 1–19.

[28] D. C. Neves da Cunha, J. Harnois-Deraps, R. Brandenberger, A. Amara, and A. Refregier, "Dark Matter Distribution Induced by a Cosmic String Wake in the Nonlinear Regime," *Phys. Rev. D* **98** no. 8, (2018) 083015, arXiv:1804.00083 [astro-ph.CO].

[29] S. Laliberte, R. Brandenberger, and D. C. N. da Cunha, "Cosmic String Wake Detection using 3D Ridgelet Transformations," arXiv:1807.09820 [astro-ph.CO].

[30] L. Lin, S. Yamanouchi, and R. Brandenberger, "Effects of Cosmic String Velocities and the Origin of Globular Clusters," *JCAP* **12** (2015) 004, arXiv:1508.02784 [astro-ph.CO].

[31] A. Barton, R. H. Brandenberger, and L. Lin, "Cosmic Strings and the Origin of Globular Clusters," *JCAP* **06** (2015) 022, arXiv:1502.07301 [astro-ph.CO].

[32] R. Brandenberger, B. Cyr, and A. V. Iyer, "Fast Radio Bursts from the Decay of Cosmic String Cusps," arXiv:1707.02397 [astro-ph.CO].

[33] T. Vachaspati, "Cosmic Sparks from Superconducting Strings," *Phys. Rev. Lett.* **101** (2008) 141301, arXiv:0802.0711 [astro-ph].

[34] L. V. Zadorozhna and B. I. Hnatyk, "Electromagnetic emission bursts from the near-cusp regions of superconducting cosmic strings," *Ukr. J. Phys.* **54** (2009) 1149–1156.

[35] Y.-F. Cai, E. Sabancilar, and T. Vachaspati, "Radio bursts from superconducting strings," *Phys. Rev. D* **85** (2012) 023530, arXiv:1110.1631 [astro-ph.CO].

[36] Y.-F. Cai, E. Sabancilar, D. A. Steer, and T. Vachaspati, "Radio Broadcasts from Superconducting Strings," *Phys. Rev. D* **86** (2012) 043521, arXiv:1205.3170 [astro-ph.CO].

[37] J. Ye, K. Wang, and Y.-F. Cai, "Superconducting cosmic strings as sources of cosmological fast radio bursts," *Eur. Phys. J. C* **77** no. 11, (2017) 720, arXiv:1705.10956 [astro-ph.HE].

[38] Y.-W. Yu, K.-S. Cheng, G. Shiu, and H. Tye, "Implications of fast radio bursts for superconducting cosmic strings," *JCAP* **11** (2014) 040, arXiv:1409.5516 [astro-ph.HE].

[39] L. V. Zadorozhna, "Fast radio bursts as electromagnetic radiation from cusps on superconducting cosmic strings," *Advances in Astronomy and Space Physics* **5** (Sept., 2015) 43–50.

[40] S. F. Bramberger, R. H. Brandenberger, P. Jreidini, and J. Quintin, "Cosmic String Loops as the Seeds of Super-Massive Black Holes," *JCAP* **06** (2015) 007, arXiv:1503.02317 [astro-ph.CO].

[41] A. Albrecht and N. Turok, "Evolution of Cosmic Strings," *Phys. Rev. Lett.* **54** (1985) 1868–1871.

[42] D. P. Bennett and F. R. Bouchet, "Evidence for a Scaling Solution in Cosmic String Evolution," *Phys. Rev. Lett.* **60** (1988) 257.

[43] B. Allen and E. P. S. Shellard, "Cosmic string evolution: a numerical simulation," *Phys. Rev. Lett.* **64** (1990) 119–122.

[44] C. Ringeval, M. Sakellariadou, and F. Bouchet, "Cosmological evolution of cosmic string loops," *JCAP* **02** (2007) 023, arXiv:astro-ph/0511646.

[45] V. Vanchurin, K. D. Olum, and A. Vilenkin, "Scaling of cosmic string loops," *Phys. Rev. D* **74** (2006) 063527, arXiv:gr-qc/0511159.

[46] L. Lorenz, C. Ringeval, and M. Sakellariadou, "Cosmic string loop distribution on all length scales and at any redshift," *JCAP* **10** (2010) 003, arXiv:1006.0931 [astro-ph.CO].

[47] J. J. Blanco-Pillado, K. D. Olum, and B. Shlaer, "Large parallel cosmic string simulations: New results on loop production," *Phys. Rev. D* **83** (2011) 083514, arXiv:1101.5173 [astro-ph.CO].

[48] J. J. Blanco-Pillado, K. D. Olum, and B. Shlaer, "The number of cosmic string loops," *Phys. Rev. D* **89** no. 2, (2014) 023512, arXiv:1309.6637 [astro-ph.CO].

[49] **NANOGrav** Collaboration, Z. Arzoumanian *et al.*, "The NANOGrav Nine-year Data Set: Limits on the Isotropic Stochastic Gravitational Wave Background," *Astrophys. J.* **821** no. 1, (2016) 13, arXiv:1508.03024 [astro-ph.GA].

[50] D. J. Fixsen *et al.*, "ARCADE 2 Measurement of the Extra-Galactic Sky Temperature at 3-90 GHz," *Astrophys. J.* **734** (2011) 5, arXiv:0901.0555 [astro-ph.CO].

[51] C. Feng and G. Holder, "Enhanced global signal of neutral hydrogen due to excess radiation at cosmic dawn," *Astrophys. J. Lett.* **858** no. 2, (2018) L17, arXiv:1802.07432 [astro-ph.CO].

[52] S. Furlanetto, S. P. Oh, and F. Briggs, "Cosmology at Low Frequencies: The 21 cm Transition and the High-Redshift Universe," *Phys. Rept.* **433** (2006) 181–301, arXiv:astro-ph/0608032.

[53] J. D. Bowman, A. E. E. Rogers, R. A. Monsalve, T. J. Mozdzen, and N. Mahesh, "An absorption profile centred at 78 megahertz in the sky-averaged spectrum," *Nature* **555** no. 7694, (2018) 67–70, arXiv:1810.05912 [astro-ph.CO].

[54] R. A. Monsalve, B. Greig, J. D. Bowman, A. Mesinger, A. E. E. Rogers, T. J. Mozdzen, N. S. Kern, and N. Mahesh, "Results from EDGES High-Band: II. Constraints on Parameters of Early Galaxies," *Astrophys. J.* **863** no. 1, (2018) 11, arXiv:1806.07774 [astro-ph.CO].

[55] R. Hills, G. Kulkarni, P. D. Meerburg, and E. Puchwein, "Concerns about modelling of the EDGES data," *Nature* **564** no. 7736, (2018) E32–E34, arXiv:1805.01421 [astro-ph.CO].

[56] O. F. Hernández, "Wouthuysen-Field absorption trough in cosmic string wakes," *Phys. Rev. D* **90** no. 12, (2014) 123504, arXiv:1403.7522 [astro-ph.CO].

[57] A. Fialkov, R. Barkana, and A. Cohen, "Constraining Baryon–Dark Matter Scattering with the Cosmic Dawn 21-cm Signal," *Phys. Rev. Lett.* **121** (2018) 011101, arXiv:1802.10577 [astro-ph.CO].

[58] R. Barkana, N. J. Outmezguine, D. Redigolo, and T. Volansky, "Strong constraints on light dark matter interpretation of the EDGES signal," *Phys. Rev. D* **98** no. 10, (2018) 103005, arXiv:1803.03091 [hep-ph].

[59] S. Fraser *et al.*, "The EDGES 21 cm Anomaly and Properties of Dark Matter," *Phys. Lett. B* **785** (2018) 159–164, arXiv:1803.03245 [hep-ph].

[60] T. W. B. Kibble, "Phase Transitions in the Early Universe," *Acta Phys. Polon. B* **13** (1982) 723.

[61] T. W. B. Kibble, "Some Implications of a Cosmological Phase Transition," *Phys. Rept.* **67** (1980) 183.

[62] E. J. Copeland, T. W. B. Kibble, and D. Austin, "Scaling solutions in cosmic string networks," *Phys. Rev. D* **45** (1992) 1000–1004.

[63] L. Perivolaropoulos, "COBE versus cosmic strings: An Analytical model," *Phys. Lett. B* **298** (1993) 305–311, arXiv:hep-ph/9208247.

[64] D. Austin, E. J. Copeland, and T. W. B. Kibble, "Evolution of cosmic string configurations," *Phys. Rev. D* **48** (1993) 5594–5627, arXiv:hep-ph/9307325.

[65] M. Hindmarsh, J. Lizarraga, J. Urrestilla, D. Daverio, and M. Kunz, "Scaling from gauge and scalar radiation in Abelian Higgs string networks," *Phys. Rev. D* **96** no. 2, (2017) 023525, arXiv:1703.06696 [astro-ph.CO].

[66] T. W. B. Kibble and N. Turok, "Selfintersection of Cosmic Strings," *Phys. Lett. B* **116** (1982) 141–143.

[67] R. H. Brandenberger, "On the Decay of Cosmic String Loops," *Nucl. Phys. B* **293** (1987) 812–828.

[68] J. H. MacGibbon and R. H. Brandenberger, "Gamma-ray signatures from ordinary cosmic strings," *Phys. Rev. D* **47** (1993) 2283–2296, arXiv:astro-ph/9206003.

[69] J. H. MacGibbon and R. H. Brandenberger, "High-energy neutrino flux from ordinary cosmic strings," *Nucl. Phys. B* **331** (1990) 153–172.

[70] U. F. Wichoski, J. H. MacGibbon, and R. H. Brandenberger, "High-energy neutrinos, photons and cosmic ray fluxes from VHS cosmic strings," *Phys. Rev. D* **65** (2002) 063005, arXiv:hep-ph/9805419.

[71] V. Berezinsky, B. Hnatyk, and A. Vilenkin, "Gamma-ray bursts from superconducting cosmic strings," *Phys. Rev. D* **64** (2001) 043004, arXiv:astro-ph/0102366.

[72] J. J. Blanco-Pillado and K. D. Olum, "Form of cosmic string cusps," *Phys. Rev. D* **59** (1999) 063508, arXiv:gr-qc/9810005. [Erratum: Phys.Rev.D 103, 029902 (2021)].

[73] H. B. Nielsen and P. Olesen, "Vortex Line Models for Dual Strings," *Nucl. Phys. B* **61** (1973) 45–61.

[74] G. R. Blumenthal and R. J. Gould, "Bremsstrahlung, synchrotron radiation, and compton scattering of high-energy electrons traversing dilute gases," *Rev. Mod. Phys.* **42** (1970) 237–270.

[75] T. Vachaspati and A. Vilenkin, "Gravitational Radiation from Cosmic Strings," *Phys. Rev. D* **31** (1985) 3052.

[76] J. H. MacGibbon and R. H. Brandenberger, "High-energy neutrino flux from ordinary cosmic strings," *Nucl. Phys. B* **331** (1990) 153–172.

[77] M. Kaplinghat, M. Chu, Z. Haiman, G. Holder, L. Knox, and C. Skordis, "Probing the reionization history of the universe using the cosmic microwave background polarization," *Astrophys. J.* **583** (2003) 24–32, arXiv:astro-ph/0207591.

[78] A. Zucca, Y. Li, and L. Pogosian, "Constraints on Primordial Magnetic Fields from Planck combined with the South Pole Telescope CMB B-mode polarization measurements," *Phys. Rev. D* **95** no. 6, (2017) 063506, arXiv:1611.00757 [astro-ph.CO].

[79] J. J. Blanco-Pillado, K. D. Olum, and J. M. Wachter, "Gravitational backreaction near cosmic string kinks and cusps," *Phys. Rev. D* **98** no. 12, (2018) 123507, arXiv:1808.08254 [gr-qc].

Chapter 3

Constraints on Superconducting Cosmic Strings from the Global 21-cm Signal before Reionization

R.H. Brandenberger, B. Cyr, and R. Shi, *Constraints on Superconducting Cosmic Strings from the Global 21-cm Signal before Reionization*, JCAP 09 (2019) 009, [arXiv:1902.08282].

Addendum for thesis

This chapter builds directly on the previous one. Here, with visiting student R. Shi, we consider the effect of a distribution of superconducting cosmic strings on the amplitude of the 21-cm brightness temperatures δT_b at cosmic dawn. For a brief overview of the reported detection of this signal by the EDGES collaborations, see the addendum for chapter 3 of this thesis.

In our previous work with T. Schaeffer, it was found that the flux of 21-cm photons produced through Bremsstrahlung and synchroton emission of a spectrum of charged pions was too low to cause any appreciable impact on the brightness temperature. To get around this issue, we considered a distribution of cosmic string loops which were superconducting (that is, they carry an electric current).

In this case, the photon production is much more efficient and we are able to derive stringent constraints on the parameter space of superconducting cosmic strings. These constraints are shown in the figures of this chapter. Note that regardless of whether the EDGES signal is physical, we are able to rule out a large range of high current, low string tension

models.

Abstract

Electromagnetic radiation from the cusp region of superconducting cosmic strings leads to a radio excess in the photon spectrum in the early universe and can produce a deep absorption feature in the global 21cm signal before the epoch of reionization. We study the constraints on the parameter space of superconducting strings which can be derived by demanding that the absorption feature is not larger in amplitude than what has recently been reported by the EDGES collaboration. We find a previously unconstrained region of high current, low tension strings would produce too strong of an absorption feature, and are thus ruled out by non-detection.

3.1 Introduction

There has recently been a lot of work exploring the observational signals of cosmic strings (see e.g. [1] for a review of recent work). Cosmic strings are one-dimensional topological defects which are solutions of the field equations in many theories beyond the Standard Model of particle physics (see e.g. [2, 3, 4] for reviews of the physics and cosmology of cosmic strings). If Nature is described by a theory which admits cosmic string solutions, then a network of cosmic strings will form during a phase transition in the early universe and persist until the present time [5, 6]. Strings lead to interesting signatures for a variety of cosmological observations. Not observing these signals will lead to constraints on the parameter space of particle physics models beyond the Standard Model [7].

Most of the recent studies of the cosmological imprints of cosmic strings have been done in the context of strings which only interact gravitationally. In this case, the network of strings is described by a single parameter, the string tension μ (usually expressed in terms of the dimensionless number $G\mu$, where G is Newton's gravitational constant). However, in many models, strings carry conserved electromagnetic currents, either bosonic or fermionic, and they are hence superconducting [8]. In a theory which has superconducting strings, currents on the string are induced during the phase transition which produces the strings, and during the later evolution of the strings through the plasma of the early universe. Superconducting cosmic strings emit electromagnetic radiation. This radiation is dominated by the cusp region on cosmic string loops, regions which move with a velocity which approaches the speed of light. Cusps are generic features of string loops, with at least one cusp per oscillation period

forming on a string loop [9]. The bursts of electromagnetic radiation from strings cusps were studied in [10], [11], [12] and [13]. The fact that this emission gives rise to spectral distortions of the CMB was investigated in [14, 15] and [16]. The connection with gamma ray bursts was explored in [17, 18, 19], and the connection with fast radio transients in [20, 21, 22, 23, 24, 25, 26] [1].

Causality implies [5, 6] that at all times after the phase transition during which the strings are formed, there will be at least one "long" string crossing each Hubble patch of space. Here, "long" refers to a string with curvature radius larger than the Hubble radius. Analytical arguments [2, 3, 4] indicate that the network of long strings approaches a "scaling" solution, according to which the distribution of strings is statistically the same at all times if lengths are scaled to the Hubble radius. This is confirmed by numerical simulations of the evolution of cosmic string networks [29, 30, 31, 32, 33, 34, 35, 36]. The network of long strings maintains its scaling property by losing energy to string loops during long string intersections. Hence, a distribution of string loops with a large range of radii R builds up. Analytical arguments (this time not supported by general causality considerations) indicate that the distribution of string loops will also approach a scaling solution. At times later than t_{eq}, the time of equal matter and radiation, the distribution of string loops is given by (see e.g. [37, 38, 39, 40, 41, 42, 43])

$$n(R,t) \,=\, \nu R^{-5/2} t_{eq}^{1/2} t^{-2} \;\text{ for }\; R_c(t) \,<\, R \,<\, \alpha t_{eq}\,, \tag{3.1}$$

and

$$n(R,t) \,\sim\, R^{-2} t^{-2} \;\text{ for }\; R \,>\, \alpha t_{eq}\,, \tag{3.2}$$

where ν is a constant which depends on the number of long string segments crossing a Hubble volume, $R_c(t)$ is a cutoff radius below which loops live less than one Hubble expansion time, and α is a constant indicating at what fraction of the Hubble radius loops are produced.

For non-superconducting strings, the dominant energy loss mechanism of string loops is gravitational radiation. Since string loops have relativistic tension, they oscillate and emit gravitational radiation. The power of gravitational radiation from a string loop is [44]

$$P_{gw} \,=\, \gamma G \mu^2\,, \tag{3.3}$$

where γ is a constant which, according to numerical simulations of gravitational wave emis-

[1] For earlier work on the connection between superconducting strings and ultra-high energy cosmic rays see [27, 28].

sion [44] is of the order $\gamma \sim 10^2$.

It can be shown that the total power of electromagnetic radiation from cusp regions, averaged over an oscillation period, is [45]

$$P_{em} \,=\, \kappa I \sqrt{\mu}\,, \tag{3.4}$$

where I is the current on the string and κ is a constant of the order 1. For a fixed value of $G\mu$ there is a critical current I_c above which electromagnetic radiation dominates, and below which gravitational radiation is more important. This critical current is given by

$$I_c \,=\, \kappa^{-1}\gamma (G\mu)^{3/2} m_{pl}\,, \tag{3.5}$$

where m_{pl} is the Planck mass. If gravitational radiation dominates, then the cutoff radius $R_c(t)$ is given by

$$R_c(t) \,=\, \gamma \beta^{-1} G\mu t\,, \tag{3.6}$$

where β is a constant which gives the mean loop length in terms of the radius (for a circular loop we would have $\beta = 2\pi$), while if electromagnetic radiation dominates we have

$$R_c(t) \,=\, \kappa \beta^{-1} I \mu^{-1/2} t\,. \tag{3.7}$$

There is another energy loss mechanism for string loops: cusp decay [46]. This mechanism is more important than gravitational radiation loss for very low tension strings, and more important than electromagnetic radiation for very small currents. Thus, the mechanism is only important in regions of parameter space where the electromagnetic radiation is small. Hence, in this work we will not consider the cusp decay channels.

The electromagnetic emission is non-thermal and concentrated at low frequencies. We consider the enhanced energy density in electromagnetic radiation for frequencies at and below the frequency of 21cm radiation. This radio excess leads to a deep absorption signal in the global 21cm signal before reionization. Such a signal was recently reported by the EDGES experiment [47, 48] with an absorption deeper than predicted by the standard cosmological paradigm. A radio excess could possibly explain this signal. In an earlier paper [49], we studied the contribution of electromagnetic radiation from cusp decays of non-superconducting strings to the radio excess and found it to be much too small to effect observations. Superconducting strings, on the other hand, produce much more electromagnetic radiation. Here we study the contribution to a possible radio excess which these strings

can produce. By demanding that the global absorption is smaller than what has been measured by the EDGES collaboration [47, 48], we can derive constraints on the parameter space of superconducting strings. We find a region of parameter space which is indeed ruled out by observations.

In the following, we will first review how a soft radio photon excess can lead to a large absorption feature in the 21cm global signal. In Section 3, we then compute the radio excess predicted by a network of superconducting cosmic string loops as a function of the cosmic string parameters $G\mu$ and I, determine their fractional contribution to the total radio spectrum of the cosmic microwave background (CMB), and derive the constraints on the parameter space which results from demanding that the induced 21cm absorption signal is not larger than what has been detected. We discuss our results and compare with previous studies of cosmological constraints on superconducting cosmic strings in the final section.

We work in natural units in which the speed of light, Planck's constant and Boltzmann's constant are set to 1. We work in the context of standard cosmology. The variable t is used for physical time, t_{eq} denotes the time of equal matter and radiation, and t_{rec} is the time of recombination (which is later than the time of equal matter and radiation). The temperature of the radiation gas is denoted by T.

3.2 Radio Excess and Global 21cm Absorption Signal

One way in which the parameter space of superconducting cosmic strings can be constrained is by the amplitude of the absorption feature in the global 21cm signal. Observing the universe through the 21cm window can provide information about the distribution of neutral hydrogen at early times, in particular before and during reionization. CMB photons passing through a cold cloud of neutral hydrogen are absorbed by exciting the hydrogen hyperfine transition (see e.g. [50] for an in-depth review of the physics of 21cm surveys). In an early paper [51] it was pointed out that the global 21cm signal can provide a tool to probe for the existence of cosmic string wakes before reionization.

There has recently been a lot of interest in the global 21cm absorption signal before the epoch of reionization as a consequence of the detection of an unexpectedly large absorption signal by the EDGES collaboration [47, 48]. The detected amplitude of the temperature decrement is at least twice what is expected in standard cosmology. Assuming a mostly

neutral IGM, the temperature decrement δT_b is given by the proportionality

$$\delta T_b \propto 1 - \frac{T_\gamma}{T_{spin}}\,, \tag{3.8}$$

where T_γ is the effective temperature of the photons at the 21cm frequency, and T_{spin} is the spin temperature of the hydrogen gas. The effective temperature of the photons, in turn, is given by

$$T_\gamma = T_{CMB} + T_{21}\,, \tag{3.9}$$

where T_{CMB} is the overall CMB black body temperature, and T_{21} is the effective temperature due to extra photons at 21cm frequencies. These effective temperatures are given in terms of the energy densities of photons in the frequency range of 21cm. Given a new source of radio photons, the boost in the amplitude of the absorption feature is given by [52] the factor

$$\mathcal{F} \sim 1 + \frac{T_{21}}{T_{CMB}}\,. \tag{3.10}$$

Following the results reported in [47, 48], there has been a flurry of work proposing ways to explain the extra absorption. A lot of the proposed models have focused on ways to reduce the spin temperature, e.g. by invoking dark matter interactions (see e.g. [53, 54, 55] for early work). On the other hand, it was pointed out in [56] that extra 21cm absorption can also be obtained if there is a new source of radio photons. In fact, an excess of the radio background has been reported by the ARCADE-2 experiment [57]. This serves as an additional piece of motivation, as the existence of cosmic strings (both superconducting and not) would produce an anomalous background.

In this work, we will compute the contribution of superconducting cosmic string loops to the radio photon background and provide bounds on the parameter space of such strings, by demanding that the absorption feature produced by the strings not exceed the amplitude reported in [47, 48] [2]. Note that if the global 21cm signal turns out to be lower than what was reported, our bounds will become stronger.

[2] In a recent paper [49] we studied the radio excess produced by the cusp decay of non-superconducting strings, but we found that the predicted radio spectrum is too low in amplitude to yield constraints on the cosmic string parameter space.

3.3 Radio Excess from Superconducting Cosmic Strings

In the following, we will compute the energy density in radio photons due to the emission from a network of loops of superconducting cosmic strings. The energy density of photons in the frequency interval $[0, \omega_{21}]$ at time t is

$$\rho^{21}(t) \,=\, \int_{t_{rec}}^{t} d\tau \frac{d\rho^{21}(\tau)}{d\tau} \left(\frac{\tau}{t}\right)^{8/3} \,, \tag{3.11}$$

where the first term inside the integral is the energy density in photons inserted per unit time, and the second factor gives the cosmological redshift of the radiation energy density in the matter dominated epoch. The energy density per unit time is given by integrating over all frequencies below the frequency ω_{21} blueshifted to time $\tau < t$

$$\omega_{21}(\tau) \,=\, \omega_{21} \left(\frac{t}{\tau}\right)^{2/3} \,, \tag{3.12}$$

and integrating over the distribution of string loops. This gives

$$\frac{d\rho^{21}(\tau)}{d\tau} \,=\, \int_{0}^{\omega_{21}(\tau)} d\omega \int_{R_c(\tau)}^{\alpha\tau} dR n(R,\tau) \frac{dP}{d\omega}(\omega) \,, \tag{3.13}$$

where the final factor is the power per unit frequency from cosmic string core region emission, and is given by [45]

$$\frac{dP}{d\omega}(\omega) \,=\, \kappa I^2 R^{1/3} \omega^{-2/3} \,. \tag{3.14}$$

The integral over R in (3.13) is dominated by the smallest value of R greater than the cutoff value $R_c(t)$. Let us focus on values of $G\mu$ and I which are sufficiently small such that the value of $R_c(t)$ at the time of reionization is smaller than αt_{eq}. In this case, we can use the expression (3.1) for $n(R,\tau)$. Inserting this and performing the integral over R, we obtain

$$\rho^{21}(t) \,=\, 3\tilde{\kappa}\nu I^2 \omega_{21}^{1/3} t_{eq}^{1/2} t^{-2} \int_{t_{rec}}^{t} d\tau R_c(\tau)^{-7/6} \left(\frac{\tau}{t}\right)^{4/9} \,, \tag{3.15}$$

where $\tilde{\kappa}$ is κ multiplied $\mathcal{O}(1)$ constants.

For currents smaller than the critical current I_c (which is a function of $G\mu$), we insert the value of the cutoff radius given by (3.6) and obtain

$$\rho^{21}(t) \,=\, 18\tilde{\kappa}\nu I^2 \omega_{21}^{1/3} t_{eq}^{1/2} t^{-2} \gamma^{-7/6} \beta^{7/6} (G\mu)^{-7/6} t^{-1/6} \,. \tag{3.16}$$

Inserting the maximal current for which this expression is valid, namely (3.5), yields

$$\rho^{21}(t) \;=\; 18\tilde{\kappa}\kappa^{-2}\nu G^{-1}\omega_{21}^{1/3}t_{eq}^{1/2}t^{-2}\gamma^{5/6}\beta^{7/6}(G\mu)^{11/6}t^{-1/6}\,. \tag{3.17}$$

For currents larger than the critical one, we insert the value of the cutoff radius given by (3.7) and obtain

$$\rho^{21}(t) \;=\; 18\tilde{\kappa}\kappa^{-7/6}\nu I^{5/6}\omega_{21}^{1/3}t_{eq}^{1/2}t^{-2}\beta^{7/6}(G\mu)^{7/12}G^{-7/12}t^{-1/6}\,. \tag{3.18}$$

Inserting the current (3.5), the minimal current for which this computation applies, yields the same result we obtained above, namely (3.17).

We now compare the magnitude of the above radio excess of photons at frequencies smaller than ν_{21} with the CMB black body photons in this frequency range. Since the value ω_{21} is in the low frequency (Rayleigh-Jeans) regime of the black body for the temperature at the time of reionization, the energy density in CMB photons is given by

$$\rho_{CMB}(t) \;=\; \frac{1}{3\pi^2}\omega_{21}^3 T(t)\,. \tag{3.19}$$

To compute the ratio $\mathcal{R} = \rho^{21}(t)/\rho_{CMB}(t)$ we make use of the Friedmann equation to relate time and temperature. Specifically, we use

$$G^{-1}t^{-2} \;=\; 6\pi\left(\frac{t}{t_{eq}}\right)^{2/3}T^4\,. \tag{3.20}$$

Inserting the value of I_c into $\rho^{21}(t)$ yields

$$\mathcal{R}(I=I_c) \;=\; \mathcal{A}\nu\gamma^{5/6}\beta^{7/6}(G\mu)^{11/6}\left(\frac{t}{t_{eq}}\right)^{1/18}\left(\frac{T}{\omega_{21}}\right)^{8/3}\left(\frac{m_{pl}}{T}\right)^{1/3}\,, \tag{3.21}$$

where $\mathcal{A}$ is a constant of the order 10^3 (assuming that κ is a constant of the order 1), and where we have left the dependence on ν, β and γ explicit. For typical values $\beta = \gamma = \nu = 10$, evaluating the result at the temperature of reionization we obtain

$$\mathcal{R}(I=I_c) \;\sim\; 10^{12}(G\mu)_6^{11/6}\,, \tag{3.22}$$

where $(G\mu)_6$ is the value of $G\mu$ in units of 10^{-6}.

For values of the current larger than I_c we have

$$\mathcal{R}(I) \;=\; \left(\frac{I}{I_c}\right)^{5/6} \mathcal{R}(I_c) \qquad (I > I_c)\,, \tag{3.23}$$

while for values smaller than I_c we have

$$\mathcal{R}(I) \;=\; \left(\frac{I}{I_c}\right)^{2} \mathcal{R}(I_c) \qquad (I < I_c)\,. \tag{3.24}$$

If the EDGES results are to be explained by excess photons at low frequencies, then the value of $\mathcal{R}$ should be of the order 1 [52]. If we demand that the distribution of superconducting string loops does not produce an absorption feature larger in amplitude than has been observed, the parameter space of strings must be constrained to yield $\mathcal{R} \leq 1$. From (3.22), (3.23) and (3.24) we see that a significant parameter space of high-tension and high-current superconducting cosmic strings is ruled out.

Our results are summarized in figures 1 and 2. In figure 1, our new constraints (the shaded blue region) are shown alongside previously computed constraints (shaded orange region, see [58] and references therein). The region above the brown diagonal line corresponds to the zone in which gravitational wave decay is the primary energy loss mechanism for the strings, and below this line they decay primarily into EM waves. We show that with our analysis, we can rule out a previously allowed region of parameter space by considering the 21cm photons emitted from superconducting strings between recombination and reionization. We do this by assuming the radiation in 21cm is not greater than what was detected by the EDGES collaboration ($\mathcal{R} \leq 1$). In figure 2, we show how these constraints can be strengthened in the event that the radiation density in 21cm produced by strings is 10% or 1% of the EDGES signal.

Assuming standard values of the constants which arise in the cosmic string distribution

$$\begin{aligned} \gamma &= 10 \\ \beta &= 10 \\ \nu &= 10 \end{aligned} \tag{3.25}$$

we find

$$I_c \;\sim\; (G\mu)_6^{3/2} 10^{10}\mathrm{GeV}\,. \tag{3.26}$$

For $I = I_c$ the constraint $\mathcal{R} < 1$ implies

$$(G\mu) \, < \, 10^{-12.5} \, . \tag{3.27}$$

This limit is marginally stronger than the limit on the string tension from pulsar timing array measurements [59], though previously constrained by BBN considerations and the Parkes Radio Survey. The pulsar timing limit on $G\mu$, however, assumes that the distribution of string loops is determined by energy loss only from gravitational radiation. Since the pulsar timing constraints are dominated by the smallest loops in the scaling distribution, the bounds are much weaker if $I > I_c$. According to the analysis of [58], the pulsar timing constraints essentially disappear for $I > I_c$. Our analysis lets us set an upper bound on the cosmic string current in this regime by requiring $\mathcal{R} < 1$ in (3.23) such that the background radiation density in 21-cm from strings doesn't exceed that of the CMB

$$I \, < \, I_c (G\mu)_6^{-11/5} 10^{-72/5} \, \sim \, (G\mu)^{-7/10} 10^{-9} \text{ GeV} \qquad (I \, > I_c) \tag{3.28}$$

Similarly, we can compute the same constraint for the regime where $I < I_c$ using (3.24)

$$I \, < \, I_c (G\mu)_6^{-11/12} 10^{-6} \, \sim \, (G\mu)^{7/12} 10^{7} \text{ GeV} \qquad (I \, < I_c) \tag{3.29}$$

Though this constraint seems degenerate with other ones compiled by [58].

3.4 Conclusions and Discussion

We have derived constraints on the parameter space of superconducting cosmic strings obtained by demanding that the induced absorption feature in the global 21cm signal before reionization not exceed the value observed by the EDGES collaboration [47, 48]. Our results are summarized in Figure 1. Note that we have implicitly assumed total efficiency in the Lyman alpha coupling of the 21cm spin temperature to the kinetic temperature of the IGM during the formation of the first stars. If the coupling efficiency was low, then a higher excess radiation would be required to produce a given decrement in the signal, and our bounds on the cosmic string parameter space would weaken.

For values of the string current I smaller than the critical current $I_c(G\mu)$, our constraints are weaker than the ones which follow from pulsar timing array measurements. The pulsar timing constraints come from gravitational radiation emitted by string loops. The effect is dominated by the smallest loops which survive more than one Hubble time. In the region

of parameter space where gravitational radiation dominates over electromagnetic radiation, the effective cutoff radius is $\gamma G\mu t$. However, for large currents in which electromagnetic radiation dominates the cutoff radius is larger, and hence the pulsar timing constraints on $G\mu$ are weaker. The analysis of [58] has shown that the pulsar timing constraint essentially disappears for $I > I_c$. In this region, our constraints rule out a large parameter space of strings with large currents.

Before concluding, it is prudent to mention some limitations of our analysis. First, we have remained agnostic to the details of the symmetry breaking scheme that forms these strings. This was done to remain as general as possible, though in doing so we have neglected to describe the best way to generate steady currents on a distribution of loops. The motion of superconducting strings through the universe will naturally produce a range of currents within the loop distribution, as the inhomogeneity of small scale magnetic fields induces different current magnitudes. Future work should consider a distribution of such currents.

As well, it has been shown that the production of low frequency photons off of cosmic string cusps will accelerate particles in the ISM and IGM to very high Lorentz factors [17, 18, 19]. This can cause a hydrodynamical flow of gas in the vicinity of a string, which is often terminated by a shock. This shock could lead to a gamma ray burst, of which it is unclear how physics at reionization could be effected. This mechanism is very difficult to track analytically, and so a more numerical approach would be beneficial in elucidating the consequences of this effect.

There have been other constraints on superconducting cosmic strings. For example, the electromagnetic radiation from string loops can locally reionize matter, and thus change the optical depth which has been measured with great accuracy by the recent CMB experiments (see e.g. [60]). The resulting constraints on the parameter space of superconducting strings has been studied in [61] and [58]. In addition, the electromagnetic radiation can lead to CMB spectral distortions, providing still further constraints. Comparing our results of Figure 1 with the results of the analysis in [58], which summarizes the constraints mentioned above (see in particular the figure 8 in [58]), we see that our analysis rules out an additional region of parameter space; a region which is particularly interesting for large values of the current.

Non-superconducting cosmic strings can provide nonlinear seeds at high redshifts, which could help explain the abundance of super-massive black holes [62]. They could also play a role in the formation of globular clusters [63, 64]. It would be interesting to study to what extent currents on superconducting strings would change those results.

Acknowledgements

The research at McGill is supported in part by funds from NSERC and from the Canada Research Chair program. BC is supported in part by a McGill Space Institute fellowship. RS would like to thank Yifu Cai for helpful discussions. We are grateful to Raul Monsalve for many stimulating discussions and for comments on the manuscript. We also thank Oscar Hernandez, Samuel Laliberté and Disrael Cunha for discussions.

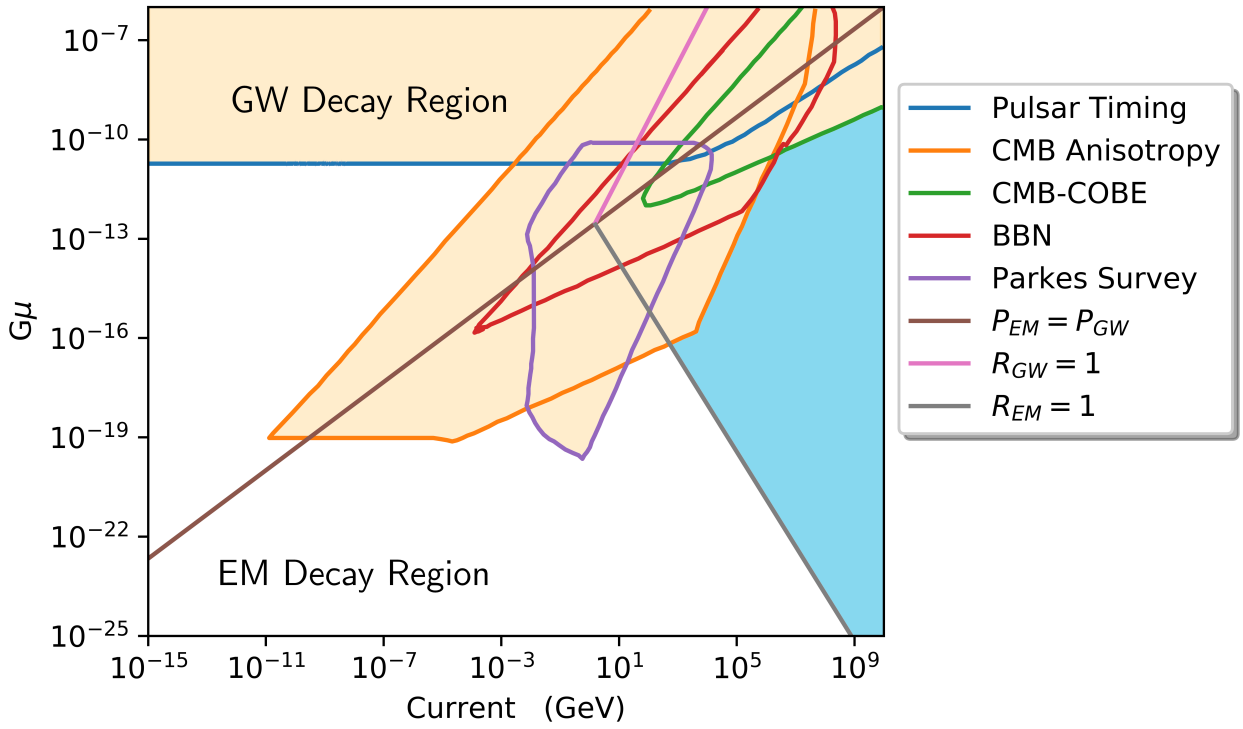

Figure 3.1: The shaded regions show the parameter space of superconducting cosmic strings which are ruled out. The light orange region corresponds to constraints from previously considered sources (see [58] and references therein for these constraints), whereas the light blue correspond to regions that are now ruled out by our analysis, assuming the global 21cm absorption signal is not larger than what was reported by the EDGES collaboration. These new regions are bound by the curves along which $\mathcal{R} = 1$ (see the main text for the definition of $\mathcal{R}$). The vertical axis gives the value of $G\mu$, the horizontal axis is the current. The diagonal brown curve corresponds to the critical current as a function of $G\mu$. Above the curve gravitational radiation is the dominate decay mechanism of the loops. Below it, electromagnetic radiation dominates.

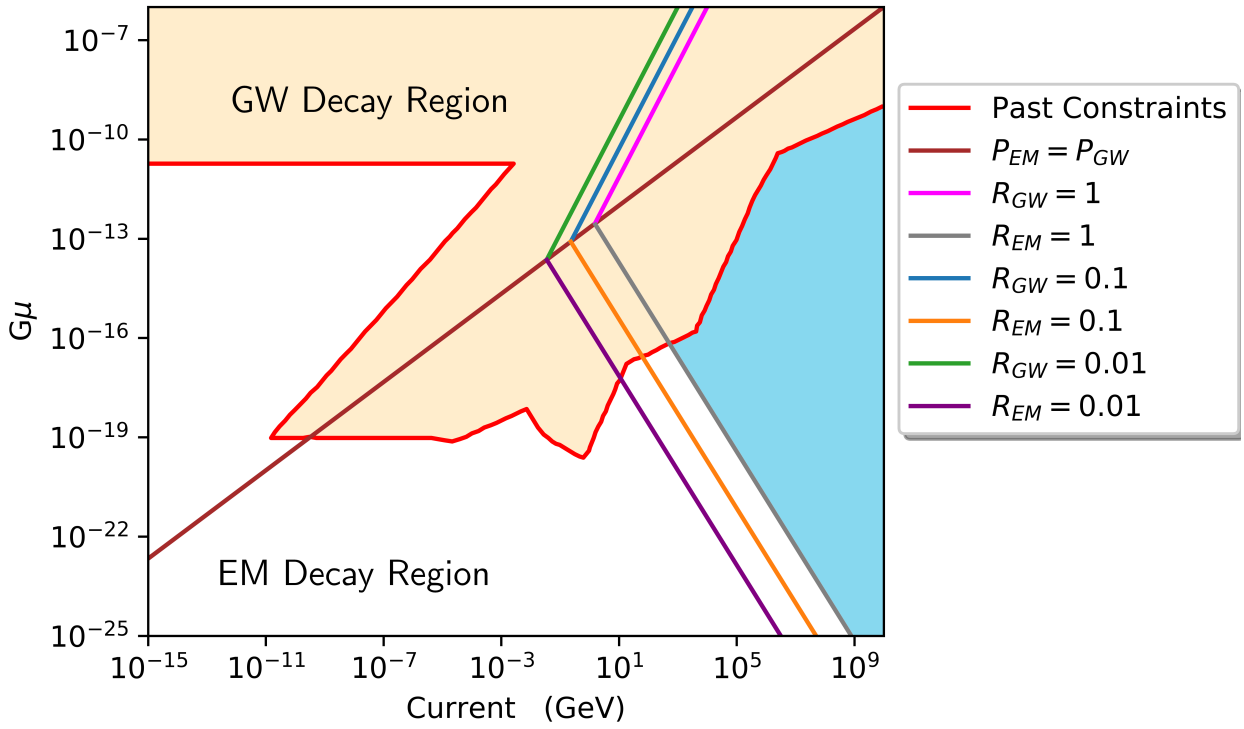

Figure 3.2: The light orange region bounded by the red curve represents the limiting constraints considered by previous works in [58]. The light blue region bounded by the grey curve corresponds to regions of the superconducting string parameter space that constrained via our analysis by requiring $\mathcal{R} \leq 1$. If the signal from strings is less than 10% of what has been reported, the constrained region extends to the orange line (requiring $\mathcal{R} \leq 0.1$). If it is less than 1%, the region extends even further to the purple line ($\mathcal{R} \leq 0.01$). These new constraints all exist in the region where the decay of loops is dominated by their energy loss into EM radiation. Constraints of this analysis from 21cm in the gravitational wave regime are plotted here in magenta, blue, and green, but they do not constrain any regions which haven't been constrained previously.

Bibliography

[1] R. H. Brandenberger, "Searching for Cosmic Strings in New Observational Windows," *Nucl. Phys. B Proc. Suppl.* **246-247** (2014) 45–57, arXiv:1301.2856 [astro-ph.CO].

[2] A. Vilenkin and E. P. S. Shellard, *Cosmic Strings and Other Topological Defects*. Cambridge University Press, 7, 2000.

[3] M. B. Hindmarsh and T. W. B. Kibble, "Cosmic strings," *Rept. Prog. Phys.* **58** (1995) 477–562, arXiv:hep-ph/9411342.

[4] R. H. Brandenberger, "Topological defects and structure formation," *Int. J. Mod. Phys. A* **9** (1994) 2117–2190, arXiv:astro-ph/9310041.

[5] T. W. B. Kibble, "Phase Transitions in the Early Universe," *Acta Phys. Polon. B* **13** (1982) 723.

[6] T. W. B. Kibble, "Some Implications of a Cosmological Phase Transition," *Phys. Rept.* **67** (1980) 183.

[7] R. H. Brandenberger, "Probing Particle Physics from Top Down with Cosmic Strings," *The Universe* **1** no. 4, (2013) 6–23, arXiv:1401.4619 [astro-ph.CO].

[8] E. Witten, "Superconducting Strings," *Nucl. Phys. B* **249** (1985) 557–592.

[9] T. W. B. Kibble and N. Turok, "Selfintersection of Cosmic Strings," *Phys. Lett. B* **116** (1982) 141–143.

[10] A. Vilenkin and T. Vachaspati, "Electromagnetic Radiation from Superconducting Cosmic Strings," *Phys. Rev. Lett.* **58** (1987) 1041–1044.

[11] D. N. Spergel, T. Piran, and J. Goodman, "Dynamics of Superconducting Cosmic Strings," *Nucl. Phys. B* **291** (1987) 847–875.

[12] E. J. Copeland, D. Haws, M. Hindmarsh, and N. Turok, "Dynamics of and Radiation From Superconducting Strings and Springs," *Nucl. Phys. B* **306** (1988) 908–930.

[13] J. J. Blanco-Pillado and K. D. Olum, "Electromagnetic radiation from superconducting string cusps," *Nucl. Phys. B* **599** (2001) 435–445, arXiv:astro-ph/0008297.

[14] N. G. Sanchez and M. Signore, "The Cosmological Microwave Background Radiation, Cosmic and Superconducting Strings," *Phys. Lett. B* **219** (1989) 413–418.

[15] N. G. Sanchez and M. Signore, "The Absence of Distortion in the Cosmic Microwave Background Spectrum and Superconducting Cosmic Strings," *Phys. Lett. B* **241** (1990) 332–335.

[16] H. Tashiro, E. Sabancilar, and T. Vachaspati, "CMB Distortions from Superconducting Cosmic Strings," *Phys. Rev. D* **85** (2012) 103522, arXiv:1202.2474 [astro-ph.CO].

[17] A. Babul, B. Paczynski, and D. Spergel, "Gamma-ray bursts from superconducting cosmic strings at large redshifts," *Astrophys. J. Lett.* **316** (1987) L49–L54.

[18] V. Berezinsky, B. Hnatyk, and A. Vilenkin, "Gamma-ray bursts from superconducting cosmic strings," *Phys. Rev. D* **64** (2001) 043004, arXiv:astro-ph/0102366.

[19] K. S. Cheng, Y.-W. Yu, and T. Harko, "High Redshift Gamma-Ray Bursts: Observational Signatures of Superconducting Cosmic Strings?," *Phys. Rev. Lett.* **104** (2010) 241102, arXiv:1005.3427 [astro-ph.HE].

[20] T. Vachaspati, "Cosmic Sparks from Superconducting Strings," *Phys. Rev. Lett.* **101** (2008) 141301, arXiv:0802.0711 [astro-ph].

[21] L. V. Zadorozhna and B. I. Hnatyk, "Electromagnetic emission bursts from the near-cusp regions of superconducting cosmic strings," *Ukr. J. Phys.* **54** (2009) 1149–1156.

[22] Y.-F. Cai, E. Sabancilar, and T. Vachaspati, "Radio bursts from superconducting strings," *Phys. Rev. D* **85** (2012) 023530, arXiv:1110.1631 [astro-ph.CO].

[23] Y.-F. Cai, E. Sabancilar, D. A. Steer, and T. Vachaspati, "Radio Broadcasts from Superconducting Strings," *Phys. Rev. D* **86** (2012) 043521, arXiv:1205.3170 [astro-ph.CO].

[24] J. Ye, K. Wang, and Y.-F. Cai, "Superconducting cosmic strings as sources of cosmological fast radio bursts," *Eur. Phys. J. C* **77** no. 11, (2017) 720, arXiv:1705.10956 [astro-ph.HE].

[25] Y.-W. Yu, K.-S. Cheng, G. Shiu, and H. Tye, "Implications of fast radio bursts for superconducting cosmic strings," *JCAP* **11** (2014) 040, arXiv:1409.5516 [astro-ph.HE].

[26] L. V. Zadorozhna, "Fast radio bursts as electromagnetic radiation from cusps on superconducting cosmic strings," *Advances in Astronomy and Space Physics* **5** (Sept., 2015) 43–50.

[27] C. T. Hill, D. N. Schramm, and T. P. Walker, "Ultrahigh-Energy Cosmic Rays from Superconducting Cosmic Strings," *Phys. Rev. D* **36** (1987) 1007.

[28] V. Berezinsky, K. D. Olum, E. Sabancilar, and A. Vilenkin, "UHE neutrinos from superconducting cosmic strings," *Phys. Rev. D* **80** (2009) 023014, arXiv:0901.0527 [astro-ph.HE].

[29] A. Albrecht and N. Turok, "Evolution of Cosmic Strings," *Phys. Rev. Lett.* **54** (1985) 1868–1871.

[30] D. P. Bennett and F. R. Bouchet, "Evidence for a Scaling Solution in Cosmic String Evolution," *Phys. Rev. Lett.* **60** (1988) 257.

[31] B. Allen and E. P. S. Shellard, "Cosmic string evolution: a numerical simulation," *Phys. Rev. Lett.* **64** (1990) 119–122.

[32] C. Ringeval, M. Sakellariadou, and F. Bouchet, "Cosmological evolution of cosmic string loops," *JCAP* **02** (2007) 023, arXiv:astro-ph/0511646.

[33] V. Vanchurin, K. D. Olum, and A. Vilenkin, "Scaling of cosmic string loops," *Phys. Rev. D* **74** (2006) 063527, arXiv:gr-qc/0511159.

[34] L. Lorenz, C. Ringeval, and M. Sakellariadou, "Cosmic string loop distribution on all length scales and at any redshift," *JCAP* **10** (2010) 003, arXiv:1006.0931 [astro-ph.CO].

[35] J. J. Blanco-Pillado, K. D. Olum, and B. Shlaer, "Large parallel cosmic string simulations: New results on loop production," *Phys. Rev. D* **83** (2011) 083514, arXiv:1101.5173 [astro-ph.CO].

[36] J. J. Blanco-Pillado, K. D. Olum, and B. Shlaer, "The number of cosmic string loops," *Phys. Rev. D* **89** no. 2, (2014) 023512, arXiv:1309.6637 [astro-ph.CO].

[37] A. Vilenkin, "Cosmological Density Fluctuations Produced by Vacuum Strings," *Phys. Rev. Lett.* **46** (1981) 1169–1172. [Erratum: Phys.Rev.Lett. 46, 1496 (1981)].

[38] N. Turok and R. H. Brandenberger, "Cosmic Strings and the Formation of Galaxies and Clusters of Galaxies," *Phys. Rev. D* **33** (1986) 2175.

[39] H. Sato, "Galaxy Formation by Cosmic Strings," *Prog. Theor. Phys.* **75** (1986) 1342.

[40] A. Stebbins, "Cosmic Strings and Cold Matter," *apjl* **303** (1986) L21.

[41] E. J. Copeland, T. W. B. Kibble, and D. Austin, "Scaling solutions in cosmic string networks," *Phys. Rev. D* **45** (1992) 1000–1004.

[42] L. Perivolaropoulos, "COBE versus cosmic strings: An Analytical model," *Phys. Lett. B* **298** (1993) 305–311, arXiv:hep-ph/9208247.

[43] D. Austin, E. J. Copeland, and T. W. B. Kibble, "Evolution of cosmic string configurations," *Phys. Rev. D* **48** (1993) 5594–5627, arXiv:hep-ph/9307325.

[44] T. Vachaspati and A. Vilenkin, "Gravitational Radiation from Cosmic Strings," *Phys. Rev. D* **31** (1985) 3052.

[45] Y.-F. Cai, E. Sabancilar, D. A. Steer, and T. Vachaspati, "Radio Broadcasts from Superconducting Strings," *Phys. Rev. D* **86** (2012) 043521, arXiv:1205.3170 [astro-ph.CO].

[46] R. H. Brandenberger, "On the Decay of Cosmic String Loops," *Nucl. Phys. B* **293** (1987) 812–828.

[47] J. D. Bowman, A. E. E. Rogers, R. A. Monsalve, T. J. Mozdzen, and N. Mahesh, "An absorption profile centred at 78 megahertz in the sky-averaged spectrum," *Nature* **555** no. 7694, (2018) 67–70, arXiv:1810.05912 [astro-ph.CO].

[48] R. A. Monsalve, B. Greig, J. D. Bowman, A. Mesinger, A. E. E. Rogers, T. J. Mozdzen, N. S. Kern, and N. Mahesh, "Results from EDGES High-Band: II. Constraints on Parameters of Early Galaxies," *Astrophys. J.* **863** no. 1, (2018) 11, arXiv:1806.07774 [astro-ph.CO].

[49] R. Brandenberger, B. Cyr, and T. Schaeffer, "On the Possible Enhancement of the Global 21-cm Signal at Reionization from the Decay of Cosmic String Cusps," *JCAP* **04** (2019) 020, arXiv:1810.03219 [astro-ph.CO].

[50] S. Furlanetto, S. P. Oh, and F. Briggs, "Cosmology at Low Frequencies: The 21 cm Transition and the High-Redshift Universe," *Phys. Rept.* **433** (2006) 181–301, arXiv:astro-ph/0608032.

[51] O. F. Hernández, "Wouthuysen-Field absorption trough in cosmic string wakes," *Phys. Rev. D* **90** no. 12, (2014) 123504, arXiv:1403.7522 [astro-ph.CO].

[52] A. Ewall-Wice, T. C. Chang, J. Lazio, O. Dore, M. Seiffert, and R. A. Monsalve, "Modeling the Radio Background from the First Black Holes at Cosmic Dawn: Implications for the 21 cm Absorption Amplitude," *Astrophys. J.* **868** no. 1, (2018) 63, arXiv:1803.01815 [astro-ph.CO].

[53] A. Fialkov, R. Barkana, and A. Cohen, "Constraining Baryon–Dark Matter Scattering with the Cosmic Dawn 21-cm Signal," *Phys. Rev. Lett.* **121** (2018) 011101, arXiv:1802.10577 [astro-ph.CO].

[54] R. Barkana, N. J. Outmezguine, D. Redigolo, and T. Volansky, "Strong constraints on light dark matter interpretation of the EDGES signal," *Phys. Rev. D* **98** no. 10, (2018) 103005, arXiv:1803.03091 [hep-ph].

[55] S. Fraser *et al.*, "The EDGES 21 cm Anomaly and Properties of Dark Matter," *Phys. Lett. B* **785** (2018) 159–164, arXiv:1803.03245 [hep-ph].

[56] C. Feng and G. Holder, "Enhanced global signal of neutral hydrogen due to excess radiation at cosmic dawn," *Astrophys. J. Lett.* **858** no. 2, (2018) L17, arXiv:1802.07432 [astro-ph.CO].

[57] D. J. Fixsen *et al.*, "ARCADE 2 Measurement of the Extra-Galactic Sky Temperature at 3-90 GHz," *Astrophys. J.* **734** (2011) 5, arXiv:0901.0555 [astro-ph.CO].

[58] K. Miyamoto and K. Nakayama, "Cosmological and astrophysical constraints on superconducting cosmic strings," *JCAP* **07** (2013) 012, arXiv:1212.6687 [astro-ph.CO].

[59] **NANOGrav** Collaboration, Z. Arzoumanian *et al.*, "The NANOGrav Nine-year Data Set: Limits on the Isotropic Stochastic Gravitational Wave Background," *Astrophys. J.* **821** no. 1, (2016) 13, arXiv:1508.03024 [astro-ph.GA].

[60] **Planck** Collaboration, N. Aghanim *et al.*, "Planck 2018 results. VI. Cosmological parameters," *Astron. Astrophys.* **641** (2020) A6, arXiv:1807.06209 [astro-ph.CO]. [Erratum: Astron.Astrophys. 652, C4 (2021)].

[61] H. Tashiro, E. Sabancilar, and T. Vachaspati, "Constraints on Superconducting Cosmic Strings from Early Reionization," *Phys. Rev. D* **85** (2012) 123535, arXiv:1204.3643 [astro-ph.CO].

[62] S. F. Bramberger, R. H. Brandenberger, P. Jreidini, and J. Quintin, "Cosmic String Loops as the Seeds of Super-Massive Black Holes," *JCAP* **06** (2015) 007, arXiv:1503.02317 [astro-ph.CO].

[63] L. Lin, S. Yamanouchi, and R. Brandenberger, "Effects of Cosmic String Velocities and the Origin of Globular Clusters," *JCAP* **12** (2015) 004, arXiv:1508.02784 [astro-ph.CO].

[64] A. Barton, R. H. Brandenberger, and L. Lin, "Cosmic Strings and the Origin of Globular Clusters," *JCAP* **06** (2015) 022, arXiv:1502.07301 [astro-ph.CO].

Part III

High Energy Signatures of Cosmic Textures

Chapter 4

Cosmic Rays and Spectral Distortions from Collapsing Textures

R.H. Brandenberger, B. Cyr, and H. Jiao, *Cosmic Rays and Spectral Distortions from Collapsing Textures*, JCAP 09 (2020) 035, [arXiv:2005.11099].

Addendum for thesis

This chapter moves away from the study of cosmic strings, instead focussing on a different class of topological defect known as a cosmic texture. Unlike cosmic strings, all of the energy in a texture configuration is stored in the gradients, there is no region of space that is trapped in a false vacuum. Cosmic textures are unstable to collapse, and are capable of releasing a significant amount of energy into photons when they do.

Preceding this work, R. Brandenberger and H. Jiao had been investigating the impacts of galaxy and black hole formation from collapsing textures. This work is an extension of their investigation, where we studied the electromagnetic consequences of texture collapse.

These collapse events happen continuously after the initial symmetry breaking, and so their energetics create different signals at different times. Textures which release energy after recombination will create a diffuse gamma ray background, which was the main object of study for H. Jiao and R. Brandenberger in this project. Alternatively, textures collapsing before recombination will source distortions to the blackbody spectrum of the cosmic microwave background, a signature that I studied in depth. We derived strong constraints on the symmetry breaking scale for cosmic textures by considering next-generation CMB spectral distortion experiments.

Abstract

We compute the energy spectrum of photons and neutrinos produced by the unwinding of a scaling distribution of cosmic textures, and discuss the implications for the spectrum of high energy cosmic rays, and for CMB spectral distortions. Textures lead to a contribution to the photon flux which scales as $E^3F(E) \sim E^{3/2}$. Hence, the tightest constraints on the texture model come from the highest energies from which primordial photons can reach us without being scattered by the CMB and other foregrounds. Textures lead to both μ type and y type distortions. While the constraints on the texture model coming from the current COBE bounds are weaker than the bounds from the angular power spectrum of the CMB, future surveys such as PIXIE can lead to stronger bounds. The high energy neutrino flux is constrained by data from the Pierre Auger experiment and yields a bound on the energy scale of textures which is competitive with CMB bounds.

4.1 Introduction

It is of great interest to study the cosmological consequences of particle physics models beyond the Standard Model which have defect solutions. The defects which inevitably form in the early universe in such models persist to the present time and lead to signatures in cosmological surveys. Thus, the study of topological defects in cosmology leads to a close connection between particle physics and cosmology (see e.g. [1] for a discussion). If evidence for defects is found in observations, we would learn which class of particle physics models beyond the Standard Model is favored. If the predicted signatures are not found, we can constrain the energy scale of particle physics models which predict the signatures. Particle physics models which predict domain wall solutions are already ruled out by cosmology [2], since they would overclose the universe. Models which predict monopoles are also constrained [3]. There has been a lot of work on the cosmological signatures of cosmic strings (see e.g. [4, 5, 6, 7]). Here, we will focus on another class of defects, namely global textures.

Low energy effective field theories in which a global symmetry is spontaneously broken such that the vacuum manifold $\mathcal{M}$ has a nontrivial third homotopy group $\Pi_3(\mathcal{M})$ admit defect solutions called *global textures* [8] (see e.g. [6, 7] for reviews of the cosmology of topological defects, including discussions of textures). Like global monopoles, textures are extended configurations of field energy with the topology of a sphere. By causality [9, 10], textures will form during the symmetry breaking phase transition in the early universe, and their initial radial extent will be comparable to the Hubble radius. The same causality

argument implies that at all late times there will be of the order one texture per Hubble volume. Hence, textures can leave potentially observable imprints even at late times.

In contrast to global string and global monopole defects, textures are not stable. A texture with initial size comparable to the Hubble radius at time t will collapse at close to the speed of light and "unwind". In this process, a fraction of the initial energy stored in the texture configuration will be released as particles. An order one fraction of the released energy ends up in the form of photons, including high energy photons and ultra-high energy neutrinos. Photons emitted in the redshift interval between $z = 10^6$ and the redshift of recombination will lead to spectral distortions of the Cosmic Microwave Background (CMB). In this paper, we compute the spectrum of high energy gamma rays produced by texture collapse, and we estimate the magnitude of the induced spectral distortions.

An example of a low energy theory which has texture solutions is quantum chromodynamics (QCD). In the limit of massless quarks, the theory has a global $SU(3) \times SU(3)$ symmetry which gets spontaneously broken to the diagonal subgroup $SU(3)$, in the process generating an octet of pseudoscalar mesons which are the Goldstone bosons of the symmetry breaking. In theories beyond the Standard Model of particle physics there may be similar global symmetries which are spontaneously broken at an energy scale η, an energy scale of new physics. Since texture configurations contain trapped energy, they can contribute to structure formation in the early universe [8, 11, 12] and induce cosmic microwave background (CMB) anisotropies. The induced CMB anisotropies have an angular power spectrum which do not have [13, 14, 15] the acoustinc oscillations which have been observed. Hence, observations of CMB anisotropies lead to an upper bound on the energy scale η of new physics with texture solutions [16]. Textures with an energy scale slightly lower than the upper bound may, however, help explain the observed cold spot in the CMB maps [17]. Since textures form nonlinear density perturbations at arbitarily early times, they may contribute to the seeds for the observed super-massive black holes at high redshifts (in the same way that cosmic string loops can [18]). This was discussed in a recent paper [19] by two of us. In fact, there is a range of values of η where the number density of nonlinear seed fluctuations at high redshifts is larger than that produced in the standard ΛCDM paradigm of early universe cosmology.

Whereas most work done on the cosmological implications of textures has focused on their gravitational effects, here we will study effects on the electromagnetic spectrum. We compute the spectrum of induced high energy cosmic rays and compare our results with the observational bounds, and we estimate the amplitude of the induced spectral distortions of the CMB.

We begin this article with a brief review of textures, focusing on the scaling solution which is achieved. In Section 3 we then compute the spectrum of photons and neutrinos emitted from textures collapsing. In the case of photons, the relevant collapse time begins at the time of recombination. As neutrino decoupling takes place long before recombination, collapsing textures in the primordial plasma will also contribute to their production. In Section 4 we compute the total energy released by textures collapsing during the time interval when the emitted photons can produce spectral distortions. We conclude with a discussion section.

We use natural units in which the speed of light, Planck's constant and Boltzmann's constant are all set to 1. We work in the context of a Friedmann-Lemaitre-Robertson-Walker metric

$$ds^2 \,=\, dt^2 - a(t)^2 d\mathbf{x}^2 \,, \tag{4.1}$$

where t is physical time, $\mathbf{x}$ are comoving spatial coordinates (we assume that the spatial curvature vanishes), and $a(t)$ is the scale factor in terms of which the Hubble parameter is defined as

$$H(t) \,=\, \frac{\dot{a}}{a} \,, \tag{4.2}$$

and its inverse is the Hubble radius. We often work in terms of the cosmological redshift $z(t)$ defined by

$$\frac{a(t_0)}{a(t)} \,\equiv\, z(t) + 1 \,. \tag{4.3}$$

4.2 Review of Global Textures and their Scaling Solution

To get a feeling for what a global texture is, consider a scalar field theory with four real scalar fields ϕ_i and a symmetry breaking potential of the standard form

$$V(\phi) \,=\, \frac{\lambda}{4}\left(\sum_{i=1}^{4} \phi_i^2 - \eta^2\right)^2 \,, \tag{4.4}$$

where η is the symmetry breaking scale and λ is a dimensionless coupling constant. At high temperatures, finite temperature corrections to the potential force $\phi(x) = 0$ at all points in space. Below the critical temperature which is of the order η (modulo coupling constants) the confining force disappears and $\phi(x)$ rolls down to a minimum of its potential. The space of field values which minimize the potential energy is called the vacuum manifold $\mathcal{M}$ and is

given by

$$\mathcal{M} = \left[\phi \;\middle|\; \sum_{i=1}^{4} \phi_i^2 = \eta^2 \right] \tag{4.5}$$

which in our case is a three sphere S^3. It has the property that the third homotopy group is nontrivial

$$\Pi_3(\mathcal{M}) \neq 1 \,. \tag{4.6}$$

All field theories with the property (4.6) have texture solutions.

By causality [9, 10] there can be no correlation on scales larger than the Hubble radius. Hence, there is a finite probability c of the order one that in any Hubble volume the field $\phi(x)$ covers the entire vacuum manifold [1]. Such a configuration winds the entire vacuum manifold.

For our Lagrangian, a texture configuration with winding number 1 and with spherically symmetric energy distribution is

$$\phi(t, x, y, z) = \eta \left(\cos\chi(r), \frac{x}{r}\sin\chi(r), \frac{y}{r}\sin\chi(r), \frac{z}{r}\sin\chi(r) \right) \tag{4.7}$$

where $r^2 = x^2 + y^2 + z^2$. The radial function vanishes at the origin (i.e. $\chi(0) = 0$) and tends to the value π as $r \to \infty$. The *effective radius* of the texture can be defined to be the radius where $\chi(r_c) = \pi/2$, i.e. the radius r_c where the texture configuration (restricted to the sphere of radius r_c in space) wraps the equator sphere of the vacuum manifold $\mathcal{M}$.

Note that, unlike for monopole, cosmic string and domain wall defects, in the case of textures it is possible for the scalar field to be everywhere in the vacuum manifold. Hence, there is no trapped potential energy, but only gradient energy. In the case of theories with a local symmetry, the gradient energy in the scalar field can be locally compensated by the gauge fields, and hence there are no well-localized local texture configurations.

The total gradient energy in the texture configuration (4.7) can decrease if r_c decreases. Since we are dealing with relativistic field theories, the speed of contraction is of the order of the speed of light. The energy density of the collapsing texture configuration becomes [22]

$$\rho(r, s) \simeq 2\frac{r^2 + 3s^2}{(r^2 + s^2)^2}\eta^2 \tag{4.8}$$

where s is the shifted time such that the collapse happens at $s = 0$. This formula is a good approximation up the radius r_c.

[1] The study of [20, 21] shows that the probability is approximately $c \simeq 0.04$.

As $s \to 0$ the gradient energy density (4.8) of the collapsing texture diverges at the origin. When the energy density at the origin becomes comparable to the potential energy, it becomes favourable for the texture configuration to "unwind", i.e. $\phi(x)$ in a region close to the center leaves the vacuum manifold and χ jumps from $\chi \sim 0$ to $\chi \sim \pi$. The time when this happens is [19]

$$s_{uw} \sim \sqrt{6\lambda^{-1}}\eta^{-1}\,, \tag{4.9}$$

and the radius of the central region where the unwinding happens is

$$r_{uw} \sim \lambda^{-1/2}\eta^{-1}\,. \tag{4.10}$$

After the unwinding, the field configuration is no longer topologically confined, and will radiate outwards. The total energy in a texture is obtained by integrating (4.8) from $r = 0$ to $r = r_c$, setting $s = r_c$ (the collapse time). The result is

$$E \sim 8\pi\eta^2 r_c\,. \tag{4.11}$$

For a texture becoming dynamical at the time t_f we can set $r_c \simeq t_f/2$, and hence the amount of energy released by a texture forming at time t_f is

$$E(t_f) \sim 4\pi\eta^2 t_f\,. \tag{4.12}$$

Textures first form during the symmetry breaking phase transition. For any sphere in space with radius R, there is a probability c of the order one that the configuration of ϕ in that sphere will wind the vacuum manifold and that hence a texture will form. Textures with radius smaller than the Hubble radius, i.e. $R < t$ will collapse. However, by causality the field configuration on larger scales is still random. Hence, at all times t, there will be a probability c that a texture of size $r_c \sim t$ will form and start to contract. This process of texture configurations entering the Hubble radius, becoming dynamical and starting to collapse will continue to the present time. This is the *scaling solution* for textures: at any time t after the phase transition, there will be c textures per Hubble radius of roughly Hubble size which begin to contract and unwind within a Hubble time. In the following we will compute the spectrum of cosmic rays produced by this scaling solution of textures.

4.3 Spectrum of Cosmic Rays Produced by Texture Collapse

The primary particles which result from the texture unwinding are ϕ quanta. The particles associated with ϕ are, however, unstable, and their decay will generate a jet of Standard Model elementary particles, in particular photons. This process is similar to the production of a jet of low energy particles in laboratory decays of unstable particles, or from the annihilation of a cosmic string cusp [23]. In the case of cosmic string cusp decay, the spectrum of resulting photons and neutrinos was computed in [24] and [25], respectively. Here we will perform a similar calculation for the photon and neutrino fluxes resulting from texture decay.

To obtain the spectra of photons and neutrinos from a texture collapse we assume that the primary particles released (the ϕ particles) decay into jets of Standard Model quarks and leptons, and that these then produce photons and neutrinos in agreement with the QCD multiplicity functions. Following [26], we take the spectra at energies $E < \eta$ from a texture collapsing at time t_f to be given by

$$\frac{dN}{dE'}(E', t_f) \, = \, \frac{f_i}{2} E(t_f) \left(\frac{\eta}{E'} \right)^{3/2} \frac{1}{\eta^2} \, , \tag{4.13}$$

where $N(E', t_f)$ is the number per unit energy interval of photons or neutrinos of energy E' at time t_f, and f_i is the fraction of the energy of texture annihilation which goes into photons $f_i = f_e$ and neutrinos $f_i = f_\nu$, respectively. The above fragmentation functions hold for energies larger than the mass of the π_0 meson.

Let us first consider the photon spectrum. If we want the energy density $d\rho/dE$ for unit interval of energy at energy E and time t, then we have to integrate over all texture formation times t_f. For each value of t_f, we need to consider the number of photons with energy E' at time t_f which redshifts to E at time t. We must finally take into account the redshifting of the number density of the produced photons. In this way, we get

$$\frac{d\rho}{dE}(E, t) \, = \, E \int_{t_i(E,t)}^{t} dt_f \frac{dN}{dE'}(E', t_f) c t_f^{-4} \frac{dE'}{dE} \left(\frac{z(t)}{z(t_f)} \right)^3 \, , \tag{4.14}$$

where we have used the fact that there are c textures for Hubble volume per Hubble time (thus giving the factors ct_f^{-4} in the above, and the Jacobian of the transformation between

E' and E. Note that in the above

$$E' \;=\; \frac{z(t_f)}{z(t)} E\,. \tag{4.15}$$

The time $t_i(E,t)$ is the larger of the following two times: the time t_c of the phase transition, and the time $t_b(E,t)$ before which all photons emitted by a texture have redshifted energy less than E by the time t. This time is given by

$$\frac{z(t_b(E,t))}{z(t)} \;=\; \frac{\eta}{E}\,. \tag{4.16}$$

Inserting (5.10) and (4.12) into (4.14) we obtain

$$\frac{d\rho}{dE}(E,t) \;\sim\; 2\pi c f_e \eta^{3/2} E^{-1/2} \int_{t_i(E,t)}^{t} dt_f t_f^{-3} \left(\frac{z(t)}{z(t_f)}\right)^{7/2}\,. \tag{4.17}$$

Evaluating the result for times before the time t_{eq} of equal matter and radiation we obtain

$$\frac{d\rho}{dE}(E,t) \;\sim\; 8\pi c f_e \eta^{3/2} E^{-1/2} t^{-2} \left[\left(\frac{t}{t_i(E,t)}\right)^{1/4} - 1\right]\,, \tag{4.18}$$

the time integral being dominated by the lower integration end.

For $t > t_{eq}$ we divide the integration over t_f into the interval before t_{eq} and the interval after t_{eq}. The contribution of textures at $t_f > t_{eq}$ gives

$$\frac{d\rho}{dE}(E,t) \;\sim\; 6\pi c f_e \eta^{3/2} E^{-1/2} t^{-2} \left[1 - \left(\frac{t_{eq}}{t}\right)^{1/3}\right]\,, \tag{4.19}$$

assuming that $t_i(E,t) < t_{eq}$. If $t_i(E,t) > t_{eq}$, then the factor t_{eq} in the above is replaced by $t_i(E,t)$.

The contribution from textures formed before t_{eq} gives

$$\begin{aligned} \frac{d\rho}{dE}(E,t) \quad &\sim \quad 8\pi c f_e \eta^{3/2} E^{-1/2} t^{-2} \\ &\left(\frac{t_{eq}}{t_i(E,t)}\right)^{1/4} \left(\frac{t_{eq}}{t}\right)^{1/3} \left[1 - \left(\frac{t_i(E,t)}{t_{eq}}\right)^{1/4}\right]\,. \end{aligned} \tag{4.20}$$

If we are interested in the spectrum of high energy cosmic rays today, then photons released from textures before t_{eq} do not contribute. Those released before a redshift of $z \sim 10^6$ will thermalize, and those created between that redshift and recombination will scatter off the

plasma and lead to spectral distortions of the CMB (as studied in the next section), but they will not survive as primary cosmic rays. Hence, in the following we will only consider the contribution (4.19).

We now compare the predicted cosmic ray flux from textures with the observational upper bounds. These bounds are usually expressed in terms of the flux $F(E)$, where

$$F(E) \,=\, E^{-1} \frac{d\rho}{dE} \,. \tag{4.21}$$

Since the measured flux and the upper flux limits decay rapidly as a function of E, the quantity which is usually used is $E^3 F(E)$. From (4.19) we see that the texture model predicts

$$E^3 F(E) \,\sim\, 6\pi c f_e (E\eta)^{3/2} t^{-2} \,, \tag{4.22}$$

which is a rapidly increasing function of E. Hence, the tightest bounds will come from the largest values of E. There is a caveat, however: as discussed in detail in [27], photons energies greater than about 10^2GeV cannot travel over cosmological distances. They scatter off the CMB and off the infrared and optical backgrounds. Hence, the strongest (but conservative) bound on the symmetry breaking scale η will come from comparing our predictions with the observational limits at $E = 10^2$GeV which are [27, 28, 29] (in the usual units used in cosmic ray physics)

$$E^3 F(E) \,<\, 10^{21} b \ \mathrm{eV}^2 \mathrm{m}^{-2} \mathrm{sec}^{-1} \mathrm{sr}^{-1} \,, \tag{4.23}$$

where we have introduced a factor b to take into account future improvements of the bound (at the moment the bound is $b = 1$). Comparing the prediction (4.22) with the observational bound (4.23) we obtain

$$G\eta^2 \,<\, \left(\frac{1}{6\pi c f_e} \right)^{4/3} 10^{7/3} b^{4/3} \left(\frac{E_2}{E} \right)^2 \,, \tag{4.24}$$

where $E_2 = 10^2$GeV. At the present time, using $b = 1$, $f_e \sim 1$ and $E = E_2$, there is no bound on the symmetry breaking scale η (since $G\eta^2$ cannot be larger than unity). This result contrasts with actual bounds [16] which come from the effects of textures on the angular power spectrum of the CMB. If scattering off of the infrared and optical backgrounds is neglected, then the photon spectra could be extrapolated up to $E = 10^5$GeV. In this case, for $f \sim 1$ there would be a bound of the form (with $b = 1$)

$$G\eta^2 \,<\, 10^{-4} \,, \tag{4.25}$$

which is still a few orders of magnitude weaker than the bound coming from the CMB.

The calculation of the high energy neutrino flux is completely analogous to the computation of the photon flux after replacing f_e by f_ν. However, neutrinos can reach us from much earlier times. For energies $E < z_{eq}^{-1}\eta$, the earliest textures producing neutrinos which today have energy E were formed at a time $t_i(E)$ given by

$$t_i(E) = t_{eq} z_{eq}^2 \left(\frac{E}{\eta}\right)^2 . \tag{4.26}$$

Inserting this result into (4.20) yields

$$E^3 F(E) \simeq 8\pi f_\nu c E \eta^2 z_{eq}^{-1} t_0^{-2} . \tag{4.27}$$

We can derive an upper bound on $G\eta^2$ by demanding that the flux (4.27) be smaller than the upper bound which follows from the Pierre Auger experiment. This experiment detected no ultra-high energy neutrino events in the accessible energy range $10^8\text{GeV} < E < 2.5 \times 10^{10}\text{GeV}$ and obtained the bound [30]

$$E^3 F(E) < 6.4 \times 10^{21} E_8 \ \text{eV}^2\text{m}^{-2}\text{s}^{-1}\text{sr}^{-1} , \tag{4.28}$$

where E_8 is the value of the energy in units of 10^8GeV. Comparing this bound with the predicted flux from (4.27) yields the constraint

$$G\eta^2 < \frac{1}{f_\nu} 10^{-9} , \tag{4.29}$$

which is in fact slightly stronger than the bound from the CMB, as long as the neutrino fragmentation fraction f_ν is not much smaller than 1. Note that the range of values of η which are ruled out by the above constraint are in the range for which $E < z_{eq}^{-1}\eta$ is satisfied for the value of the energy $E = 10^8$GeV, a condition which was assumed in the calculation. This is a self-consistency check of our analysis.

To conclude our discussion of limits from ultra-high energy neutrinos, we must check that the neutrinos indeed can travel freely until the present time beginning at the redshift $z(t_i(E))$. As discussed in [25], the neutrino free streaming redshift $z_{IA}(E)$ below which neutrinos of energy E can freely stream to us is given by

$$z_{IA} \sim 3 \times 10^{10} \left(\frac{E}{1\text{GeV}}\right)^{0.35} . \tag{4.30}$$

Evaluated at the energy $E = 10^8$GeV we find that neutrino interactions are indeed negligible (i.e. $z_{IA} > z(t_i(E))$) if η is smaller than about 10^{16}GeV. Larger values of η are not of great interest to us since textures with such a scale are already ruled out by the CMB data.

4.4 Induced Spectral Distortions

Photons emitted in the redshift range between $z_1 \simeq 3 \times 10^6$ and the time of recombination cannot fully thermalize and give rise to CMB spectral distortions[2]. Roughly speaking, those emitted between z_1 and $z_2 \sim 10^5$ yield μ distortions, those emitted between z_2 and recombination give rise to y distortions (see e.g. [32] [33] for reviews).

A μ distortion is sourced when energy release occurs in a redshift window where photon number changing interactions (Bremsstrahlung and double Compton scattering) are frozen out, and only a kinetic equilibrium can be reached in the photon plasma. The spectrum then acquires a Bose-Einstein like correction, where the μ parameter is given by the expression

$$\mu \equiv -\frac{1}{0.7}\int_{z_{\rm C}}^{\infty} dz \frac{1}{\rho_\gamma}\frac{dU}{dz}\cdot e^{-(z/z_{\rm DC})^{5/2}}, \tag{4.31}$$

Where ρ_γ is the usual photon energy density at a redshift z, while $z_{\rm DC} \approx 2 \times 10^6$ is the approximate redshift at which double Compton scattering freezes out for the usual values of Helium abundance and matter energy density. $z_{\rm C} \approx 10^5$ is the redshift that Compton scattering freezes out, marking an end to the μ era. Finally, dU/dz is the rate of energy density injection from the decay of cosmic textures, given by

$$\frac{dU}{dz} = -8\pi c f_e \frac{\eta^2}{t_0^2} z^3 \tag{4.32}$$

This is computed by taking the number density of textures per unit time and multiplying by their individual energy release, so at the time of formation, t_f, we have $dU/dt_f = ct_f^{-4}\cdot E(t_f)$. We also consider the fact that textures produced in the μ distortion window will collapse within a Hubble time, releasing a fraction, f, of their energy into photons. The exponential in (4.31) acts to damp out contributions for $z > z_{\rm DC}$, so with this in mind we can find that the induced μ distortion is

$$\mu \approx \frac{8\pi}{0.7} c f_e (G\eta^2) \ln\left(\frac{z_{\rm DC}}{z_{\rm C}}\right) \sim 6 f (G\eta^2) \tag{4.33}$$

[2]The effect is similar to the one produced by cusp annihilation from cosmic string loops which has been studied in [31].

Where we have made use of $c \approx 0.04$, and noting that the CMB energy density at redshift z is $\rho_\gamma \approx (3/4)G^{-1}t_0^{-2}z^4$.

A primordial[3] y-distortion is induced in the CMB spectrum for energy releases in the redshift range between recombination and $z_{\rm C}$, as we are no longer able to even sustain a kinetic equilibrium in the photon plasma. This distortion is primarily sourced by the fact that external energy injection heats up the pre-recombination electrons, which transfer their non-thermal energy to the rest of the photons. Traditionally, the y parameter is written as

$$y = \int_{t_{\rm C}}^{t_{\rm rec}} dt \frac{T_e - T}{m_e} n_e \sigma_T \tag{4.34}$$

where T_e is the electron temperature, T is the CMB photon temperature, n_e is the number density of free electrons at time t, and σ_T is the Thomson scattering cross section. It is manifest from this expression that a decoupling between the electron and photon temperatures will induce a y-distortion. Under reasonable assumptions (neglecting cosmic expansion when compared to the timescale of Compton scattering, and assuming the injected photons perturb the electron temperature only slightly), one can recast this expression in a more applicable way to energy release scenarios

$$y \approx -\frac{1}{4}\int_{z_{\rm rec}}^{z_{\rm C}} dz \frac{1}{\rho_\gamma}\frac{dU}{dz} \tag{4.35}$$

Since the energy release mechanism we have is insensitive to the transition between the y and μ eras, we can simply use (4.32) once again to compute our contribution to the y distortion. Doing this yields

$$y \approx \frac{8\pi}{3} c f_e(G\eta^2) \ln\left(\frac{z_{\rm C}}{z_{\rm rec}}\right) \sim 1.5 f(G\eta^2) \tag{4.36}$$

At the present time, the best bounds on μ and y are from the COBE satellite

$$\mu < 9 \times 10^{-5}\,, \quad \text{COBE} \tag{4.37}$$

$$y < 10^{-5}\,, \qquad \text{COBE} \tag{4.38}$$

Of these two bounds, the y distortion yields the tightest constraint on the parameter space

$$f_e(G\eta^2) < 6.7 \times 10^{-6}\,. \tag{4.39}$$

[3]y-distortions are also sourced after recombination, for example through the upscattering of CMB photons as they pass through hot clumps of electrons in our line-of-sight

Given that $f_e < 1$, this bound is slightly weaker than the constraint which comes from the CMB angular power spectrum. The proposed PIXIE experiment will have a sensitivity of [34]

$$\mu < 10^{-8}\,, \;\; \text{PIXIE}\,, \tag{4.40}$$

$$y < 2 \times 10^{-9}\,, \;\; \text{PIXIE}\,, \tag{4.41}$$

and with this experiment the bound on the scale η could be strengthened to read (this time from the proposed sensitivity on the μ parameter)

$$f_e(G\eta^2) < 1.7 \times 10^{-9}\,, \tag{4.42}$$

If no distortions are seen. This bound would be significantly stronger than the current bounds from the CMB. Since these textures would decay through the entire (μ and y) distortion window, they could be probed even more precisely as decays around $z_{\rm C}$ may encode information on the exact time dependence of the energy release. A lack of a detection of this form would put serious constraints on symmetry breaking patterns that would give rise to textures in the early universe.

Note that due to their feeble interactions with the primordial plasma, neutrinos from texture collapse do not lead to any spectral distortions.

4.5 Conclusions and Discussion

We have studied the emission of photons and neutrinos from a network of unwinding cosmic textures. We computed the spectrum of high energy cosmic rays and compared the results with the current observational bounds. For photons, the bounds satisfied for all values of the energy scale η of the textures which are compatible with the constraints from the angular power spectrum of the CMB. In the case of neutrinos, we obtain an upper bound on the symmetry breaking scale η which is comparable (and possibly slightly stronger) than the bounds from the CMB angular power spectrum. We then computed the induced spectral distortions of the CMB produced by textures unwinding in the redshift interval between $z = 10^6$ and recombination. Whereas the current bounds from the COBE experiment are not competitive with the CMB angular power spectrum constraint, future missions such as PIXIE will be able to yield stronger constraints on η.

The photon flux from unwinding textures can effect more cosmological observables. For example, the extra photon radiation at radio wavelengths may lead to an absorption feature

[35] in the global 21cm signal, in the same way that decaying cosmic string loops may yield such a signal [36, 37, 38]. It is unlikely, however, that unwinding events can explain the origins of fast radio bursts (FRBs), as the decay pattern to low energy photons suffers from similar problems to those photons produced off of cosmic string cusps [39]. On top of that, the number density of these undwinding events is much smaller than that of string loops studied in [39], and so this model would also suffer from being unable to explain the current number densities of FRBs.

Global monopoles [40] are monopole defects in a theory with a global symmetry. The number density and topology of these defects is similar to that of textures. Note that for a global monopole, the total energy of a monopoe is also comparable to that of a texture because the energy is dominated by the long range gradients, as it is for global textures. Whereas global monopoles are stable, unlike textures, monopole-antimonopole annihilation will lead to a scaling solution of defects very similar to that of textures, except that the constant c describing the number density of these defects, will be different ($c \sim 1.2$ [41]). The spectrum of cosmic rays and the induced CMB spectral distortions will hence be analogous to the ones studied here. Since the value of c is larger by a factor of about 30, the resulting bounds on $G\eta^2$ will be tighter by a similar factor.

Acknowledgement

RB wishes to thank the Pauli Center and the Institutes of Theoretical Physics and of Particle- and Astrophysics of the ETH for hospitality. The research of RB at McGill is supported in part by funds from NSERC and from the Canada Research Chair program. BC thanks support from a Vanier-CGS fellowship and from NSERC. HJ is supported in part by the Undergraduate Education Office of USTC. She also wishes to thank Professor Lavinia Heisenberg for an invitation to the ETH. We wish to thank an anonymous referee for suggesting we consider not only the photon but also the neutrino spectrum.

Bibliography

[1] R. H. Brandenberger, "Probing Particle Physics from Top Down with Cosmic Strings," *The Universe* **1** no. 4, (2013) 6–23, arXiv:1401.4619 [astro-ph.CO].

[2] Y. B. Zeldovich, I. Y. Kobzarev, and L. B. Okun, "Cosmological Consequences of the Spontaneous Breakdown of Discrete Symmetry," *Zh. Eksp. Teor. Fiz.* **67** (1974) 3–11.

[3] Y. B. Zeldovich and M. Y. Khlopov, "On the Concentration of Relic Magnetic Monopoles in the Universe," *Phys. Lett. B* **79** (1978) 239–241.

[4] A. Vilenkin and E. P. S. Shellard, *Cosmic Strings and Other Topological Defects*. Cambridge University Press, 7, 2000.

[5] M. B. Hindmarsh and T. W. B. Kibble, "Cosmic strings," *Rept. Prog. Phys.* **58** (1995) 477–562, arXiv:hep-ph/9411342.

[6] R. H. Brandenberger, "Topological defects and structure formation," *Int. J. Mod. Phys. A* **9** (1994) 2117–2190, arXiv:astro-ph/9310041.

[7] R. Durrer, M. Kunz, and A. Melchiorri, "Cosmic structure formation with topological defects," *Phys. Rept.* **364** (2002) 1–81, arXiv:astro-ph/0110348.

[8] N. Turok, "Global Texture as the Origin of Cosmic Structure," *Phys. Rev. Lett.* **63** (1989) 2625.

[9] T. W. B. Kibble, "Phase Transitions in the Early Universe," *Acta Phys. Polon. B* **13** (1982) 723.

[10] T. W. B. Kibble, "Some Implications of a Cosmological Phase Transition," *Phys. Rept.* **67** (1980) 183.

[11] A. K. Gooding, D. N. Spergel, and N. Turok, "The Formation of galaxies and quasars in a texture seeded CDM cosmogony,".

[12] D. N. Spergel and N. G. Turok, "Textures and cosmic structure," *Sci. Am.* **266** (1992) 36–43.

[13] J. Magueijo, A. Albrecht, D. Coulson, and P. Ferreira, "Doppler peaks from active perturbations," *Phys. Rev. Lett.* **76** (1996) 2617–2620, arXiv:astro-ph/9511042.

[14] U.-L. Pen, U. Seljak, and N. Turok, "Power spectra in global defect theories of cosmic structure formation," *Phys. Rev. Lett.* **79** (1997) 1611–1614, arXiv:astro-ph/9704165.

[15] L. Perivolaropoulos, "Spectral analysis of microwave background perturbations induced by cosmic strings," *Astrophys. J.* **451** (1995) 429–435, arXiv:astro-ph/9402024.

[16] A. Lopez-Eiguren, J. Lizarraga, M. Hindmarsh, and J. Urrestilla, "Cosmic Microwave Background constraints for global strings and global monopoles," *JCAP* **07** (2017) 026, arXiv:1705.04154 [astro-ph.CO].

[17] M. Cruz, E. Martinez-Gonzalez, P. Vielva, J. M. Diego, M. Hobson, and N. Turok, "The CMB cold spot: texture, cluster or void?," *Mon. Not. Roy. Astron. Soc.* **390** (2008) 913, arXiv:0804.2904 [astro-ph].

[18] S. F. Bramberger, R. H. Brandenberger, P. Jreidini, and J. Quintin, "Cosmic String Loops as the Seeds of Super-Massive Black Holes," *JCAP* **06** (2015) 007, arXiv:1503.02317 [astro-ph.CO].

[19] R. Brandenberger and H. Jiao, "Cosmic Textures and Global Monopoles as Seeds for Super-Massive Black Holes," *JCAP* **02** (2020) 002, arXiv:1908.04585 [astro-ph.CO].

[20] T. Prokopec, "Formation of topological and nontopological defects in the early universe," *Phys. Lett. B* **262** (1991) 215–221.

[21] R. A. Leese and T. Prokopec, "Monte Carlo simulation of texture formation," *Phys. Rev. D* **44** (1991) 3749–3759.

[22] N. Turok and D. Spergel, "Global Texture and the Microwave Background," *Phys. Rev. Lett.* **64** (1990) 2736.

[23] R. H. Brandenberger, "On the Decay of Cosmic String Loops," *Nucl. Phys. B* **293** (1987) 812–828.

[24] J. H. MacGibbon and R. H. Brandenberger, "Gamma-ray signatures from ordinary cosmic strings," *Phys. Rev. D* **47** (1993) 2283–2296, arXiv:astro-ph/9206003.

[25] J. H. MacGibbon and R. H. Brandenberger, "High-energy neutrino flux from ordinary cosmic strings," *Nucl. Phys. B* **331** (1990) 153–172.

[26] C. T. Hill, D. N. Schramm, and T. P. Walker, "Ultrahigh-Energy Cosmic Rays from Superconducting Cosmic Strings," *Phys. Rev. D* **36** (1987) 1007.

[27] U. F. Wichoski, J. H. MacGibbon, and R. H. Brandenberger, "High-energy neutrinos, photons and cosmic ray fluxes from VHS cosmic strings," *Phys. Rev. D* **65** (2002) 063005, arXiv:hep-ph/9805419.

[28] S. P. Swordy, "The Energy Spectra and Anisotropies of Cosmic Rays," *ssr* **99** (Oct., 2001) 85–94.

[29] A. De Angelis and M. Pimenta, *Introduction to Particle and Astroparticle Physics: Multimessenger Astronomy and its Particle Physics Foundations*. Undergraduate Lecture Notes in Physics. Springer Nature, Heidelberg, 2018.

[30] **Pierre Auger** Collaboration, A. Aab *et al.*, "Improved limit to the diffuse flux of ultrahigh energy neutrinos from the Pierre Auger Observatory," *Phys. Rev. D* **91** no. 9, (2015) 092008, arXiv:1504.05397 [astro-ph.HE].

[31] M. Anthonisen, R. Brandenberger, A. Laguë, I. A. Morrison, and D. Xia, "Cosmic Microwave Background Spectral Distortions from Cosmic String Loops," *JCAP* **02** (2016) 047, arXiv:1509.07998 [astro-ph.CO].

[32] J. Chluba and R. A. Sunyaev, "The evolution of CMB spectral distortions in the early Universe," *Mon. Not. Roy. Astron. Soc.* **419** (2012) 1294–1314, arXiv:1109.6552 [astro-ph.CO].

[33] H. Tashiro, "CMB spectral distortions and energy release in the early universe," *PTEP* **2014** no. 6, (2014) 06B107.

[34] A. Kogut *et al.*, "The Primordial Inflation Explorer (PIXIE): A Nulling Polarimeter for Cosmic Microwave Background Observations," *JCAP* **07** (2011) 025, arXiv:1105.2044 [astro-ph.CO].

[35] J. D. Bowman, A. E. E. Rogers, R. A. Monsalve, T. J. Mozdzen, and N. Mahesh, "An absorption profile centred at 78 megahertz in the sky-averaged spectrum," *Nature* **555** no. 7694, (2018) 67–70, arXiv:1810.05912 [astro-ph.CO].

[36] R. Brandenberger, B. Cyr, and T. Schaeffer, "On the Possible Enhancement of the Global 21-cm Signal at Reionization from the Decay of Cosmic String Cusps," *JCAP* **04** (2019) 020, arXiv:1810.03219 [astro-ph.CO].

[37] R. Brandenberger, B. Cyr, and R. Shi, "Constraints on Superconducting Cosmic Strings from the Global 21-cm Signal before Reionization," *JCAP* **09** (2019) 009, arXiv:1902.08282 [astro-ph.CO].

[38] S. Laliberte and R. Brandenberger, "Ionization from cosmic strings at cosmic dawn," *Phys. Rev. D* **101** no. 2, (2020) 023528, arXiv:1907.08022 [astro-ph.CO].

[39] R. Brandenberger, B. Cyr, and A. V. Iyer, "Fast Radio Bursts from the Decay of Cosmic String Cusps," arXiv:1707.02397 [astro-ph.CO].

[40] M. Barriola and A. Vilenkin, "Gravitational Field of a Global Monopole," *Phys. Rev. Lett.* **63** (1989) 341.

[41] D. P. Bennett and S. H. Rhie, "Cosmological evolution of global monopoles and the origin of large scale structure," *Phys. Rev. Lett.* **65** (1990) 1709–1712.

Part IV

Cosmic String Loops and Black Holes

Chapter 5

Intermediate Mass Black Hole Seeds from Cosmic String Loops

R.H. Brandenberger, B. Cyr, and H. Jiao, *Intermediate mass black hole seeds from cosmic string loops*, Phys.Rev.D 104 (2021) 12, 123501, [arXiv:2103.14057].

Addendum for thesis

This chapter sees a return to cosmic string loop phenomenology, this time in the form of black hole formation in the vicinity of a loop. This problem had been studied in the past by a variety of authors, including R. Brandenberger who was originally interested in determining if cosmic strings could act as the seeds for the supermassive black holes residing at the centres of galaxies.

Our motivation for this project came from the LIGO experiment, which detects gravitational wave signatures of merging black holes. Using an extensive template bank of gravitational waveforms produced by numerical simulations, LIGO is able to infer the masses of the original black holes in a merger. The LIGO collaboration (at this point in 2020) had detected a handful of events coming from black holes with masses $65M_{\odot} \leq M_{BH} \leq 135M_{\odot}$. This mass range is often referred to as the *mass gap* window, as collapsing stars which would naively source such black holes undergo what is known as a pair-instability supernova, a process which leaves no black hole remnant.

The origin of these black holes remains a mystery, and so we investigated whether a distribution of cosmic string loops could produce them. Our analysis was rather basic, predicting the number distribution of mass gap black holes which could form in the vicinity

of a string loop, to be compared with data once a more complete sample of merging black holes is obtained.

Abstract

We demonstrate that cosmic string loops may provide a joint resolution of two mysteries surrounding recently observed black holes. For a string tension in an appropriate range, large radius string loops have the potential to provide the nonlinearities in the early universe which seed supermassive black holes. The more numerous smaller radius string loops can then seed intermediate mass black holes, including those with a mass in the region between $65M_\odot$ and $135M_\odot$ in which standard black hole formation scenarios predict no black holes are able to form, but which have recently been detected by the LIGO/VIRGO collaboration. We find that there could be as many as 10^6 of intermediate mass black holes per galaxy, providing a tantalizing target for gravitational wave observatories to look for.

5.1 Introduction

In this Letter we suggest that cosmic strings may provide a joint resolution of two puzzles in astrophysics. On one hand, as already investigated in [1], string loops may explain the origin of the seeds about which super-massive black holes (SMBHs) accrete. On the other hand, smaller loops can lead to the formation of intermediate mass black holes, in particular black holes in the "mass gap" range between $65M_\odot$ and $135M_\odot$ where standard stellar black hole formation scenarios predict that no black holes should exist. Such black holes, however, have been detected by the LIGO/VIRGO collaboration [2].

Observations indicate the presence of black holes of mass larger than $10^9 M_\odot$ at redshifts greater or equal to $z = 6$ [3, 4, 5]. In fact, each galaxy in the low redshift universe appears to harbour a SMBH of mass greater or equal to $10^6 M_\odot$. In the context of the current cosmological paradigm, the ΛCDM model with an almost scale-invariant spectrum of nearly Gaussian primordial density fluctuations, it is not possible to explain the origin of these massive early black holes if accretion is limited by the Eddington rate [1]. For a review article on supermassive black hole formation the reader is referred to [6]. As studied in [1], cosmic string loops with an appropriate radius can provide nonlinear seeds at high redshifts which can resolve this puzzle.

Cosmic strings exist as solutions of the field equations in a wide range to particle physics models beyond the *Standard Model*. If Nature is described by such a theory, then a network

of strings inevitably forms in the early universe and persists to the present time. For a review article the reader is referred to [7, 8, 9, 10]. The network of strings contains loops with a continuous range of radii. String loops represent nonlinear density fluctuations. Hence, string loops may seed black holes with a continuous range of masses. As will be reviewed in the next section, the number density of string loops increases as the loop radius decreases. If the parameters of the string model are tuned such that the observed number density of super-massive black holes results, the model will predict a distribution of black holes of intermediate mass, in particular of mass in the "mass gap" region. Here, we compute the mass distribution of the resulting black hole seeds and show that they may explain the LIGO/VIRGO data.

In the following section we briefly review how cosmic strings form and evolve in an expanding universe. In Section 3 we discuss the mystery of the origin of SMBHs and the possible role which Eddington accretion about string loops can play. Our analysis is summarized in Section 4. The string network is determined by a single free parameter, the string tension. We fix this parameter such that we obtain the observed number density of SMBHs. We then compute the predicted distribution of nonlinear seeds of smaller mass which may evolve into intermediate mass black holes (IMBHs). We conclude with a summary and discussion of our results.

We will use natural units in which the speed of light, Planck's constant and Boltzmann's constant are all set to 1. We work in the context of a homogeneous and isotropic background metric with scale factor $a(t)$ (t being time). The present time is denoted by t_0, the time of equal matter and radiation by t_{eq} (and the corresponding temperatures are T_0 and T_{eq}, respectively). Instead of time, we will often use cosmological redshift $z(t)$ given by

$$z(t) + 1 \equiv \frac{a(t_0)}{a(t)} \,. \tag{5.1}$$

Newton's gravitational constant is denoted by G, and it defines the Planck mass m_{pl} via $G = m_{pl}^{-2}$. The Hubble radius is the inverse expansion rate and plays a role in the description of the network of strings.

5.2 Cosmic String Formation and Evolution

A subset of particle physics models beyond the Standard Model admit solutions of their field equations which correspond to linear topological defects analogous to vortex lines in

superconductors and superfluids [7, 8, 9, 10]. If Nature is described by such a model, then a network of strings inevitably [11, 12] forms in the early universe and persists to the present time. Typically, topological defects form during a symmetry breaking phase transition when a scalar order parameter takes on a nonvanishing expectation value. If the manifold of possible low temperature expectation values of the order parameter has the topology of a circle, then the defects are one-dimensional strings. They represent narrow tubes of trapped energy [1], and they are characterized by their tension μ. The tension is related to the energy scale η of symmetry breaking via $\mu \sim \eta^2$. The trapped energy density leads to gravitational effects which in turn produce distinctive signals for strings in various observational windows (see e.g. [13]).

Cosmic strings cannot have any ends. The network of strings which forms in the symmetry breaking phase transition consists of *long* strings (strings whose curvature radius is larger than the Hubble radius) and loops. The network rapidly approaches a *scaling solution* in which the statistical properties of the strings are the same at all times if all length are scaled to the Hubble radius. The scaling solution is maintained by the long strings intersecting and giving off energy in the form of string loops. The string loops, in turn, oscillate, emit gravitational radiation and gradually decay. There are good analytical arguments to expect the string network to scale (see e.g. [7, 8, 9, 10]). The scaling of the network of long strings is also clearly established based on numerical simulations [14, 15, 16]. Simulations making use of the Nambu-Goto effective action for strings also establish the scaling of the loop distribution [17, 18, 19, 20, 21, 22, 23], while some simulations of cosmic string evolution using the field theory equations [24] indicate that the long strings more efficiently lose energy to particles, and that in consequence the distribution of string loops does not scale. We will here assume that the results of the Nambu-Goto simulations are correct.

According to the one-scale model [25, 26, 27] (supported by the Nambu-Goto simulations) [2], the number density per unit radius of loops at any given time $t > t_{eq}$ is given by

$$n(R,t) = \begin{cases} NR^{-5/2}t^{-2}t_{eq}^{1/2} & R \geq \gamma G\mu t \\ \text{const} & R < R_{gw} \equiv \gamma G\mu t \end{cases} \tag{5.2}$$

where N and γ are constants. Here, R is the radius of the loop and $n(R,t)$ gives the number density of loops per R interval [3]. R_{gw} is the radius below which a loop will live less than

[1] In this paper we will assume that the strings are not superconducting.

[2] We will return to a discussion of the caveats of using this model in the concluding section.

[3] Note that multiplying $n(R,t)$ by R yields the number density of loops with radius greater or equal to R, which is dominated by loops of radius between R and $2R$.

one Hubble expansion time before decaying. The constant N is determined by the number of long strings per Hubble volume and by the length of loop (in units of the Hubble radius) when it forms, while the constant γ is determined by the strength of gravitational radiation from string loops. Based on the results of numerical simulations [17, 18, 19, 20, 21, 22, 23] we will take $N \sim 6 \times 10^{-3}$ and $\gamma \sim 10^2$. Note that the above formula is modified for loops which form after t_{eq} and reads

$$n(R,t) \sim N' R^{-2} t^{-2} . \tag{5.3}$$

where N' is of the same order of magnitude of N. These loops, however, will only play a role for the final considerations in this work.

String loops can also lose energy by *cusp annihilation* [28]. As can be shown [29], for any loop of radius R there will be at least one cusp formed per oscillation time R. A cusp is a point on the string - treated according to the Nambu-Goto action - which moves at exactly the speed of light. At this point, the loop doubles back on itself. Since strings have a finite thickness $w \sim \eta^{-1}$, there will be a region near the cusp where the string segments on either side of the cusp point overlap. Locally, this region looks like a string-antistring configuration, and it will hence decay explosively giving rise to a burst of particles. The overlap region has length $l_c \sim w^{1/2} R^{1/2}$ [30], and hence the energy lost by cusp annihilation per unit time is of the order

$$P_{\text{cusp}} \sim w^{1/2} \mu R^{-1/2} . \tag{5.4}$$

In comparison, the energy loss per unit time of a string loop due to gravitational radiation is [31]

$$P_{\text{grav}} \sim \gamma G \mu^2 . \tag{5.5}$$

Hence, for small values of μ, cusp annihilation will dominate. The critical value μ_c of μ below which cusp annihilation dominates depends on the string radius R and can be obtained by equating (5.4) and (5.5), keeping in mind that $w \sim \mu^{-1/2}$ and is

$$G\mu_c \sim \gamma^{-4/5} G^{1/5} R^{-2/5} . \tag{5.6}$$

Thus, the larger the loop radius, the less is the relative importance of cusp evaporation. For

loops at the gravitational radiation cutoff R_{gw}, the condition on μ_c yields

$$G\mu_c \sim \gamma^{-6/7} \left(\frac{T_{eq}}{m_{pl}}\right)^{4/7} \sim 10^{-17}\,, \tag{5.7}$$

where we have used the value $\gamma = 10^2$. For values of $G\mu$ smaller than this critical value, the loop distribution changes compared to (5.2). However, in this work we will not be considering values of $G\mu$ smaller than $G\mu_c$.

Note that string loops are not exactly circular. We will introduce a constant β to parametrize the mean length $l(R)$ of a loop of radius R, namely

$$l(R) \equiv \beta R\,. \tag{5.8}$$

For circular loops, $\beta = 2\pi$, though in general one expects $\beta \sim \mathcal{O}(10)$. Since cosmic strings carry energy, their gravitational effects lead to imprints in many observational windows. These imprints are highly non-Gaussian and typically most visible in position space maps. Well known are the line discontinuities which long strings produce in cosmic microwave background (CMB) temperature maps [32, 33]. The current upper bound on the string tension from not having observed these signals is [34, 35, 36] $G\mu < 10^{-7}$, and searches for these signals using wavelet statistics [37, 38] and machine learning methods [39, 40] have the potential of reducing this bound by one or two orders of magnitude. Long strings moving through space produce *wakes*, planar density perturbations in the plane mapped out by the moving string [41, 42, 43, 44, 45]. Wakes, in turn, lead to specific signals in B-mode CMB polarization maps: rectangles in the sky with a uniform polarization direction and linearly increasing signal amplitude [46]. They also lead to wedge-shaped regions of extra absorption in 21cm redshift maps during the dark ages [47].

String loops lead to spherical (if the center of mass velocity is small) or filamentary (if the center of mass velocity is large) overdensities. Originally, this mechanism was postulated to be the dominant source of structure formation [48, 49, 50, 51], but the required value of $G\mu$ exceeds the abovementioned upper bound. Thus, string loops are only a supplementary source of nonlinear structures. The role of string loops in seeding ultra-compact mini-halos was explored in [52], and the role in seeding globular clusters was studied in [53, 54]. Here, we study the role of string loops in seeding SMBHs and IMBHs.

The tightest current constraints on the string tension come from pulsar timing limits on the amplitude of stochastic gravitational waves [55, 56]. The limits come about since string loops decay by emitting gravitational radiation resulting in a scale-invariant spectrum of

gravitational waves over a large range of wavelengths (with specific signatures coming from the cusp annihilation process). The current limits are $G\mu < 10^{-10}$, and the recent NANOgrav results could [57] be interpreted as being due to cosmic strings with a value of $G\mu$ of this order of magnitude. The cusp annihilation process also produces jets of particles whose role in contributing to the spectrum of high energy cosmic rays was explored in [58, 59, 60, 61], and which will contribute to the global 21cm signal [62, 63, 64, 65], which may play a role in explaining Fast Radio Bursts [66], and in magnetogenesis [67].

Since cosmic strings inevitably arise in a large class of particle physics models beyond the Standard Model, searching for string signals in new observational windows is an interesting way to probe particle physics. Since many of the string signals grow in amplitude as the energy scale η increases, cosmology provides an approach to probe particle physics models which is complementary to accelerator probes (which are more sensitive if the energy scale η of the new physics is low). Improved upper bounds on the string tension from cosmology will allow us to constrain larger sets of particle physics models (for more discussion on this point see [68].

5.3 Eddington Accretion and Super-Massive Black Hole Formation

The origin of SMBHs is an important open question in astrophysics. A conservative approach (see e.g. [6] for a review) is to assume that the seeds of the SMBHs are black holes formed after the death of Population III stars which are expected to have masses in the range of $10^2 - 10^3 M_\odot$. These seed black holes are then assumed to accrete matter. The Eddington rate is often taken to be a good estimate for the highest accretion rate onto these seed black holes. But, according to the canonical ΛCDM paradigm of early universe cosmology, there are not enough nonlinear seeds at early times in order to explain the origin of the observed $10^9 M_\odot$ black holes at redshifts greater than $z = 6$. As pointed out in [1], string loops can provide a sufficient number of nonlinear seeds in the early universe, even for small values of the string tension. For values of the string tension significantly lower than the current upper bounds, linear accretion onto the string loops is insufficient to explain the high mass of the observed SMBHs, and thus it is reasonable to assume that nonlinear accretion at a rate comparable to the Eddington rate takes place. We will denote by $\mathcal{E}_1$ the enhancement of the increase in mass for these SMBH seeds compared to linear theory.

Since there is a continuous distribution of string loop masses with a number density which

increases as the mass decreases, the string model for seeding SMBHs predicts a distribution of black holes of smaller masses, and in particular black holes in the "mass gap" mass range. Since accretion onto smaller loops is more difficult than accretion onto larger loops, we expect the nonlinear accretion factor for smaller loops to be less. The reason is that for smaller black hole masses, the horizon area is less, and infalling matter has to be directed more precisely in direction towards the black hole, while the thermal correlation length of the accreting matter is independent of the loop size. We will denote that enhancement factor for IMBHs by $\mathcal{E}_2$, noting that it is reasonable to expect that $\mathcal{E}_2 \sim 1$, indicating a scenario in which no Eddington accretion has taken place onto these smaller black holes.

5.4 Resulting Distribution of Intermediate Mass Black Holes

In this section we will compute the expected number density of string-seeded IMBH assuming that the string model is normalized such that it yields one SMBH seed per galaxy. More specifically, we will demand that the model yield one string loop per volume d_g^3 (where d_g is the comoving radius of the region which collapses to form a large galaxy) capable of seeding a SMBH of mass M_{SM} at $z = 0$, which we will take to be $10^6 M_\odot$ later in the analysis. When inserting numbers we will use $d_g = 10^{2/3}$Mpc [69]. Allowing for an enhancement of the accretion onto the string loop by a factor of $\mathcal{E}_1$ (e.g. by Eddington accretion) compared to the linear perturbation theory growth rate), the condition on $G\mu$ becomes

$$\beta \mu R (z_{eq} + 1) \mathcal{E}_1 \, = \, M_{SM} \, , \tag{5.9}$$

where the radius R must be chosen in order to obtain the correct number density of loops, i.e. (see (5.2))

$$N R^{-3/2} t_{eq}^{1/2} t_0^{-2} d_g^3 \, = \, 1 \, . \tag{5.10}$$

Combining (5.9) and (5.10) yields

$$G\mu \, = \, \beta^{-1} N^{-2/3} (z_{eq} + 1)^{-1/2} \mathcal{E}_1^{-1} \left(\frac{t_0}{d_g} \right)^2 \frac{G}{t_0} M_{SM} \, . \tag{5.11}$$

Inserting the values of G, d_g, M_{SM}, and t_0, and using $\beta = 10$ yields

$$G\mu \sim 2 \times 10^{-14} N^{-2/3} \mathcal{E}_1^{-1} \,. \tag{5.12}$$

The mass gap we are interested in today is $[M_{IM}^{\min}, M_{IM}^{\max}]$ with $M_{IM}^{\min} = 65\, M_\odot$ and $M_{IM}^{\max} = 130\, M_\odot$. As one would expect, black holes in this mass range are also seeded by string loops that fall within a range, R_{IM}^{min} and R_{IM}^{max}. Assuming all black holes in this mass range have the same Eddington factor, $\mathcal{E}_2$, (where $\mathcal{E}_2 \leq \mathcal{E}_1$), their masses grow as

$$M_{IM}^{\min/\max} = \beta\mu(z_{eq}+1) R_{IM}^{\min/\max} \mathcal{E}_2 \,, \tag{5.13}$$

The resulting number N_{IMBH} of string loops inside a galaxy capable of seeding black holes in the IMBH range is then given by

$$N_{IMBH} \sim N t_{eq}^{1/2} t_0^{-2} d_g^3 R_{IM}^{\min\, -3/2} \left(1 - \left(\frac{R_{IM}^{\min}}{R_{IM}^{\max}}\right)^{3/2}\right) , \tag{5.14}$$

In fact, it is reasonable to use $\mathcal{E}_2 = 1$. Inserting the expression for d_g^3 from (5.10), where R is the radius of a loop responsible for accreting a black hole of mass M_{SM}, and relating R to M_{SM} via (5.9) yields our main result

$$N_{IMBH} \sim \left(\frac{\mathcal{E}_2}{\mathcal{E}_1}\right)^{3/2} \left(\frac{M_{SM}}{M_{IM}^{\min}}\right)^{3/2} \left(1 - \left(\frac{M_{IM}^{\min}}{M_{IM}^{\max}}\right)^{3/2}\right) \tag{5.15}$$

We can see that requiring one SMBH per galaxy completely sets the shape of the number distribution of all other black holes formed from cosmic strings, as we would expect in the one-scale model (aside from the different Eddington accretion factors). The number of IMBHs per galaxy is mostly determined by the ratio of SMBH to IMBH masses, with a small correction coming from the small but finite range of IMBHs in the mass gap. Inserting our numbers yields our main prediction of IMBHs per galaxy

$$N_{IMBH} \sim 10^6 \left(\frac{\mathcal{E}_2}{\mathcal{E}_1}\right)^{3/2} \tag{5.16}$$

If we assume that no loop accretes matter at a rate larger than what linear theory predicts, then we need a value of $G\mu \sim 10^{-13}$ in order to explain the origin of the SMBHs (taking $N^{-2/3} = 10$), and we obtain $N_{IMBH} \sim 10^6$. This value of $G\mu$ is consistent with the upper bound on $G\mu$ due to gravitational radiation constraints [55, 56]. No super-linear (in

particular no Eddington) accretion is required to explain the origin of the nonlinear seeds required to explain the abundance of SMBHs. For smaller values of $G\mu$ we would require some amount of Eddington accretion in order to explain the number density of SMBHs. In that case, the predicted number of IMBH candidates would be smaller than what is given in (5.15) unless the smaller loops also undergo similar Eddington accretion.

We have normalized our calculations to yield one SMBH of mass of at least $10^6 M_\odot$ per galaxy. As long as the loops are created in the radiation phase, the number density $n(> M)$ of supermassive seed scales with the seed mass greater than M (using the fact that the linear accretion factor for all of these loops is the same and hence M is proportional to the loop radius R) as[4]

$$n_{>M} \propto M^{-3/2}\,. \tag{5.17}$$

For loops created in the matter period, we have (see (5.3)) $n(R) \sim R^{-2}$. Furthermore, the linear growth factor is reduced since formation after matter-radiation equality means less time to accrete. In particular, the linear growth factor, GF, now depends on R

$$GF(R) = GF(R_c)(z_{eq}+1)\left(\frac{t_{eq}}{R}\right)^{2/3}, \tag{5.18}$$

where R_c is the radius of the loop formed at the time t_{eq}. Hence, taking into account this radius-dependent growth factor we have

$$n(M) \propto M^{-4}\,, \tag{5.19}$$

and hence the number density of seeds with mass greater or equal to M scales as

$$n_{>M} \propto M^{-3} \tag{5.20}$$

Thus, the mean separation d_M of seeds with mass greater or equal to M (for large masses) scales as

$$d_M = d_6 \frac{M}{M_6}\left(\frac{M_6}{M_{eq}}\right)^{1/2}, \tag{5.21}$$

where M_{eq} is the mass of a seed from a loop created at time t_{eq}, and we use $M_6 = 10^6 M_\odot$

[4]Note that $n(M)$ is the number density of black holes per unit mass, and $n_{>M}$ is the number density of SMBH seeds for masses greater than $10^6\, M_\odot$.

and d_6 to be the mean separation of the corresponding seeds.

Making use of $R_c = t_{eq}$ (loops form with size of order the Hubble radius) and the value of $G\mu$ from (5.12) we obtain

$$M_{eq} \simeq \beta\mu t_{eq}(z_{eq}+1)\mathcal{E}_{eq} \sim 2.4 \times 10^8 N^{-2/3}\frac{\mathcal{E}_{eq}}{\mathcal{E}_1}M_\odot\,, \tag{5.22}$$

where $\mathcal{E}_{eq}$ is the Eddington growth rate of loops formed at t_{eq}. Inserting into (5.21) the value of $d_g = 10^{2/3}$Mpc, and the value of M_{eq} from (5.22) we get

$$d_9 \sim 0.3\text{Gpc}N^{1/3}\left(\frac{\mathcal{E}_1}{\mathcal{E}_{eq}}\right)^{1/2} \tag{5.23}$$

for the mean separation of seeds which can accrete SMBHs of mass $10^9 M_\odot$.

Assuming no Eddington accretion or an Eddington accretion factor independent of mass for these superheavy objects, and using the value $N = 6 \times 10^{-3}$ from numerical simulations [17, 18, 19, 20, 21, 22, 23], our model thus predicts one SMBH of mass greater than $10^9 M_\odot$ per volume d_9^3 with $d_9 \simeq 60$Mpc, which agrees well with the observed separation of such black hole monsters [69].

5.5 Conclusions and Discussion

We have studied the implications of the proposal that both super-massive black holes (SMBHs) and intermediate black holes (IMBHs) could originate from cosmic string loop seeds. The cosmic string model contains (in principle) one free parameter, namely the string tension. Normalizing the string tension to yield one candidate seed per galaxy which can develop into a SMBH of mass greater or equal to $10^6 M_\odot$, we predicted the number per galaxy of IMBHs capable of seeding black holes in the "mass gap" window of $65\,M_\odot - 130\,M_\odot$. This number is 10^6 modulo Eddington accretion factors. We can also predict the mean separation d_9 of loops capable of seeding monster SMBHs of mass greater than $10^9 M_\odot$. We obtain $d_9 \sim 60$Mpc.

Our model predicts a continuum of black hole masses inside any galaxy, from one SMBH with mass greater or equal to $10^6 M_\odot$ down to a lower cutoff mass M_c given by

$$M_c \sim \gamma G\mu\mu t_{eq}(z_{eq}+1) \tag{5.24}$$

(modulo Eddington accretion factors). Would-be black holes with a smaller mass than this

would have to be formed from string loops that would have decayed by matter-radiation equality, and therefore would not have undergo any efficient accretion. Inserting the value of the string tension from (5.12), we find

$$M_c \sim 10^{-2}\,\gamma(z_{eq}+1)^{-1/2}\mathcal{E}_1^{-2}M_\odot\,, \tag{5.25}$$

which, using the value of $\gamma \sim 10^2$ from studies of gravitational radiation from string loops [31], is about $10^{-2}M_\odot$, assuming no Eddington accretion.

We expect that the accretion onto these cosmic string loops collapses into a black hole before structure formation takes place. Therefore, the formation and merger history of binary systems of these IMBHs will closely resemble that of primordial black holes (see for example [70, 71, 72, 73])

Note that in our scenario, the string loop-seeded black holes provide a negligible fractional contribution Ω_{BH} to the dark matter density

$$\Omega_{BH} \simeq 12\pi \times \beta\gamma^{-1}(G\mu)^{1/2}N \sim 0.4 \times 10^{-2}N^{2/3}\,, \tag{5.26}$$

being dominated by black holes of mass near the cutoff mass M_c, and hence our model is consistent with observational bounds on the black hole contribution to the total energy budget of the universe (see e.g. [74, 75]).

It is important to mention a caveat related to our analysis. While there is no debate that the distribution of long strings converges to a scaling distribution, there is still a lot of uncertainty concerning the exact nature of the distribution of loops. If the field theory simulations of [24] give the correct distributions of strings in a cosmological setting, then there are no stable long-lived loops and our mechanism does not work. The Nambu-Goto simulations of cosmic string evolution indicate, however, that the distribution of loops takes on a scaling distribution. We have considered the original one-scale model [25, 26, 27] for the distribution of loops, assuming implicitly that they are formed at a fixed fraction of the Hubble radius. Other loop generation mechanisms have been discussed (see e.g. [76, 77]). These lead to a distribution of loop radii which differs from what is assumed in Eqs. (5.2) and (5.3). However, the differences are mostly for loop radii comparable and smaller to the gravitational radiation cutoff R_{gw}. While these differences are very important when calculating the gravitational wave signatures of a cosmic string distribution (since it is small loops which dominate the gravitational wave emission, see e.g. the recent study of [78]), they are much less important for our considerations. They will mostly effect the predicted

number of intermediate mass black holes at the low mass end.

In our analysis we have also assumed that loops, once formed, do not fragment into smaller loops. If this is not the case, then the redshifting is not the only important factor which determines the loop distribution. The numerical Nambu-Goto simulations [17, 18, 19, 20, 21, 22, 23] do not see evidence the cascading fragmentation.

Note that there are other mechanisms in early universe models which can lead to nonlinear seeds early on (see e.g. [79, 80, 81]. What is special about the cosmic string scenario is that a scaling distribution of seeds is generated. Phase transitions without a resulting scaling defect network will typically generate seeds with a narrow range of sizes.

Acknowledgement

RB wishes to thank the Pauli Center and the Institutes of Theoretical Physics and of Particle- and Astrophysics of the ETH for hospitality. The research of RB and HJ at McGill is supported in part by funds from NSERC and from the Canada Research Chair program. BC thanks support from a Vanier-CGS fellowship and from NSERC. RB wishes to thank Ken Olum and Marta Volonteri for discussions. JH acknowledges fellowships from Hydro-Quebec (through the McGill Physics Department) and from the McGill Space Institute.

Bibliography

[1] S. F. Bramberger, R. H. Brandenberger, P. Jreidini, and J. Quintin, "Cosmic String Loops as the Seeds of Super-Massive Black Holes," *JCAP* **06** (2015) 007, arXiv:1503.02317 [astro-ph.CO].

[2] **LIGO Scientific, Virgo** Collaboration, R. Abbott *et al.*, "GW190521: A Binary Black Hole Merger with a Total Mass of $150M_{\odot}$," *Phys. Rev. Lett.* **125** no. 10, (2020) 101102, arXiv:2009.01075 [gr-qc].

[3] E. Banados *et al.*, "The Discovery of a Highly Accreting, Radio-loud Quasar at $z = 6.82$," *Astrophys. J.* **909** no. 1, (2021) 80, arXiv:2103.03295 [astro-ph.CO].

[4] E. Banados *et al.*, "An 800-million-solar-mass black hole in a significantly neutral Universe at redshift 7.5," *Nature* **553** no. 7689, (2018) 473–476, arXiv:1712.01860 [astro-ph.GA].

[5] L. Jiang *et al.*, "The Final SDSS High-Redshift Quasar Sample of 52 Quasars at z>5.7," *Astrophys. J.* **833** no. 2, (2016) 222, arXiv:1610.05369 [astro-ph.GA].

[6] M. Volonteri, "Formation of Supermassive Black Holes," *Astron. Astrophys. Rev.* **18** (2010) 279–315, arXiv:1003.4404 [astro-ph.CO].

[7] A. Vilenkin and E. P. S. Shellard, *Cosmic Strings and Other Topological Defects*. Cambridge University Press, 7, 2000.

[8] M. B. Hindmarsh and T. W. B. Kibble, "Cosmic strings," *Rept. Prog. Phys.* **58** (1995) 477–562, arXiv:hep-ph/9411342.

[9] R. H. Brandenberger, "Topological defects and structure formation," *Int. J. Mod. Phys. A* **9** (1994) 2117–2190, arXiv:astro-ph/9310041.

[10] R. Durrer, M. Kunz, and A. Melchiorri, "Cosmic structure formation with topological defects," *Phys. Rept.* **364** (2002) 1–81, arXiv:astro-ph/0110348.

[11] T. W. B. Kibble, "Phase Transitions in the Early Universe," *Acta Phys. Polon. B* **13** (1982) 723.

[12] T. W. B. Kibble, "Some Implications of a Cosmological Phase Transition," *Phys. Rept.* **67** (1980) 183.

[13] R. H. Brandenberger, "Searching for Cosmic Strings in New Observational Windows," *Nucl. Phys. B Proc. Suppl.* **246-247** (2014) 45–57, arXiv:1301.2856 [astro-ph.CO].

[14] A. Albrecht and N. Turok, "Evolution of Cosmic Strings," *Phys. Rev. Lett.* **54** (1985) 1868–1871.

[15] D. P. Bennett and F. R. Bouchet, "Evidence for a Scaling Solution in Cosmic String Evolution," *Phys. Rev. Lett.* **60** (1988) 257.

[16] B. Allen and E. P. S. Shellard, "Cosmic string evolution: a numerical simulation," *Phys. Rev. Lett.* **64** (1990) 119–122.

[17] C. Ringeval, M. Sakellariadou, and F. Bouchet, "Cosmological evolution of cosmic string loops," *JCAP* **02** (2007) 023, arXiv:astro-ph/0511646.

[18] V. Vanchurin, K. D. Olum, and A. Vilenkin, "Scaling of cosmic string loops," *Phys. Rev. D* **74** (2006) 063527, arXiv:gr-qc/0511159.

[19] L. Lorenz, C. Ringeval, and M. Sakellariadou, "Cosmic string loop distribution on all length scales and at any redshift," *JCAP* **10** (2010) 003, arXiv:1006.0931 [astro-ph.CO].

[20] J. J. Blanco-Pillado, K. D. Olum, and B. Shlaer, "Large parallel cosmic string simulations: New results on loop production," *Phys. Rev. D* **83** (2011) 083514, arXiv:1101.5173 [astro-ph.CO].

[21] J. J. Blanco-Pillado, K. D. Olum, and B. Shlaer, "The number of cosmic string loops," *Phys. Rev. D* **89** no. 2, (2014) 023512, arXiv:1309.6637 [astro-ph.CO].

[22] P. Auclair, C. Ringeval, M. Sakellariadou, and D. Steer, "Cosmic string loop production functions," *JCAP* **06** (2019) 015, arXiv:1903.06685 [astro-ph.CO].

[23] J. J. Blanco-Pillado and K. D. Olum, "Direct determination of cosmic string loop density from simulations," *Phys. Rev. D* **101** no. 10, (2020) 103018, arXiv:1912.10017 [astro-ph.CO].

[24] M. Hindmarsh, J. Lizarraga, J. Urrestilla, D. Daverio, and M. Kunz, "Scaling from gauge and scalar radiation in Abelian Higgs string networks," *Phys. Rev. D* **96** no. 2, (2017) 023525, arXiv:1703.06696 [astro-ph.CO].

[25] E. J. Copeland, T. W. B. Kibble, and D. Austin, "Scaling solutions in cosmic string networks," *Phys. Rev. D* **45** (1992) 1000–1004.

[26] L. Perivolaropoulos, "COBE versus cosmic strings: An Analytical model," *Phys. Lett. B* **298** (1993) 305–311, arXiv:hep-ph/9208247.

[27] D. Austin, E. J. Copeland, and T. W. B. Kibble, "Evolution of cosmic string configurations," *Phys. Rev. D* **48** (1993) 5594–5627, arXiv:hep-ph/9307325.

[28] R. H. Brandenberger, "On the Decay of Cosmic String Loops," *Nucl. Phys. B* **293** (1987) 812–828.

[29] T. W. B. Kibble and N. Turok, "Selfintersection of Cosmic Strings," *Phys. Lett. B* **116** (1982) 141–143.

[30] J. J. Blanco-Pillado and K. D. Olum, "Form of cosmic string cusps," *Phys. Rev. D* **59** (1999) 063508, arXiv:gr-qc/9810005. [Erratum: Phys.Rev.D 103, 029902 (2021)].

[31] T. Vachaspati and A. Vilenkin, "Gravitational Radiation from Cosmic Strings," *Phys. Rev. D* **31** (1985) 3052.

[32] N. Kaiser and A. Stebbins, "Microwave Anisotropy Due to Cosmic Strings," *Nature* **310** (1984) 391–393.

[33] R. Moessner, L. Perivolaropoulos, and R. H. Brandenberger, "A Cosmic string specific signature on the cosmic microwave background," *Astrophys. J.* **425** (1994) 365–371, arXiv:astro-ph/9310001.

[34] T. Charnock, A. Avgoustidis, E. J. Copeland, and A. Moss, "CMB constraints on cosmic strings and superstrings," *Phys. Rev. D* **93** no. 12, (2016) 123503, arXiv:1603.01275 [astro-ph.CO].

[35] C. Dvorkin, M. Wyman, and W. Hu, "Cosmic String constraints from WMAP and the South Pole Telescope," *Phys. Rev. D* **84** (2011) 123519, arXiv:1109.4947 [astro-ph.CO].

[36] **Planck** Collaboration, P. A. R. Ade *et al.*, "Planck 2013 results. XXV. Searches for cosmic strings and other topological defects," *Astron. Astrophys.* **571** (2014) A25, arXiv:1303.5085 [astro-ph.CO].

[37] L. Hergt, A. Amara, R. Brandenberger, T. Kacprzak, and A. Refregier, "Searching for Cosmic Strings in CMB Anisotropy Maps using Wavelets and Curvelets," *JCAP* **06** (2017) 004, arXiv:1608.00004 [astro-ph.CO].

[38] J. D. McEwen, S. M. Feeney, H. V. Peiris, Y. Wiaux, C. Ringeval, and F. R. Bouchet, "Wavelet-Bayesian inference of cosmic strings embedded in the cosmic microwave background," *Mon. Not. Roy. Astron. Soc.* **472** no. 4, (2017) 4081–4098, arXiv:1611.10347 [astro-ph.IM].

[39] R. Ciuca and O. F. Hernández, "A Bayesian Framework for Cosmic String Searches in CMB Maps," *JCAP* **08** (2017) 028, arXiv:1706.04131 [astro-ph.CO].

[40] R. Ciuca, O. F. Hernández, and M. Wolman, "A Convolutional Neural Network For Cosmic String Detection in CMB Temperature Maps," *Mon. Not. Roy. Astron. Soc.* **485** (2019) 1377, arXiv:1708.08878 [astro-ph.CO].

[41] J. Silk and A. Vilenkin, "COSMIC STRINGS AND GALAXY FORMATION," *Phys. Rev. Lett.* **53** (1984) 1700–1703.

[42] M. Rees, "Baryon concentrations in string wakes at $z \sim 200$: implications for galaxy formation and large-scale structure," *Mon. Not. Roy. Astron. Soc.* **222** (1986) 27.

[43] T. Vachaspati, "Cosmic Strings and the Large-Scale Structure of the Universe," *Phys. Rev. Lett.* **57** (1986) 1655–1657.

[44] A. Stebbins, S. Veeraraghavan, R. H. Brandenberger, J. Silk, and N. Turok, "Cosmic String Wakes," *Astrophys. J.* **322** (1987) 1–19.

[45] D. C. Neves da Cunha, J. Harnois-Deraps, R. Brandenberger, A. Amara, and A. Refregier, "Dark Matter Distribution Induced by a Cosmic String Wake in the Nonlinear Regime," *Phys. Rev. D* **98** no. 8, (2018) 083015, arXiv:1804.00083 [astro-ph.CO].

[46] R. J. Danos, R. H. Brandenberger, and G. Holder, "A Signature of Cosmic Strings Wakes in the CMB Polarization," *Phys. Rev. D* **82** (2010) 023513, arXiv:1003.0905 [astro-ph.CO].

[47] R. H. Brandenberger, R. J. Danos, O. F. Hernandez, and G. P. Holder, "The 21 cm Signature of Cosmic String Wakes," *JCAP* **12** (2010) 028, arXiv:1006.2514 [astro-ph.CO].

[48] A. Vilenkin, "Cosmological Density Fluctuations Produced by Vacuum Strings," *Phys. Rev. Lett.* **46** (1981) 1169–1172. [Erratum: Phys.Rev.Lett. 46, 1496 (1981)].

[49] N. Turok and R. H. Brandenberger, "Cosmic Strings and the Formation of Galaxies and Clusters of Galaxies," *Phys. Rev. D* **33** (1986) 2175.

[50] H. Sato, "Galaxy Formation by Cosmic Strings," *Prog. Theor. Phys.* **75** (1986) 1342.

[51] A. Stebbins, "Cosmic Strings and Cold Matter," *apjl* **303** (1986) L21.

[52] M. Anthonisen, R. Brandenberger, and P. Scott, "Constraints on cosmic strings from ultracompact minihalos," *Phys. Rev. D* **92** no. 2, (2015) 023521, arXiv:1504.01410 [astro-ph.CO].

[53] L. Lin, S. Yamanouchi, and R. Brandenberger, "Effects of Cosmic String Velocities and the Origin of Globular Clusters," *JCAP* **12** (2015) 004, arXiv:1508.02784 [astro-ph.CO].

[54] A. Barton, R. H. Brandenberger, and L. Lin, "Cosmic Strings and the Origin of Globular Clusters," *JCAP* **06** (2015) 022, arXiv:1502.07301 [astro-ph.CO].

[55] J. J. Blanco-Pillado, K. D. Olum, and X. Siemens, "New limits on cosmic strings from gravitational wave observation," *Phys. Lett. B* **778** (2018) 392–396, arXiv:1709.02434 [astro-ph.CO].

[56] **NANOGRAV** Collaboration, Z. Arzoumanian *et al.*, "The NANOGrav 11-year Data Set: Pulsar-timing Constraints On The Stochastic Gravitational-wave Background," *Astrophys. J.* **859** no. 1, (2018) 47, arXiv:1801.02617 [astro-ph.HE].

[57] J. J. Blanco-Pillado, K. D. Olum, and J. M. Wachter, "Comparison of cosmic string and superstring models to NANOGrav 12.5-year results," *Phys. Rev. D* **103** no. 10, (2021) 103512, arXiv:2102.08194 [astro-ph.CO].

[58] J. H. MacGibbon and R. H. Brandenberger, "Gamma-ray signatures from ordinary cosmic strings," *Phys. Rev. D* **47** (1993) 2283–2296, arXiv:astro-ph/9206003.

[59] J. H. MacGibbon and R. H. Brandenberger, "High-energy neutrino flux from ordinary cosmic strings," *Nucl. Phys. B* **331** (1990) 153–172.

[60] C. T. Hill, D. N. Schramm, and T. P. Walker, "Ultrahigh-Energy Cosmic Rays from Superconducting Cosmic Strings," *Phys. Rev. D* **36** (1987) 1007.

[61] U. F. Wichoski, J. H. MacGibbon, and R. H. Brandenberger, "High-energy neutrinos, photons and cosmic ray fluxes from VHS cosmic strings," *Phys. Rev. D* **65** (2002) 063005, arXiv:hep-ph/9805419.

[62] O. F. Hernández, "Wouthuysen-Field absorption trough in cosmic string wakes," *Phys. Rev. D* **90** no. 12, (2014) 123504, arXiv:1403.7522 [astro-ph.CO].

[63] R. Brandenberger, B. Cyr, and T. Schaeffer, "On the Possible Enhancement of the Global 21-cm Signal at Reionization from the Decay of Cosmic String Cusps," *JCAP* **04** (2019) 020, arXiv:1810.03219 [astro-ph.CO].

[64] R. Brandenberger, B. Cyr, and R. Shi, "Constraints on Superconducting Cosmic Strings from the Global 21-cm Signal before Reionization," *JCAP* **09** (2019) 009, arXiv:1902.08282 [astro-ph.CO].

[65] S. Laliberte and R. Brandenberger, "Ionization from cosmic strings at cosmic dawn," *Phys. Rev. D* **101** no. 2, (2020) 023528, arXiv:1907.08022 [astro-ph.CO].

[66] R. Brandenberger, B. Cyr, and A. V. Iyer, "Fast Radio Bursts from the Decay of Cosmic String Cusps," arXiv:1707.02397 [astro-ph.CO].

[67] R. H. Brandenberger and X.-m. Zhang, "Anomalous global strings and primordial magnetic fields," *Phys. Rev. D* **59** (1999) 081301, arXiv:hep-ph/9808306.

[68] R. H. Brandenberger, "Probing Particle Physics from Top Down with Cosmic Strings," *The Universe* **1** no. 4, (2013) 6–23, arXiv:1401.4619 [astro-ph.CO].

[69] F. Shankar, "Black Hole Demography: From scaling relations to models," *Class. Quant. Grav.* **30** (2013) 244001, arXiv:1307.3289 [astro-ph.CO].

[70] Z.-C. Chen and Q.-G. Huang, "Merger Rate Distribution of Primordial-Black-Hole Binaries," *Astrophys. J.* **864** no. 1, (2018) 61, arXiv:1801.10327 [astro-ph.CO].

[71] Y. Wu, "Merger history of primordial black-hole binaries," *Phys. Rev. D* **101** no. 8, (2020) 083008, arXiv:2001.03833 [astro-ph.CO].

[72] L. Liu, Z.-K. Guo, and R.-G. Cai, "Effects of the surrounding primordial black holes on the merger rate of primordial black hole binaries," *Phys. Rev. D* **99** no. 6, (2019) 063523, arXiv:1812.05376 [astro-ph.CO].

[73] L. Liu, Z.-K. Guo, and R.-G. Cai, "Effects of the merger history on the merger rate density of primordial black hole binaries," *Eur. Phys. J. C* **79** no. 8, (2019) 717, arXiv:1901.07672 [astro-ph.CO].

[74] B. Carr, K. Kohri, Y. Sendouda, and J. Yokoyama, "Constraints on primordial black holes," *Rept. Prog. Phys.* **84** no. 11, (2021) 116902, arXiv:2002.12778 [astro-ph.CO].

[75] D. Gaggero, G. Bertone, F. Calore, R. M. T. Connors, M. Lovell, S. Markoff, and E. Storm, "Searching for Primordial Black Holes in the radio and X-ray sky," *Phys. Rev. Lett.* **118** no. 24, (2017) 241101, arXiv:1612.00457 [astro-ph.HE].

[76] J. Polchinski and J. V. Rocha, "Analytic study of small scale structure on cosmic strings," *Phys. Rev. D* **74** (2006) 083504, arXiv:hep-ph/0606205.

[77] L. Lorenz, C. Ringeval, and M. Sakellariadou, "Cosmic string loop distribution on all length scales and at any redshift," *JCAP* **10** (2010) 003, arXiv:1006.0931 [astro-ph.CO].

[78] **LIGO Scientific, Virgo, KAGRA** Collaboration, R. Abbott *et al.*, "Constraints on Cosmic Strings Using Data from the Third Advanced LIGO–Virgo Observing Run," *Phys. Rev. Lett.* **126** no. 24, (2021) 241102, arXiv:2101.12248 [gr-qc].

[79] S. G. Rubin, A. S. Sakharov, and M. Y. Khlopov, "The Formation of primary galactic nuclei during phase transitions in the early universe," *J. Exp. Theor. Phys.* **91** (2001) 921–929, arXiv:hep-ph/0106187.

[80] M. Y. Khlopov, S. G. Rubin, and A. S. Sakharov, "Strong primordial inhomogeneities and galaxy formation," arXiv:astro-ph/0202505.

[81] M. Y. Khlopov, S. G. Rubin, and A. S. Sakharov, "Primordial structure of massive black hole clusters," *Astropart. Phys.* **23** (2005) 265, arXiv:astro-ph/0401532.

Chapter 6

Massive black holes at high redshifts from superconducting cosmic strings

B. Cyr, H. Jiao, and R.H. Brandenberger, *Massive black holes at high redshifts from superconducting cosmic strings*, Mon.Not.Roy.Astron.Soc (under review), [arXiv:2202.01799].

Addendum for thesis

In this final chapter, we considered a much more detailed approach to the possibility of black hole formation around a cosmic string loop. In the previous chapter (and in previous works in the literature), one assumed that a cosmic string loop in place at early times would accrete enough matter to collapse into a black hole. However, the precise mechanism from which this collapse occurs was never properly investigated.

This article takes a closer look at the dynamics of the primordial gas cloud surrounding a cosmic string loop after recombination. We invoke what is known as the *direct collapse* scenario, in which a primordial gas can collapse monolithically if it satisfies a number of conditions.

In studying which range of cosmic string parameters are necessary to satisfy the direct collapse conditions, we are able to confidently predict when a black hole is likely to form near a string loop. This addresses assumptions made in previous literature, and in particular we show that black hole formation is not trivial. One cannot expect black hole formation around the majority of string loops. These facts have wide-reaching implications for future works studying cosmic string seeded black holes.

Abstract

The observation of quasars at high redshifts presents a mystery in the theory of black hole formation. In order to source such objects, one often relies on the presence of *heavy seeds* ($M \approx 10^{4-6}\, M_\odot$) in place at early times. Unfortunately, the formation of these heavy seeds are difficult to realize within the standard astrophysical context. Here, we investigate whether superconducting cosmic string loops can source sufficiently strong overdensities in the early universe to address this mystery. We review a set of *direct collapse* conditions under which a primordial gas cloud will undergo monolithic collapse into a massive black hole (forming with a mass of $M_{BH} \approx 10^5\, M_\odot$ at $z \approx 300$ in our scenario), and systematically show how superconducting cosmic string loops can satisfy such conditions in regions of the $G\mu - I$ parameter space.

6.1 Introduction

The origin of the active galactic nuclei (AGN) at redshifts higher than $z = 7$ which are believed to harbour super-massive black holes with masses up to $10^9\, M_\odot$ is a growing mystery for astrophysics and cosmology [1, 2, 3, 4]. In order to form such an AGN, a nonlinear overdensity needs to be present at early times. Unless a prolonged period of super-Eddington accretion is invoked, then according to the standard cosmological model (ΛCDM), the number density of such nonlinear seeds at high redshifts is insufficient [5] to explain the observed abundance of high redshift AGNs.

One way to resolve this problem is to consider a cosmological model with large primordial non-Gaussianities in the required mass range. A natural candidate for such non-Gaussianities are cosmic string loops which inevitably arise in a large class of particle physics models beyond the Standard Model. A causality argument [6, 7] ensures that if Nature is described by a field theory which has cosmic string solutions, then a network of strings will form in the early universe and persist to the present time. In [5] it was pointed out that cosmic string loops could provide the seeds for the observed high redshift super-massive black holes. More recently [8], we studied the distribution of such seeds and pointed out that the distribution of seeds can be consistent with both the number density of super-massive and mass-gap black holes.

A key question not addressed in the previous works is the mechanism by which the nonlinear fluctuations induced by a string loop can collapse to form a black hole. This is the problem we address in this paper. We show that in the case of superconducting strings, all

of the criteria for *Direct Collapse Black Hole Formation* can be satisfied in a range of cosmic string parameter values.

In the following section, we give a brief review of cosmic strings, discussing current constraints and highlighting their potential as seeds of supermassive black holes at high redshifts. In Section III we study accretion onto superconducting string loops. Section IV follows with a systematic study of the direct collapse criteria, and a proof-of-concept on how superconducting strings can efficiently meet these criteria. We conclude in Section V, discussing possible implications of these early black holes, as well as limitations of our study that we plan to address in the future.

6.2 Cosmic String Overview

Topological defects are objects that may form at the interface of cosmological phase transitions, provided that the vacuum manifold after such a transition is degenerate, and not simply connected. In three spatial dimensions, there are three classes of defects that are stable (preserved by a topological charge), domain walls from disconnected vacua, cosmic strings from a 1-sphere vacuum manifold, and monopoles from a 2-sphere vacuum manifold. Additionally, a vacuum manifold with a 3-sphere topology gives rise to cosmic textures which can source interesting phenomenological signatures (for example, in the cosmic microwave background [9] [10]) even though they are not stable. In this work, we focus on an observational implication of cosmic strings.

Cosmic strings are nearly one dimensional objects that may form in the very early universe (see e.g. [11, 12, 13] for in-depth reviews). If the symmetry breaking patterns at high energies admit cosmic string solutions, the Kibble mechanism [6, 7] states that they must form, and will permeate the universe. Strings have a small but finite width, whose interiors consist of a condensate of gauge and scalar fields which were present in the previously unbroken phase. An attractive feature of regular cosmic string theories is that they possess only one free parameter, μ, the string tension. If the symmetry breaking scale for cosmic string formation is η, the tension is simply related by $\mu \sim \eta^2$. In the literature, this is usually expressed as the dimensionless quantity $G\mu$ where G is Newton's constant. Certain symmetry breaking patterns (for example [14, 15, 16]) can give rise to cosmic strings which carry a current (I) and are therefore referred to as superconducting. In this work, we will remain agnostic to the microphysics of the symmetry breaking, and so the parameter space is extended to include the current as a second free parameter. Phenomenological signatures of strings are often sensitive to larger values of $G\mu$, and thus also offer a way to probe particle physics from

the top-down, complementary to accelerator experiments such as the Large Hadron Collider [17].

If cosmic strings form, they exist as both long strings (with curvature radius greater than the Hubble radius), and a distribution of smaller (sub-Hubble) string loops which form from the intersections and self-intersections of the long strings. It is understood that the distribution of long strings follows a scaling relation, but the nature of the loop distribution is more uncertain. Nambu-Goto simulations model the strings as truly one dimensional, and find that the loops also follow a scaling relation [18, 19, 20, 21, 22, 23, 24, 25], whereas Abelian-Higgs field theory simulations find a negligible fraction of energy in the loops [26, 27, 28]. The origin of this discrepancy is a long-standing problem with no clear answer thus far. Our work represents a proof-of-concept and therefore makes no assumption on the properties of the underlying loop distribution, aside from requiring that loops form and persist for at least a Hubble time.

Originally, cosmic strings were thought as an alternative mechanism to seed perturbations observed in the cosmic microwave background (CMB), requiring a string tension of $G\mu \sim 10^{-6}$ [29, 30, 31, 32]. However, cosmic strings don't give rise to acoustic oscillations, and so the now detailed studies of the angular power spectrum of the CMB rule out cosmic strings as the dominant source of structure formation, setting a robust bound of $G\mu \leq 10^{-7}$ [33, 34, 35] [36, 37, 38]. Long strings can also source line discontinuities in CMB temperature maps, which have the possibility of strengthening this bound by a couple orders of magnitude [39, 40] [41, 42, 43, 44, 45, 46, 47]. In addition to these bounds, a distribution of cosmic string loops will produce a stochastic background of gravitational waves [48] which could be detected by current generation pulsar timing arrays, or next generation gravitational wave observatories such as LISA [49]. Recently, the NANOGrav [50], PPTA [51], and EPTA [52] collaborations have reported on the detection of a common-spectrum process which has been validated by the International Pulsar Timing Array group [53]. If this signal has a cosmic string origin, it may be sourced by a loop distribution with string tension $G\mu \sim 10^{-10}$ [54]. Alternatively, if this signal is not due to string loops, a stronger bound of $G\mu \leq 10^{-11}$ can be placed on the string tension assuming that the loop distribution follows a scaling relation (as is seen in Nambu-Goto simulations).

Besides sourcing a gravitational wave background, string loops have been considered in a wide variety of contexts. Work has been done on modelling the progenitors of fast radio bursts (FRBs), where annihilations of microstructure (cusps) on both regular [55] and superconducting loops [56, 57, 58, 59, 60, 61, 62] could source the signal. In addition, these cusp annihilations may also influence the global 21-cm signal by injecting additional photons

into the background, heating it up. While this effect is small for ordinary string loops [63], new regions of parameter space were constrained in the context of superconducting loops [64]. String loops are regions of trapped energy, and thus are also capable of sourcing significant gravitational potentials at early times. The high redshift formation of galaxies and stars can lead to constraints coming from early reionization and structure formation [65, 66, 67], though these are roughly the same as the CMB bound, $G\mu \leq 10^{-7}$. Accretion onto loops was studied in detail in [68], where the formation of ultra-compact minihalos was considered. Superconducting strings can also source gamma ray bursts at high redshift [69].

Due to their gravitational potential, string loops have been proposed as the solution to some astrophysical mysteries, such as the origin of globular clusters [70, 71], as well as supermassive and intermediate mass black holes [5, 8]. Another astrophysical mystery is the observation of high redshift quasars, which are thought to host central black holes of mass $10^{8-9}\, M_\odot$ at redshifts $z \geq 7$ [3]. These objects are challenging to explain within the standard paradigm, as black holes formed through the typical stellar channels do not have enough time to accrete this much mass without a prolonged period of hyper-Eddington accretion [72].

If string loops exist, they would be present at very high redshifts and persist through cosmic time, making them ideal candidates to source and seed these supermassive black holes (SMBHs). However, a question that has not been addressed clearly in recent proposals, is how the nonlinearity sourced by the string loop can collapse into a black hole at early times. In matching to observations, this is often assumed to be the case, and hence the main purpose of this work is to investigate if this collapse truly does take place.

A cosmic string loop of radius R has mass $M_{loop} = \beta\mu R$ (where $\beta = 2\pi$ refers to a circular loop). As string loops oscillate about their centre of mass, one can ask if a given loop ever satisfies the Hoop conjecture, that is, does its total mass ever reside within its Schwarzschild radius. For low string tensions ($G\mu \ll 10^{-3}$) the Hoop conjecture is satisfied for a negligible fraction of string loops, leading to the conclusion that loop collapse into black holes is difficult to realize in nature [73, 74]. However, this need not be true when one considers not just the loop, but also its immediate environment. One should note that in full numerical relativity, it has been shown that for large values of the string tension ($G\mu \sim 10^{-2}$), it is possible for the loops to collapse on their own [75, 76]. However, such high tensions are ruled out for cosmologically stable strings.

Much work has gone into attempting to source these high redshift SMBHs within a standard ΛCDM universe. One of the most promising avenues is the monolithic collapse of a pristine gas cloud, capable of producing an initially massive ($M_{BH,i} \approx 10^5\, M_\odot$) black hole a mere million years after the collapse begins [77, 78, 79, 80, 81, 82] [83, 84, 85]. In order to

produce a so-called *Direct Collapse Black Hole* (DCBH), a number of favourable conditions within the gas cloud must be met. Unfortunately, one of the conditions (the presence of a strong Lyman-Werner background, see below for details) is exceedingly difficult to satisfy given only standard ΛCDM (see [83, 84, 85] and references therein). In this work, we show that for superconducting cosmic strings, there is a region of parameter space which satisfies all of the DCBH criteria and therefore may allow for the early formation of high mass black holes.

6.3 Accretion onto Superconducting Cosmic String Loops

String loops typically form with curvature radii some fraction of the Hubble radius, $R \sim \alpha t_f$, where t_f is the time of loop formation and $\alpha \sim \mathcal{O}(0.1)$ (see [11, 12, 13] for details). After formation, these loops gradually lose energy through a variety of mechanisms which produce gravitational waves and particle content, such as cusp annihilations, kinks, and the overall oscillatory motion of the loop. For values of the string tension and current that we are most interested in, $G\mu \geq 10^{-17}$, the production of gravitational waves is the dominant energy loss mechanism for the loops [48] (hence why, for a given loop distribution, one gets strong constraints from the non-detection of a stochastic gravitational wave background from pulsar timing). As the strength of these processes depend on the radius of the loop, one can define a gravitational cutoff radius at time t as $R_c^{GW}(t) = \gamma\beta^{-1}G\mu t$ (where $\gamma \sim \mathcal{O}(100)$ from simulations), where loops with $R < R_c^{GW}$ will lose all of their energy and decay within one Hubble time. We use the "sudden decay" approximation, in which a loop with radius $R > R_c^{GW}$ maintains its size until it no longer satisfies this condition.

If the strings are superconducting (that is, the loops carry a current I), their direct coupling to electromagnetism enhances the energy loss to photons and charged fermions [59]. One can define a critical current, $I_c = \gamma\kappa^{-1}(G\mu)^{3/2}m_{pl}$ (where m_{pl} is the Planck mass and $\kappa \sim \mathcal{O}(1)$), and if the current on the string is $I > I_c$, the electromagnetic decay channel is dominant. The value of the cutoff radius depends on this current through

$$R_c(t) = \begin{cases} R_c^{GW}(t) = \gamma\beta^{-1}G\mu t & I < I_c \\ R_c^{EM}(t) = \kappa\beta^{-1}\frac{I}{m_{pl}}(G\mu)^{-1/2}t & I \geq I_c. \end{cases} \tag{6.1}$$

String loops act as early non-linearities in the density field, and will accrete the surrounding dark matter and baryons. A detailed study of this accretion was performed in [68] for

string loops forming and persisting during the radiation and matter dominated eras, with applications to ultra-compact minihalos in mind.

We adopt their analysis, which describes the spherical infall of matter from the nearly smooth (linear) background density field at early times. As one would expect, string loops that exist in the radiation dominated era accrete at a highly inefficient rate, yielding a total non-linear mass at t_{eq} of at most twice the loop mass, depending on if the loop had decayed by that point. However, once a loop enters the matter dominated epoch, its dark matter halo grows steadily, following the expression

$$M_{DM}(z) = M_{loop}\left(\frac{z_{eq}+1}{z+1}\right) \qquad (z \leq z_{eq}). \tag{6.2}$$

This growth occurs through the decoupling of spherical shells of dark matter from the Hubble flow, turning around at a physical distance from the centre of the loop, r_{TA}. These shells fall to the centre of the halo on free-fall timescales, during which many shell-crossings occur, and the matter subsequently virializes. The density profiles of these string-seeded halos follow a $\rho \sim r^{-9/4}$ profile [86, 87, 88], steeper than the usual $\rho \sim r^{-2}$ observed from Gaussian fluctuations [89]. Heuristically, the physical picture for the formation of an early massive gas cloud is this:

1. String loops are formed before matter-radiation equality and accrete at a negligible rate.

2. At t_{eq}, dark matter begins falling into the potential wells sourced by the string loops. However, before recombination the Jeans mass is very large ($M_J \approx 10^{12}\,M_\odot$) and so the baryonic matter remains unbound to the newly forming halo.

3. After recombination the Jeans mass drops rapidly (to roughly $\approx 10^5\,M_\odot$), and baryons collapse into string-seeded dark matter halos satisfying $M(z) > M_J$, where they virialize to a uniform temperature, T_{vir}. We show a more detailed computation of this in the following section.

These accretion dynamics were originally formulated for a non-superconducting cosmic string. In Appendix A, we review the basic arguments of [68] more quantitatively, and show that the additional radiation pressure produced by a superconducting cosmic string doesn't perturb the picture described above in any major way. We will now show that a gas cloud formed in this way is capable of satisfying conditions which would lead to its monolithic collapse into a massive, high redshift black hole.

6.4 Direct Collapse Conditions

The formation of stellar mass black holes in our universe is a fairly well understood process: once the internal temperature of a star is no longer high enough to mediate nuclear interactions, the star collapses under its own gravitational force, often leading to a supernova and a remnant. For sufficiently massive stars, this remnant cannot be sustained by neutron degeneracy pressure and collapses into a black hole. The LIGO-Virgo collaboration has confirmed that these stellar mass ($\mathcal{O}(1)\, M_\odot \leq M_{BH} \leq \mathcal{O}(100)\, M_\odot$) black holes are indeed ubiquitous in nature [90, 91, 92].

However, observations of high redshift quasars suggest that supermassive black holes are already in place at early times. The most robust high redshift black hole observation to date has a mass of $1.6 \times 10^9\, M_\odot$ at $z = 7.642$ [3], although there have recently been observations of two galaxy candidates [93] at $z \sim 13$, which may be interpreted as quasars hosting black holes of order $M_{BH} \approx 10^8\, M_\odot$ [94]. Conservatively, a population of "light" black hole seeds (initial mass $M_{BH} \sim 10^2\, M_\odot$) will form through the collapse of Pop III stars. However, there is simply not enough time for them to grow to these supermassive objects by $z \sim \mathcal{O}(10)$ unless super or hyper-Eddington accretion can be reliably sustained (see [72] and references therein).

The formation of "heavy" seeds (initial mass $M_{BH} \sim 10^{4-6}\, M_\odot$) on the other hand, offers a more realistic way to form supermassive black holes at high redshift. These heavy seeds can be formed through runaway merger processes of lighter black holes or Pop III stars in highly dense environments [95, 96], or through the monolithic collapse of a metal-free gas cloud [77, 78, 79, 80, 81, 82] [83, 84, 85]. Unfortunately, both of these formation channels are still quite difficult to realize in the standard cosmological and astrophysical context, and hence the origin of high redshift SMBHs still remains an open question.

In order for a gas cloud to collapse without fragmentation, a number of conditions must be met,

1. The cloud must contain sufficient material to collapse and feed an initial protostar or seed black hole. If we want the final seed mass to be $M \approx 10^5\, M_\odot$, we require at least this much baryonic matter in our string-seeded overdensities.

2. The atomic cooling threshold of the halo must be met in order to trigger the collapse without fragmentation. This requires the virial temperature of the halo to be $T_{vir} = 10^4\,\mathrm{K}$ (or higher).

3. In order to reach the atomic cooling threshold, low temperature cooling pathways

must be suppressed. Low temperature cooling occurs via heavy elements or molecular hydrogen being present in the halo. Therefore, we demand that our early formed halos haven't undergone star formation that would pollute it with metals. Additionally, a Lyman-Werner (LW) background of $J_c \approx 10^{-44} - 10^{-42}\,\mathrm{GeV}^3$ is required to quench the formation of molecular hydrogen.

If these conditions are met, a direct collapse event may occur. In such an event, the gas cloud collapses nearly isothermally, forming a rapidly accreting protostar at the centre[1]. Following the work of [83, 84, 85], this central protostar is initially quite light ($M_i \approx 0.2\,M_\odot$), but accretes at a rate of roughly $\dot{M} \approx 20 c_s^3/G \approx 1\,M_\odot/\mathrm{yr}$ [99] provided that the temperature remains as high as $T_{vir} \sim 10^4\,\mathrm{K}$ during the collapse. At this accretion rate, the protostar exhibits an instability at roughly $M \approx 2 - 3.5 \times 10^5\,M_\odot$, collapsing into a black hole of similar mass [100, 101].

It is clear that for standard astrophysical galaxies, the requirement for H_2 dissociation processes such as a strong Lyman-Werner background is difficult to realize. In principle, this background can be produced by star formation in the galaxy, though this would quickly pollute the galaxy with various metals, in violation with the *pristine mass* condition. One possibility would be to source the necessary LW background from a nearby star-forming galaxy, though this also requires a tuned scenario.

If a superconducting cosmic string resides at the centre of these protogalaxies, however, there is the possibility of sourcing this background without requiring any star formation. Therefore, within a given region of the $G\mu - I$ parameter space, loops with a radius $R > R_c^{BH}$ (where R_c^{BH} is the critical loop radius for black hole formation) will undergo a gravitational collapse. We emphasize that it is not the loop itself that is collapsing, but instead the baryonic matter in the string-seeded overdensity that forms the black hole. In the following subsections, we show that superconducting cosmic strings present ideal environments to source direct collapse black holes at very early times.

6.4.1 Sufficient Pristine Mass

In order to grow a protostar to the point that it can undergo a collapse into a black hole with mass $M_{BH} \approx 10^5\,M_\odot$, we require at least that much pristine, baryonic material. As we are envisioning a picture in which these gas clouds collapse shortly after recombination, no

[1] see figures 7, 9 and 11 of [83, 84, 85] as well as [97, 98, 99] for detailed simulations and semi-numerical modelling of this process.

star formation is expected to have occurred and so the requirement on pristine material is trivially satisfied.

Eq. (6.2) represents the growth rate of the dark matter halo after matter radiation equality. Baryons remain unbound to the halo until recombination due to a high Jeans mass. After recombination, however, the Jeans mass drops rapidly to a roughly constant value [102],

$$M_J \approx 1.35 \times 10^5 \left(\frac{\Omega_m h^2}{0.15}\right)^{-1/2} M_\odot. \tag{6.3}$$

Dark matter halos with $M \geq M_J$ will begin capturing baryons quickly following recombination. The physical radius that a shell of matter which is beginning to collapse at a redshift z would have in the absence of a string loop is given by the non-linear radius, r_{nl},

$$r_{nl}(z) = \left(\frac{3\beta\mu R}{4\pi\rho(z)} \cdot \frac{1+z_{eq}}{1+z}\right)^{1/3}. \tag{6.4}$$

This is related to the turn-around radius by $r_{nl} = 2r_{TA}$. Since we are at very early times, we assume that both the dark matter and baryonic density fields are smooth, and thus the total baryonic mass inside this radius is

$$M_b(z) = \frac{\Omega_b(z)}{\Omega_M(z)}\beta\mu R\left(\frac{1+z_{eq}}{1+z}\right) \qquad (z < z_{rec}). \tag{6.5}$$

The baryon fraction $\Omega_b/\Omega_M \approx 1/6$ and is roughly constant in time. If we require $M_b \geq 10^5\, M_\odot$ in order to form direct collapse black holes, we can see that the condition for baryonic infall ($M_{DM}(z) \geq M_J(z)$) is automatically satisfied. Therefore, in order to have enough pristine baryonic matter in the halo, we require

$$G\mu \geq \frac{\Omega_M}{\Omega_b}\frac{G}{\beta}\frac{1}{R}\left(\frac{z+1}{z_{eq}+1}\right) \times 10^5\, M_\odot \tag{6.6}$$

or, in units of $c = \hbar = k_b = 1$ with $\beta = 10$

$$G\mu \geq 2 \times 10^{-13} \left(\frac{t_{eq}}{R}\right) \left(\frac{z+1}{z_{eq}+1}\right). \tag{6.7}$$

Recall that at any time t (or redshift z) loops form with radius $R_{form} = \alpha t$, and loops with gravitational cutoff radius $R_c^{GW} = \gamma\beta^{-1}G\mu t$ decay away (we will be concerned with values of the current $I < I_c$, meaning that gravitational emission is the dominant decay mechanism). Expressing t in terms of t_{eq} this means that during the matter epoch loops exist with a range of radii

$$\gamma\beta^{-1}G\mu \left(\frac{1+z_{eq}}{1+z}\right)^{3/2} t_{eq} \;\leq\; R \;\leq\; \alpha \left(\frac{1+z_{eq}}{1+z}\right)^{3/2} t_{eq}. \tag{6.8}$$

However, we need our loops to be in place by t_{eq} so that they may grow their dark matter halos until recombination, therefore our range of accessible string radii is

$$\gamma\beta^{-1}G\mu t_{eq} \;\leq\; R \;\leq\; \alpha t_{eq}. \tag{6.9}$$

We will be most interested in the case where the baryons fall into the halo right after recombination. Therefore, some fraction of the loop distribution with $R > R_c^{BH}$ will attract $M_b \geq 10^5\, M_\odot$ in the initial baryonic collapse at z_{rec}. The value of R_c^{BH} can be computed by rearranging (6.7) for a given value of $G\mu$

$$R_c^{BH} = \frac{2 \times 10^{-13}}{G\mu} t_{eq} \left(\frac{z+1}{z_{eq}+1}\right). \tag{6.10}$$

At a given redshift, this implies that loops with radii in the range

$$R_C^{BH} \leq R \leq \alpha t_{eq} \tag{6.11}$$

will accrete a sufficient amount of gas to collapse into a $10^5\, M_\odot$ black hole.

Note that the fact that the strings are superconducting is irrelevant for this condition, so both ordinary and superconducting cosmic strings are capable of sourcing massive gas clouds in the early universe (as was considered in eg. [65, 66]).

6.4.2 Atomic Cooling Threshold

The second criterion required to kickstart a direct collapse procedure is the formation of an atomic cooling halo. An atomic cooling halo is characterized by its inability to cool at low temperatures ($T_{vir} \leq 10^4\,\mathrm{K}$) through the usual pathways of molecular hydrogen or other heavy elements. As a result, the halo is unable to cool until it reaches a gas temperature of $T_{vir} \approx 8000\,\mathrm{K}$ when cooling via atomic line transitions in hydrogen begins. The lack of heavy elements in string-seeded overdensities was justified in the previous section, and we will discuss the quenching of H_2 in the following section. Here we compute the virial temperature of a string-seeded halo and show that it is above the atomic cooling threshold, implying that a collapse will indeed take place, provided that the halo satisfies the *sufficient mass* criteria above.

As mentioned above, after recombination the Jeans mass drops rapidly and baryons fall into the halo. Again, we consider the spherical collapse model where shells of baryonic and dark matter turn around and fall towards the centre. The typical timescale for this infall is the free-fall time. When the mass of the infalling shell is much less than the halo mass, it can be approximated by

$$t_{ff} \approx \sqrt{\frac{3\pi}{32G\bar{\rho}}}, \tag{6.12}$$

where $\bar{\rho}$ is the background energy density. Using the critical density, one can find that the free-fall time is roughly a Hubble time, $t_{ff} \approx (\pi/2)H^{-1}$. It is important to note that during a free-fall time, the collapsing shells of matter will cross one another, interacting and bringing the halo into an equilibrium [103]. Therefore, t_{ff} is identified with the virialization timescale, when the gas in the halo reaches a uniform temperature, T_{vir} which we will now compute. For clarity, a shell turning around at recombination has a free-fall time of $t_{ff}(z_{rec}) \approx 0.85\,\mathrm{Myr}$, implying that it forms a virialized halo at roughly $z \approx 500$.

The virial theorem provides a relationship between the gravitational and thermal energy of a halo

$$\frac{Gm_h M_{nl}}{r_{vir}} = \frac{3}{2}T_{vir}, \tag{6.13}$$

where m_h is the mass of hydrogen (the dominant baryonic constituent), M_{nl} is the total nonlinear mass in a sphere of radius r_{nl}, and r_{vir} is the virial radius of the halo, related to

the turn-around and non-linear radii by $r_{vir} = (1/2)r_{TA} = (1/4)r_{nl}$. Recall that eq (6.4) provides us with the redshift at which a certain shell becomes nonlinear, allowing us to determine the virial temperature of a string-seeded halo simply as a function of redshift. After evaluating numerical factors and setting $\beta = 10$, we find the virial temperature of a halo at redshift z to be

$$T_{vir}(z) \approx 8 \times 10^{13}\,\mathrm{K}\,(G\mu)^{2/3} \left(\frac{R}{t_{eq}}\right)^{2/3} \left(\frac{1+z}{1+z_{eq}}\right)^{1/3}. \tag{6.14}$$

It is important to note that this expression must be evaluated at the redshift when a particular shell goes nonlinear. Therefore, even though shells that go nonlinear at recombination don't virialize until $z \approx 500$, their temperature must be evaluated at z_{rec}. The reason being that shells decoupling from the Hubble flow after recombination have not undergone sufficient shell crossings at $z = 500$ to virialize and thus don't contribute to the temperature.

In order to trigger atomic cooling, our halo must reach $T_{vir} \geq 8000\,\mathrm{K}$ allowing us to once again relate the string tension with the radius of a particular loop. This yields the constraint

$$G\mu \geq 9.7 \times 10^{-16} \left(\frac{t_{eq}}{R}\right) \left(\frac{1+z_{eq}}{1+z}\right)^{1/2}. \tag{6.15}$$

This constraint is degenerate with the sufficient mass conditions. As the halo grows in mass, its virial temperature drops modestly as energy is diffused from the hot inner regions of the halo to the colder shells which fall in later. At a redshift of $z \sim 90$ this constraint becomes the dominant one. We are primarily concerned with the baryonic matter falling in shortly after recombination, and as a result, if the mass constraint is satisfied, the virial temperature of the halo will automatically be above the atomic cooling threshold. The critical loop radius will remain the same as in eq (6.10), and this condition is also not sensitive to the superconducting nature of our string loops.

6.4.3 Lyman-Werner Background

If a gas cloud becomes massive enough, structure formation theory tells us that it will collapse and fragment, leading to abundant star formation. In order for this fragmentation to occur, the gas must remain relatively cool ($T \leq 10^4\,\mathrm{K}$). Low temperature cooling in gas clouds can occur when heavy elements are present, which are usually sourced by an epoch of prior star

formation in the halo. In a string-seeded halo, no such star formation has taken place, and so our gas is pristine, consisting of only hydrogen atoms.

However, cooling can also occur via the collisional excitation of molecular hydrogen, unless a sufficiently strong flux of Lyman-Werner photons ($E_\gamma \approx 10 - 13\,\mathrm{eV}$) is present. Lyman-Werner photons possess enough energy to quickly dissociate any newly formed H_2 allowing the halo to heat up to the atomic cooling threshold ($T \approx 10^4\,\mathrm{K}$), where the fragmentation of a collapsing gas cloud no longer occurs. The typical flux necessary to properly irradiate an optically thick, collapsing gas cloud is roughly [83, 84, 85]

$$\begin{aligned} J_c &\approx (10^{-18} - 10^{-16})\,\mathrm{erg\ s^{-1}cm^{-2}Hz^{-1}\,Sr^{-1}} \\ &\approx 2 \times (10^{-44} - 10^{-42})\,\mathrm{GeV}^3, \end{aligned} \tag{6.16}$$

where we quote the second line in natural units.

This condition, which is necessary for the monolithic collapse of a gas cloud, is notoriously difficult to realize within standard astrophysics and cosmology. Lyman-Werner backgrounds are usually sourced by the first stars in a halo. This presents a problem, as it also introduces metals into the halo, and therefore will not prevent cooling. Superconducting cosmic strings, on the other hand, can source such a background without star formation.

Superconducting strings carry a current, I, and are capable of emitting large bursts of electromagnetic radiation. The energy injection spectrum of a loop with radius R and current I is given by [59]

$$\frac{dP}{d\omega} = \kappa I^2 R^{1/3} \omega^{-2/3}. \tag{6.17}$$

To estimate the flux in Lyman-Werner photons, we consider an optically thick gas which traps photons emitted by the string (in the band $10\,\mathrm{eV} \leq E_\gamma \leq 13\,\mathrm{eV}$) at times after recombination. By integrating (6.17) over a Hubble time at redshift z and dividing by the virialized volume we obtain the following expression for the energy density per unit frequency at the frequency ω

$$\frac{d\rho}{d\omega} \approx \frac{32}{3\pi}\frac{\kappa}{\beta} I^2 (G\mu)^{-2} R^{-2/3} \omega^{-2/3} t_{eq}^{-1} \times \left(\frac{1+z}{1+z_{eq}}\right)^{5/2} \left(1 - \left(\frac{1+z}{1+z_{rec}}\right)^{3/2}\right). \tag{6.18}$$

Expressing the current in units of the critical current I_c, and inserting values for the Lyman-Werner frequency ω, the Planck mass and t_{eq} we obtain flux of

$$J \approx 10^{-34} \left(\frac{G\mu}{10^{-10}}\right)^2 \left(\frac{I}{I_c}\right)^2 \left(\frac{R}{t_{eq}}\right)^{-2/3} \left(\frac{1+z}{1+z_{eq}}\right)^{5/2} \times \left(1 - \left(\frac{1+z}{1+z_{rec}}\right)^{3/2}\right) \text{GeV}^3, \tag{6.19}$$

where we have evaluated the numerical constants as $\kappa = 1$ and $\gamma = 100$. Shells of matter turning around at recombination will virialize and begin to collapse at $z \approx 500$, and so we evaluate at this redshift. Recall that for $I < I_c$ the dominant energy loss mechanism for the strings is gravitational waves, while for $I > I_c$ it is electromagnetic emission. By requiring that we have a flux $J \geq J_c \approx 10^{-43}\,\text{GeV}^3$, we find a constraint in the $G\mu$-I plane

$$G\mu \geq 4 \times 10^{-14} \left(\frac{I}{I_c}\right)^{-1} \left(\frac{R}{t_{eq}}\right)^{1/3}, \tag{6.20}$$

when we evaluate at $z = 500$, the black hole collapse redshift. Recall that any string loop with $R_c^{BH} \leq R \leq \alpha t_{eq}$ is capable of accreting enough mass to satisfy the direct collapse criteria. One may rightly worry that the radiation from a superconducting string could induce a strong pressure force which disturbs the accretion dynamics. We refer the reader to Appendix A where we consider these effects in more detail. By requiring that these pressure forces remain small, a complementary upper bound can be set on the string tension

$$G\mu \leq 10^{-2} \left(\frac{I}{I_c}\right)^{-3} \left(\frac{R}{t_{eq}}\right)^{5}. \tag{6.21}$$

For a given loop radius R which satisfies the sufficient mass constraint, there exists a wedge in the $G\mu$-I plane which can produce a strong enough Lyman-Werner background, while not

sourcing enough radiation pressure to disturb the accretion.

Thus far we have remained agnostic to whether these loops exist as part of a scaling loop distribution as indicated by Nambu-Goto simulations, or whether they exist in relative isolation with no scaling solution and a negligible cosmological abundance. However, we must now make a comment, as if string loops are abundant, many authors (eg: [67, 104, 64]) have attempted to constrain the $G\mu$-I parameter space. In the case where loops are not abundant, these constraints generally don't apply and one may view the wedge formed by (6.20) and (6.21) as the allowed region of parameter space.

If loops are abundant, it would appear from fig. 8 of [104] that this current wedge is already constrained. However, there exist a number of caveats that make it difficult to do a straightforward comparison between our work and the usual constraints in the literature.

First, these constraints assume that all loops in the network are superconducting, with the same uniform current I, regardless of loop size. Early work on superconducting cosmic strings pointed out that the current generated on a string is dependent on the local external magnetic field at the time and place of loop formation [14, 15, 16]. Therefore, as a proof-of-concept work, it is possible that significant fluctuations in the magnetic field on length scales comparable to the radius of the loop could induce anomalously large currents on a small fraction of the loop distribution. This would source a strong Lyman-Werner background in this small fraction of loops, satisfying the criterion for direct collapse black hole formation, while remaining consistent with the constraints from [104].

Furthermore, if one has a scaling solution of loops, the observational signatures are often dominated by loops with the smallest radii, as they are the most abundant. The CMB anisotropy constraints [104] overlap significantly with our target parameter values, but these constraints are strongly dominated by string loops that decay at recombination. The loops we consider here are necessarily much larger, as we require them not to decay before redshifts of at least $z \approx 500$ (in the case of mass shells turning around at recombination). This implies that the currents on our larger loops need not be as small as those on the ones decaying at recombination. In fact, one might also expect that since these two populations of loops form at different times, they will likely possess different currents as the external magnetic fields evolve between their formation times.

Finally, there is also the possibility that if a scaling loop distribution exists, not all of the loops need to be superconducting. Therefore, the strength of the constraints in the $G\mu$-I plane will scale depending on the fraction of superconducting loops in the network, and the characteristic radii of the loops that do carry a current. Note also that we consider only the Lyman-Werner photons from the central loop. If a distribution of loops exists, a number of

smaller loops will also be present in each halo and will also contribute to the dissociating photon background.

We conclude this section by remarking that regardless of whether a string loop belongs to an abundant distribution, or is produced in relative isolation, equations (6.20) and (6.21) provide upper and lower bounds for the string tension given a current and loop radius. This maps out a wedge in parameter space where a strong enough Lyman-Werner background is present to dissociate molecular hydrogen, but the radiation pressure does not significantly perturb the accretion dynamics.

6.5 Discussion and Conclusions

The progenitors of black holes at high redshifts inferred through quasar observations remains a tantalizing mystery in astrophysics and cosmology. At the moment, the most intuitive candidate is to invoke hyper-Eddington growth onto a stellar mass black hole formed through the death of a Pop III star. However, the conditions necessary for such rapid accretion are not well understood, and strong feedback will likely cause severe limitations on the growth rates of such objects.

Another hypothesis is to invoke the direct collapse of a massive gas cloud at earlier times, as then only slow growth is necessary to grow them from an initial mass of roughly $M_i \approx 10^5\,M_\odot$ to their observed masses of $M_f \approx 10^{8-9}\,M_\odot$ at redshifts of $z \approx 8-13$. The conditions for such a collapse have been known for some time: a gas cloud with sufficient mass, and a lack of cooling pathways at low temperatures will collapse without fragmentation when it reaches the atomic cooling threshold. Unfortunately, it is difficult for typical gaseous halos to satisfy these conditions simultaneously. However, in the presence of a superconducting cosmic string loop, we have shown that these conditions can indeed be satisfied.

What we have presented above is a proof-of-concept work showing that if superconducting cosmic strings exist, they act as nonlinear seeds at early times (around matter-radiation equality). For a range of parameters, they first grow a dark matter halo at t_{eq}, and begin accreting gas shortly after recombination. Using the spherical collapse model, we have argued that a virialized halo is in place roughly one Hubble time after the turnaround time for the first shell of matter (namely, at around $z \approx 500$). Electromagnetic emission from the superconducting string sources a strong Lyman-Werner background, ensuring that no molecular hydrogen is present. Therefore, these string-seeded halos can efficiently satisfy all of the direct collapse criteria, and may collapse into black holes. The time between the initial monolithic collapse of the gas cloud, and the $10^5\,M_\odot$ black hole formation is about

1 Myr, implying that these black holes have formed by $z \approx 300$.

We have decided not to speculate on whether these string seeded black holes can match the observed abundance of high redshift quasars. We leave this to future work due to a number of caveats and subtleties that arise when applying this idea to a network of string loops. As mentioned in the previous subsection, the loops that can give rise to these halos are necessarily quite large ($R \gg R_c^{GW}$). Constraints on the $G\mu - I$ plane (see [104]) are usually sourced mainly by the smallest loops, since they are the most abundant. As a result, one needs to revisit how sensitive these constraints (particularly the ones coming from CMB anisotropies) are to currents on the larger loops before directly applying them to our model. Also, as currents on the loops are generated at the time of formation by local electromagnetic fields, it is likely that loops with different radii have different currents. Large fluctuations of the magnetic field on very small scales may also cause some loops to develop an unusually strong current. Each of these nuances must be understood before a proper abundance computation can be performed for these string-seeded black holes.

Furthermore, we have assumed spherical accretion in the rest frame of the string loop. While this will likely be a good approximation for some fraction of a string loop network, in general one should consider the loop velocity distribution. The relative velocity between the loop and its surrounding medium weakens the efficiency of accretion, making it more difficult to fulfil the *sufficient mass* criterion above. Historically, stringent bounds on the cosmic string tension $G\mu$ have been made weaker by considering this effect, such as in the case of early star formation [66] and ultra-compact minihalos [68] from string loops.

We have presented a proof-of-concept to show that in the regions of parameter space outlined by equations (6.7), (6.20), and (6.21), superconducting string loops can seed gaseous halos which will collapse into early time supermassive black holes. While this represents a possible resolution of the high redshift quasar mystery, one should be cautious in applying these results to a network of string loops without addressing our above concerns. Nevertheless, this represents an important step in validating phenomenological models of black hole formation from cosmic strings.

Acknowledgements

The research at McGill is supported in part by funds from NSERC and from the Canada Research Chair program. BC is grateful for support from a Vanier-CGS doctoral scholarship. HJ is supported in part by a Trottier award from the McGill Space institute. We would like

to thank Pratika Dayal and Maxime Trebitsch for valuable discussions at an early stage, as well as Marta Volonteri and Patrick Peter for correspondence and encouragement.

Appendix A - Accretion Dynamics and Pressure Forces

Here we summarize the main points of [68] which explored the detailed accretion dynamics of dark matter onto cosmic string loops. Both our work and theirs adopt the "sudden decay" approximation, in which the slow gravitational decay of the loop is neglected until the loop radius falls below the gravitational cutoff. This implies that once formed, loops keep their radius at $R_f = \alpha t_f$ until decay. The time of decay is then related to the time of formation by

$$t_d = \frac{\alpha}{\gamma G \mu} t_f. \tag{6.22}$$

The authors of [68] then consider the spherical collapse [105] of dark matter onto initially isothermal fluctuations sourced by the string loops. Spherical shells are considered a physical distance $r(x)$ from the centre of the loop with

$$r(x) = a(x)b(x)\zeta_i, \qquad x = \frac{a(t)}{a(t_{eq})}, \tag{6.23}$$

where $a(x)$ is the scale factor, ζ_i is the initial comoving coordinate associated with the shell at time t_i, and $b(x)$ compares this physical distance in the case with a loop present, and without. A shell is said to turn around when $\dot{r} = 0$, and so the rest of the work is dedicated to solving the dynamical equation for $b(x)$ in different regimes [106],

$$x(x+1)\frac{d^2b}{dx^2} + \left(1 + \frac{3}{2}x\right)\frac{db}{dx} + \frac{1}{2}\left(\frac{1+\Phi}{b^2} - b\right) = 0. \tag{6.24}$$

The gravitational perturbation is simply $\Phi = \delta M / M(r)$ where $\delta M = M_{loop}$ is the loop mass, and $M(r)$ is the total mass enclosed within physical radius r.

For loops that form in the radiation era, it was found that even before t_{eq}, mass shells will turn around and fall onto the seed. If the loop forms and decays before t_{eq}, the total growth of the overdensity in the radiation era (with $x > x_d$) is given by

$$M(x) = 2x_d M_{loop} \frac{3x+2}{3x_d+2} \qquad (x_d < x < 1), \tag{6.25}$$

where $x_d = a(t_d)/a(t_{eq})$ is the time when the loop decays. If the loop has not decayed yet, the growth was found to be linear in x at all times, following

$$M(x) = 2xM_{loop} \qquad (x_f < 1 \text{ and } 1 < x < x_d). \tag{6.26}$$

Since at t_{eq} we have $x = 1$, this implies that a loop will build up an overdensity with mass $M(t_{eq}) = 2M_{loop}$ at matter-radiation equality. In our work we conservatively set the linear growth rate of the dark matter halo to be $M(x) = M_{loop}x$ in agreement with these results.

Superconducting strings produce a radiation field which can source an additional pressure force on the infalling matter. To estimate this effect, we consider the ratio of the gravitational binding force of a halo at redshift z to the radiation pressure force coming from photons in that halo. For a density profile of the form $\rho(r) = \rho(r_{vir})(r_{vir}/r)^{\alpha}$, the gravitational binding energy is

$$U_{grav} = -\frac{16\pi^2 G}{(3-\alpha)(5-2\alpha)}\rho^2(r)r^5. \tag{6.27}$$

Under the conservative assumption that all electromagnetic radiation produced by the string loop between recombination and the redshift of matter infall (denoted here by z where the physical distance from the centre of the loop to the shell is $r(z)$) remains bound to the halo, the radiation pressure is

$$P = \frac{3}{4\pi}\kappa I^2 r^{-3}(R\omega_c)^{1/3} t_{eq} \left(\frac{1+z_{eq}}{1+z}\right)^{3/2} \times \left(1 - \left(\frac{1+z}{1+z_{rec}}\right)^{3/2}\right). \tag{6.28}$$

The radiation pressure depends on a cutoff frequency, and we adopt the one used in [107, 108, 109, 104], $\omega_c \sim \mu^{3/2} I^{-3} (\beta R)^{-1}$. Cosmic string seeded halos have density profiles with $\alpha = 9/4$, therefore we find that the ratio of the gravitational to the radiation pressure force

(evaluated at the virial radius) is

$$\frac{F_g}{F_r} \approx 5 \times 10^8 \left(\frac{R}{t_{eq}}\right)^{5/3} \left(\frac{G\mu}{10^{-10}}\right)^{7/6} \left(\frac{I}{\mathrm{GeV}}\right)^{-1} \times \left(\frac{1+z}{1+z_{rec}}\right)^{5/6} \left(1 - \left(\frac{1+z}{1+z_{rec}}\right)^{3/2}\right)^{-1} . \tag{6.29}$$

In units of the critical current $I_c = \gamma \kappa^{-1} (G\mu)^{3/2} m_{pl}$, we find

$$\frac{F_g}{F_r} \approx 500 \left(\frac{R}{t_{eq}}\right)^{5/3} \left(\frac{G\mu}{10^{-10}}\right)^{-1/3} \left(\frac{I}{I_c}\right)^{-1} \times \left(\frac{1+z}{1+z_{rec}}\right)^{5/6} \left(1 - \left(\frac{1+z}{1+z_{rec}}\right)^{3/2}\right)^{-1} . \tag{6.30}$$

The range of parameters we consider above are roughly consistent with the implied values here. For $F_g/F_r > 1$ the gravitational force dominates, and so only in extreme cases of very high currents or very small loops does the additional radiation pressure cause an appreciable effect to the accretion dynamics, thus we neglect it in our analysis. We do, however, use this expression to estimate upper bound on string loop currents in equation (6.21) of the main text.

Bibliography

[1] M. Volonteri and M. J. Rees, "Rapid growth of high redshift black holes," *Astrophys. J.* **633** (2005) 624–629, arXiv:astro-ph/0506040.

[2] M. Volonteri, "Formation of Supermassive Black Holes," *Astron. Astrophys. Rev.* **18** (2010) 279–315, arXiv:1003.4404 [astro-ph.CO].

[3] J. Yang *et al.*, "Probing Early Supermassive Black Hole Growth and Quasar Evolution with Near-infrared Spectroscopy of 37 Reionization-era Quasars at 6.3 $<$ z $\leq$ 7.64," *Astrophys. J.* **923** no. 2, (2021) 262, arXiv:2109.13942 [astro-ph.GA].

[4] M. Volonteri, M. Habouzit, and M. Colpi, "The origins of massive black holes," *Nature Rev. Phys.* **3** no. 11, (2021) 732–743, arXiv:2110.10175 [astro-ph.GA].

[5] S. F. Bramberger, R. H. Brandenberger, P. Jreidini, and J. Quintin, "Cosmic String Loops as the Seeds of Super-Massive Black Holes," *JCAP* **06** (2015) 007, arXiv:1503.02317 [astro-ph.CO].

[6] T. W. B. Kibble, "Some Implications of a Cosmological Phase Transition," *Phys. Rept.* **67** (1980) 183.

[7] T. W. B. Kibble, "Phase Transitions in the Early Universe," *Acta Phys. Polon. B* **13** (1982) 723.

[8] R. Brandenberger, B. Cyr, and H. Jiao, "Intermediate mass black hole seeds from cosmic string loops," *Phys. Rev. D* **104** no. 12, (2021) 123501, arXiv:2103.14057 [astro-ph.CO].

[9] R. Brandenberger, B. Cyr, and H. Jiao, "Cosmic Rays and Spectral Distortions from Collapsing Textures," *JCAP* **09** (2020) 035, arXiv:2005.11099 [astro-ph.CO].

[10] M. Cruz, N. Turok, P. Vielva, E. Martinez-Gonzalez, and M. Hobson, "A Cosmic Microwave Background feature consistent with a cosmic texture," *Science* **318** (2007) 1612–1614, arXiv:0710.5737 [astro-ph].

[11] R. H. Brandenberger, "Topological defects and structure formation," *Int. J. Mod. Phys. A* **9** (1994) 2117–2190, arXiv:astro-ph/9310041.

[12] M. B. Hindmarsh and T. W. B. Kibble, "Cosmic strings," *Rept. Prog. Phys.* **58** (1995) 477–562, arXiv:hep-ph/9411342.

[13] A. Vilenkin and E. P. S. Shellard, *Cosmic Strings and Other Topological Defects*. Cambridge University Press, 7, 2000.

[14] E. Witten, "Superconducting Strings," *Nucl. Phys. B* **249** (1985) 557–592.

[15] J. P. Ostriker, A. C. Thompson, and E. Witten, "Cosmological Effects of Superconducting Strings," *Phys. Lett. B* **180** (1986) 231–239.

[16] E. M. Chudnovsky, G. B. Field, D. N. Spergel, and A. Vilenkin, "SUPERCONDUCTING COSMIC STRINGS," *Phys. Rev. D* **34** (1986) 944–950.

[17] R. H. Brandenberger, "Probing Particle Physics from Top Down with Cosmic Strings," *The Universe* **1** no. 4, (2013) 6–23, arXiv:1401.4619 [astro-ph.CO].

[18] A. Albrecht and N. Turok, "Evolution of Cosmic Strings," *Phys. Rev. Lett.* **54** (1985) 1868–1871.

[19] D. P. Bennett and F. R. Bouchet, "Evidence for a Scaling Solution in Cosmic String Evolution," *Phys. Rev. Lett.* **60** (1988) 257.

[20] B. Allen and E. P. S. Shellard, "Cosmic string evolution: a numerical simulation," *Phys. Rev. Lett.* **64** (1990) 119–122.

[21] C. Ringeval, M. Sakellariadou, and F. Bouchet, "Cosmological evolution of cosmic string loops," *JCAP* **02** (2007) 023, arXiv:astro-ph/0511646.

[22] V. Vanchurin, K. D. Olum, and A. Vilenkin, "Scaling of cosmic string loops," *Phys. Rev. D* **74** (2006) 063527, arXiv:gr-qc/0511159.

[23] L. Lorenz, C. Ringeval, and M. Sakellariadou, "Cosmic string loop distribution on all length scales and at any redshift," *JCAP* **10** (2010) 003, arXiv:1006.0931 [astro-ph.CO].

[24] J. J. Blanco-Pillado, K. D. Olum, and B. Shlaer, "Large parallel cosmic string simulations: New results on loop production," *Phys. Rev. D* **83** (2011) 083514, arXiv:1101.5173 [astro-ph.CO].

[25] J. J. Blanco-Pillado, K. D. Olum, and B. Shlaer, "The number of cosmic string loops," *Phys. Rev. D* **89** no. 2, (2014) 023512, arXiv:1309.6637 [astro-ph.CO].

[26] N. Bevis, M. Hindmarsh, M. Kunz, and J. Urrestilla, "CMB power spectrum contribution from cosmic strings using field-evolution simulations of the Abelian Higgs model," *Phys. Rev. D* **75** (2007) 065015, arXiv:astro-ph/0605018.

[27] M. Hindmarsh, J. Lizarraga, J. Urrestilla, D. Daverio, and M. Kunz, "Scaling from gauge and scalar radiation in Abelian Higgs string networks," *Phys. Rev. D* **96** no. 2, (2017) 023525, arXiv:1703.06696 [astro-ph.CO].

[28] M. Hindmarsh, J. Lizarraga, J. Urrestilla, D. Daverio, and M. Kunz, "Type I Abelian Higgs strings: evolution and Cosmic Microwave Background constraints," *Phys. Rev. D* **99** no. 8, (2019) 083522, arXiv:1812.08649 [astro-ph.CO].

[29] A. Vilenkin, "Cosmological Density Fluctuations Produced by Vacuum Strings," *Phys. Rev. Lett.* **46** (1981) 1169–1172. [Erratum: Phys.Rev.Lett. 46, 1496 (1981)].

[30] N. Turok and R. H. Brandenberger, "Cosmic Strings and the Formation of Galaxies and Clusters of Galaxies," *Phys. Rev. D* **33** (1986) 2175.

[31] M. Izawa and H. Sato, "GALAXY FORMATION BY COSMIC STRINGS AND COOLING OF BARYONIC MATTER," *Prog. Theor. Phys.* **78** (1987) 1219–1224.

[32] A. Stebbins, "Cosmic Strings and Galaxy Formation: Current Status," in *13th Texas Symposium on Relativistic Astrophysics*. 4, 1987.

[33] L. Perivolaropoulos, "Spectral analysis of microwave background perturbations induced by cosmic strings," *Astrophys. J.* **451** (1995) 429–435, arXiv:astro-ph/9402024.

[34] J. Magueijo, A. Albrecht, D. Coulson, and P. Ferreira, "Doppler peaks from active perturbations," *Phys. Rev. Lett.* **76** (1996) 2617–2620, arXiv:astro-ph/9511042.

[35] U.-L. Pen, U. Seljak, and N. Turok, "Power spectra in global defect theories of cosmic structure formation," *Phys. Rev. Lett.* **79** (1997) 1611–1614, arXiv:astro-ph/9704165.

[36] C. Dvorkin, M. Wyman, and W. Hu, "Cosmic String constraints from WMAP and the South Pole Telescope," *Phys. Rev. D* **84** (2011) 123519, arXiv:1109.4947 [astro-ph.CO].

[37] **Planck** Collaboration, P. A. R. Ade *et al.*, "Planck 2013 results. XXV. Searches for cosmic strings and other topological defects," *Astron. Astrophys.* **571** (2014) A25, arXiv:1303.5085 [astro-ph.CO].

[38] T. Charnock, A. Avgoustidis, E. J. Copeland, and A. Moss, "CMB constraints on cosmic strings and superstrings," *Phys. Rev. D* **93** no. 12, (2016) 123503, arXiv:1603.01275 [astro-ph.CO].

[39] N. Kaiser and A. Stebbins, "Microwave Anisotropy Due to Cosmic Strings," *Nature* **310** (1984) 391–393.

[40] R. Moessner, L. Perivolaropoulos, and R. H. Brandenberger, "A Cosmic string specific signature on the cosmic microwave background," *Astrophys. J.* **425** (1994) 365–371, arXiv:astro-ph/9310001.

[41] S. Amsel, J. Berger, and R. H. Brandenberger, "Detecting Cosmic Strings in the CMB with the Canny Algorithm," *JCAP* **04** (2008) 015, arXiv:0709.0982 [astro-ph].

[42] A. Stewart and R. Brandenberger, "Edge Detection, Cosmic Strings and the South Pole Telescope," *JCAP* **02** (2009) 009, arXiv:0809.0865 [astro-ph].

[43] R. J. Danos and R. H. Brandenberger, "Canny Algorithm, Cosmic Strings and the Cosmic Microwave Background," *Int. J. Mod. Phys. D* **19** (2010) 183–217, arXiv:0811.2004 [astro-ph].

[44] L. Hergt, A. Amara, R. Brandenberger, T. Kacprzak, and A. Refregier, "Searching for Cosmic Strings in CMB Anisotropy Maps using Wavelets and Curvelets," *JCAP* **06** (2017) 004, arXiv:1608.00004 [astro-ph.CO].

[45] J. D. McEwen, S. M. Feeney, H. V. Peiris, Y. Wiaux, C. Ringeval, and F. R. Bouchet, "Wavelet-Bayesian inference of cosmic strings embedded in the cosmic microwave background," *Mon. Not. Roy. Astron. Soc.* **472** no. 4, (2017) 4081–4098, arXiv:1611.10347 [astro-ph.IM].

[46] R. Ciuca and O. F. Hernández, "A Bayesian Framework for Cosmic String Searches in CMB Maps," *JCAP* **08** (2017) 028, arXiv:1706.04131 [astro-ph.CO].

[47] R. Ciuca, O. F. Hernández, and M. Wolman, "A Convolutional Neural Network For Cosmic String Detection in CMB Temperature Maps," *Mon. Not. Roy. Astron. Soc.* **485** (2019) 1377, arXiv:1708.08878 [astro-ph.CO].

[48] T. Vachaspati and A. Vilenkin, "Gravitational Radiation from Cosmic Strings," *Phys. Rev. D* **31** (1985) 3052.

[49] **LISA** Collaboration, P. Amaro-Seoane *et al.*, "Laser Interferometer Space Antenna," arXiv:1702.00786 [astro-ph.IM].

[50] **NANOGrav** Collaboration, Z. Arzoumanian *et al.*, "The NANOGrav 12.5 yr Data Set: Search for an Isotropic Stochastic Gravitational-wave Background," *Astrophys. J. Lett.* **905** no. 2, (2020) L34, arXiv:2009.04496 [astro-ph.HE].

[51] B. Goncharov *et al.*, "On the Evidence for a Common-spectrum Process in the Search for the Nanohertz Gravitational-wave Background with the Parkes Pulsar Timing Array," *Astrophys. J. Lett.* **917** no. 2, (2021) L19, arXiv:2107.12112 [astro-ph.HE].

[52] S. Chen *et al.*, "Common-red-signal analysis with 24-yr high-precision timing of the European Pulsar Timing Array: inferences in the stochastic gravitational-wave background search," *Mon. Not. Roy. Astron. Soc.* **508** no. 4, (2021) 4970–4993, arXiv:2110.13184 [astro-ph.HE].

[53] J. Antoniadis *et al.*, "The International Pulsar Timing Array second data release: Search for an isotropic gravitational wave background," *Mon. Not. Roy. Astron. Soc.* **510** no. 4, (2022) 4873–4887, arXiv:2201.03980 [astro-ph.HE].

[54] J. J. Blanco-Pillado, K. D. Olum, and J. M. Wachter, "Comparison of cosmic string and superstring models to NANOGrav 12.5-year results," *Phys. Rev. D* **103** no. 10, (2021) 103512, arXiv:2102.08194 [astro-ph.CO].

[55] R. Brandenberger, B. Cyr, and A. V. Iyer, "Fast Radio Bursts from the Decay of Cosmic String Cusps," arXiv:1707.02397 [astro-ph.CO].

[56] T. Vachaspati, "Cosmic Sparks from Superconducting Strings," *Phys. Rev. Lett.* **101** (2008) 141301, arXiv:0802.0711 [astro-ph].

[57] L. V. Zadorozhna and B. I. Hnatyk, "Electromagnetic emission bursts from the near-cusp regions of superconducting cosmic strings," *Ukr. J. Phys.* **54** (2009) 1149–1156.

[58] Y.-F. Cai, E. Sabancilar, and T. Vachaspati, "Radio bursts from superconducting strings," *Phys. Rev. D* **85** (2012) 023530, arXiv:1110.1631 [astro-ph.CO].

[59] Y.-F. Cai, E. Sabancilar, D. A. Steer, and T. Vachaspati, "Radio Broadcasts from Superconducting Strings," *Phys. Rev. D* **86** (2012) 043521, arXiv:1205.3170 [astro-ph.CO].

[60] J. Ye, K. Wang, and Y.-F. Cai, "Superconducting cosmic strings as sources of cosmological fast radio bursts," *Eur. Phys. J. C* **77** no. 11, (2017) 720, arXiv:1705.10956 [astro-ph.HE].

[61] Y.-W. Yu, K.-S. Cheng, G. Shiu, and H. Tye, "Implications of fast radio bursts for superconducting cosmic strings," *JCAP* **11** (2014) 040, arXiv:1409.5516 [astro-ph.HE].

[62] L. V. Zadorozhna, "Fast radio bursts as electromagnetic radiation from cusps on superconducting cosmic strings," *Advances in Astronomy and Space Physics* **5** (Sept., 2015) 43–50.

[63] R. Brandenberger, B. Cyr, and T. Schaeffer, "On the Possible Enhancement of the Global 21-cm Signal at Reionization from the Decay of Cosmic String Cusps," *JCAP* **04** (2019) 020, arXiv:1810.03219 [astro-ph.CO].

[64] R. Brandenberger, B. Cyr, and R. Shi, "Constraints on Superconducting Cosmic Strings from the Global 21-cm Signal before Reionization," *JCAP* **09** (2019) 009, arXiv:1902.08282 [astro-ph.CO].

[65] K. D. Olum and A. Vilenkin, "Reionization from cosmic string loops," *Phys. Rev. D* **74** (2006) 063516, arXiv:astro-ph/0605465.

[66] B. Shlaer, A. Vilenkin, and A. Loeb, "Early structure formation from cosmic string loops," *JCAP* **05** (2012) 026, arXiv:1202.1346 [astro-ph.CO].

[67] H. Tashiro, E. Sabancilar, and T. Vachaspati, "Constraints on Superconducting Cosmic Strings from Early Reionization," *Phys. Rev. D* **85** (2012) 123535, arXiv:1204.3643 [astro-ph.CO].

[68] M. Anthonisen, R. Brandenberger, and P. Scott, "Constraints on cosmic strings from ultracompact minihalos," *Phys. Rev. D* **92** no. 2, (2015) 023521, arXiv:1504.01410 [astro-ph.CO].

[69] A. Babul, B. Paczynski, and D. Spergel, "Gamma-ray bursts from superconducting cosmic strings at large redshifts," *Astrophys. J. Lett.* **316** (1987) L49–L54.

[70] L. Lin, S. Yamanouchi, and R. Brandenberger, "Effects of Cosmic String Velocities and the Origin of Globular Clusters," *JCAP* **12** (2015) 004, arXiv:1508.02784 [astro-ph.CO].

[71] A. Barton, R. H. Brandenberger, and L. Lin, "Cosmic Strings and the Origin of Globular Clusters," *JCAP* **06** (2015) 022, arXiv:1502.07301 [astro-ph.CO].

[72] F. Pacucci and A. Loeb, "The search for the farthest quasar: consequences for black hole growth and seed models," *Mon. Not. Roy. Astron. Soc.* **509** no. 2, (2021) 1885–1891, arXiv:2110.10176 [astro-ph.GA].

[73] S. W. Hawking, "Black Holes From Cosmic Strings," *Phys. Lett. B* **231** (1989) 237–239.

[74] A. Polnarev and R. Zembowicz, "Formation of Primordial Black Holes by Cosmic Strings," *Phys. Rev. D* **43** (1991) 1106–1109.

[75] T. Helfer, J. C. Aurrekoetxea, and E. A. Lim, "Cosmic String Loop Collapse in Full General Relativity," *Phys. Rev. D* **99** no. 10, (2019) 104028, arXiv:1808.06678 [gr-qc].

[76] J. C. Aurrekoetxea, T. Helfer, and E. A. Lim, "Coherent Gravitational Waveforms and Memory from Cosmic String Loops," *Class. Quant. Grav.* **37** no. 20, (2020) 204001, arXiv:2002.05177 [gr-qc].

[77] M. G. Haehnelt and M. J. Rees, "The formation of nuclei in newly formed galaxies and the evolution of the quasar population," *Mon. Not. Roy. Astron. Soc.* **263** (1993) 168–178.

[78] M. Umemura, A. Loeb, and E. L. Turner, "Early cosmic formation of massive black holes," *Astrophys. J.* **419** (1993) 459, arXiv:astro-ph/9303004.

[79] A. Loeb and F. A. Rasio, "Collapse of primordial gas clouds and the formation of quasar black holes," *Astrophys. J.* **432** (1994) 52, arXiv:astro-ph/9401026.

[80] D. J. Eisenstein and A. Loeb, "Origin of quasar progenitors from the collapse of low spin cosmological perturbations," *Astrophys. J.* **443** (1995) 11, arXiv:astro-ph/9401016.

[81] V. Bromm and A. Loeb, "Formation of the first supermassive black holes," *Astrophys. J.* **596** (2003) 34–46, arXiv:astro-ph/0212400.

[82] M. C. Begelman, M. Volonteri, and M. J. Rees, "Formation of supermassive black holes by direct collapse in pregalactic halos," *Mon. Not. Roy. Astron. Soc.* **370** (2006) 289–298, arXiv:astro-ph/0602363.

[83] Z. Haiman, T. Abel, and M. J. Rees, "The radiative feedback of the first cosmological objects," *Astrophys. J.* **534** (2000) 11–24, arXiv:astro-ph/9903336.

[84] S. P. Oh and Z. Haiman, "Second-generation objects in the universe: radiative cooling and collapse of halos with virial temperatures above 10^4 kelvin," *Astrophys. J.* **569** (2002) 558, arXiv:astro-ph/0108071.

[85] K. Inayoshi, E. Visbal, and Z. Haiman, "The Assembly of the First Massive Black Holes," *Ann. Rev. Astron. Astrophys.* **58** (2020) 27–97, arXiv:1911.05791 [astro-ph.GA].

[86] J. A. Fillmore and P. Goldreich, "Self-similiar gravitational collapse in an expanding universe," *Astrophys. J.* **281** (1984) 1–8.

[87] E. Bertschinger, "Self - similar secondary infall and accretion in an Einstein-de Sitter universe," *Astrophys. J. Suppl.* **58** (1985) 39.

[88] M. Vogelsberger, S. D. M. White, R. Mohayaee, and V. Springel, "Caustics in growing Cold Dark Matter Haloes," *Mon. Not. Roy. Astron. Soc.* **400** (2009) 2174, arXiv:0906.4341 [astro-ph.CO].

[89] J. F. Navarro, C. S. Frenk, and S. D. M. White, "The Structure of cold dark matter halos," *Astrophys. J.* **462** (1996) 563–575, arXiv:astro-ph/9508025.

[90] **LIGO Scientific, Virgo** Collaboration, B. P. Abbott *et al.*, "GWTC-1: A Gravitational-Wave Transient Catalog of Compact Binary Mergers Observed by

LIGO and Virgo during the First and Second Observing Runs," *Phys. Rev. X* **9** no. 3, (2019) 031040, arXiv:1811.12907 [astro-ph.HE].

[91] **LIGO Scientific, Virgo** Collaboration, R. Abbott *et al.*, "GWTC-2: Compact Binary Coalescences Observed by LIGO and Virgo During the First Half of the Third Observing Run," *Phys. Rev. X* **11** (2021) 021053, arXiv:2010.14527 [gr-qc].

[92] **LIGO Scientific, VIRGO, KAGRA** Collaboration, R. Abbott *et al.*, "GWTC-3: Compact Binary Coalescences Observed by LIGO and Virgo During the Second Part of the Third Observing Run," arXiv:2111.03606 [gr-qc].

[93] Y. Harikane, A. K. Inoue, K. Mawatari, T. Hashimoto, S. Yamanaka, Y. Fudamoto, H. Matsuo, Y. Tamura, P. Dayal, L. Y. A. Yung, A. Hutter, F. Pacucci, Y. Sugahara, and A. M. Koekemoer, "A Search for H-Dropout Lyman Break Galaxies at z~12-16," *arXiv e-prints* (Dec., 2021) arXiv:2112.09141, arXiv:2112.09141 [astro-ph.GA].

[94] F. Pacucci, P. Dayal, Y. Harikane, A. K. Inoue, and A. Loeb, "Are the Newly-Discovered $z \sim 13$ Drop-out Sources Starburst Galaxies or Quasars?," arXiv:2201.00823 [astro-ph.GA].

[95] S. F. Portegies Zwart and S. L. W. McMillan, "The Runaway growth of intermediate-mass black holes in dense star clusters," *Astrophys. J.* **576** (2002) 899–907, arXiv:astro-ph/0201055.

[96] T. C. N. Boekholt, D. R. G. Schleicher, M. Fellhauer, R. S. Klessen, B. Reinoso, A. M. Stutz, and L. Haemmerle, "Formation of massive seed black holes via collisions and accretion," *Mon. Not. Roy. Astron. Soc.* **476** no. 1, (2018) 366–380, arXiv:1801.05841 [astro-ph.GA].

[97] K. Omukai, R. Schneider, and Z. Haiman, "Can Supermassive Black Holes Form in Metal-Enriched High-Redshift Protogalaxies ?," *Astrophys. J.* **686** (2008) 801, arXiv:0804.3141 [astro-ph].

[98] R. Fernandez, G. L. Bryan, Z. Haiman, and M. Li, "H_2 suppression with shocking inflows: testing a pathway for supermassive black hole formation," *Mon. Not. Roy. Astron. Soc.* **439** no. 4, (2014) 3798–3807, arXiv:1401.5803 [astro-ph.CO].

[99] K. Inayoshi, K. Omukai, and E. J. Tasker, "Formation of an embryonic supermassive star in the first galaxy," *Mon. Not. Roy. Astron. Soc.* **445** (2014) 109, arXiv:1404.4630 [astro-ph.GA].

[100] H. Umeda, T. Hosokawa, K. Omukai, and N. Yoshida, "The Final Fates of Accreting Supermassive Stars," *Astrophys. J. Lett.* **830** no. 2, (2016) L34, arXiv:1609.04457 [astro-ph.SR].

[101] T. E. Woods, A. Heger, D. J. Whalen, L. Haemmerle, and R. S. Klessen, "On the Maximum Mass of Accreting Primordial Supermassive Stars," *Astrophys. J. Lett.* **842** no. 1, (2017) L6, arXiv:1703.07480 [astro-ph.SR].

[102] A. Loeb, "First light," in *36th Saas-Fee Advanced Course of the Swiss Society for Astrophysics and Astronomy: First Light in the Universe*, pp. 1–159. 2008. arXiv:astro-ph/0603360.

[103] H. Mo, F. Van den Bosch, and S. White, *Galaxy formation and evolution*. Cambridge University Press, 2010.

[104] K. Miyamoto and K. Nakayama, "Cosmological and astrophysical constraints on superconducting cosmic strings," *JCAP* **07** (2013) 012, arXiv:1212.6687 [astro-ph.CO].

[105] Y. B. Zeldovich, "Gravitational instability: An Approximate theory for large density perturbations," *Astron. Astrophys.* **5** (1970) 84–89.

[106] E. W. Kolb and I. I. Tkachev, "Large amplitude isothermal fluctuations and high density dark matter clumps," *Phys. Rev. D* **50** (1994) 769–773, arXiv:astro-ph/9403011.

[107] A. Vilenkin and T. Vachaspati, "Electromagnetic Radiation from Superconducting Cosmic Strings," *Phys. Rev. Lett.* **58** (1987) 1041–1044.

[108] D. N. Spergel, T. Piran, and J. Goodman, "Dynamics of Superconducting Cosmic Strings," *Nucl. Phys. B* **291** (1987) 847–875.

[109] J. J. Blanco-Pillado and K. D. Olum, "Electromagnetic radiation from superconducting string cusps," *Nucl. Phys. B* **599** (2001) 435–445, arXiv:astro-ph/0008297.

Conclusions

Conclusions

Topological defects offer a truly extraordinary way to probe the high energy regime of our universe. The cosmological longevity of a network of cosmic strings ensures that interesting phenomenology will be present in every observable epoch of the universe (provided the symmetry breaking happens at sufficiently high scales). This thesis is evidence of that fact, with investigations into signatures of topological defects spanning redshifts ranging from $z \approx 10^6$ ($t \approx 1\,\mathrm{yr}$ after the big bang, coming from distortions of the CMB blackbody in chapter 4), all the way down to $z \approx 0$ ($t \approx 13\,\mathrm{Gyr}$ with black hole observations in chapter 5). While this thesis performs a random walk through different phenomenological signatures of topological defects, there still remains an enormous number of novel approaches waiting to be explored.

On the immediate horizon, follow-up work is in progress to expand on the set of conditions necessary to induce black hole collapse near a cosmic string loop. Currently, the values of $G\mu$ and $\mathcal{I}$ necessary to satisfy the direct collapse conditions lands us in a heavily constrained region of parameter space (see figure 1.3). These constraints, however, rely on assumptions about the string network that may not be well-founded (for example, that every string loop in the distribution has the same current at all times). Work is currently underway to reinterpret some of these constraints under more realistic assumptions.

Ultimately, we would like to make a low-redshift statement regarding the mass function of string-seeded black holes in order to compare with quasar observations at $z \geq 7$. To do so, we need to track the evolution of these black holes from their formation ($z \approx \mathcal{O}(100)$). Analytically, this is a challenging problem, and so we are collaborating with researchers abroad to answer this question in a semi-numerical way using *merger tree* codes. These codes simulate the mergers of galaxies and follow the subsequent evolution of the black holes residing in such galaxies.

As advancements in observational techniques improve, a variety of interesting new avenues of detection become available to us. Of particular interest to the author are anisotropic CMB spectral distortion signatures. Thus far constraints from CMB spectral distortions are

on global (or sky-averaged) scales. String loops gravitate, however, and so there exists the possibility that they may cluster with one another. In such a case, their induced distortion signatures will also be clustered. Once a method exists to search for anisotropic distortions, this will a prime target to search for. Developing such a method is a prime focus during the next academic appointment for the author.

The next generation of 21-cm cosmology experiments are well underway, with high sensitivity intensity maps upcoming from the HERA collaboration. In contrast to CMB observations, these maps contain explicit data over different redshifts, which can be used to hunt for topological defects. Anisotropies induced by both the long strings and loops in these 21-cm maps will open new windows into constraining $G\mu$.

Overall, this thesis represents a look into the evolution of the authors research interests during the course of the PhD. With many interesting topics ready to be explored, we now eagerly await the next stage in our journey through the cosmos.